
Methods¹

Expedition 329 Scientists²

Chapter contents

Introduction, operations, and curation	1
Lithostratigraphy, igneous petrology, alteration, and structural geology	5
Paleontology and biostratigraphy	12
Paleomagnetism	14
Biogeochemistry	15
Microbiology	24
Physical properties	34
Downhole measurements	41
References	43
Figures	50
Tables	69

Introduction, operations, and curation

Information assembled in this chapter will help the reader understand the basis for shipboard observations and preliminary conclusions of Integrated Ocean Drilling Program (IODP) Expedition 329. It will also enable the interested investigator to identify data and select samples for further analysis. Information presented here concerns only shipboard operations and analyses described in the site chapters (Sites U1365–U1371). Methods used by various investigators for shore-based analyses of Expedition 329 samples and data will be described in individual publications in various professional journals and the Expedition Research Results chapters of this *Proceedings* volume. This introductory section provides an overview of operations, curatorial conventions, and general core handling and analysis.

Site locations

At all Expedition 329 sites, GPS coordinates from precruise site surveys were used to position the vessel on site. The only seismic system used during the cruise was the Syquest Bathy 2010 CHIRP subbottom profiler, which was monitored on the approach to each site to confirm the seafloor depth with that from the precruise survey. Once the vessel was positioned at a site, the thrusters were lowered and a positioning beacon was dropped to the seafloor. The dynamic positioning control of the vessel uses navigational input from the GPS and triangulation to the seafloor beacon, weighted by the estimated positional accuracy. The final hole position was the mean position calculated from the GPS data collected over the time that the hole was occupied.

Coring and drilling operations

The advanced piston corer (APC), extended core barrel (XCB), and rotary core barrel (RCB) systems were used during Expedition 329. These standard coring systems and their characteristics are summarized in Graber et al. (2002). The APC system cuts soft-sediment cores with minimal coring disturbance relative to other IODP coring systems. After the APC core barrel is lowered through the drill pipe and lands near the bit, the drill pipe is pressurized until the shear pins that attach the inner barrel to the outer barrel fail. The inner barrel then advances into the formation and cuts the core. The driller can detect a successful cut, or “full stroke,” from the pressure gauge on the rig floor. The XCB system is de-

¹Expedition 329 Scientists, 2011. Methods. In D'Hondt, S., Inagaki, F., Alvarez Zarikian, C.A., and the Expedition 329 Scientists, *Proc. IODP, 329*: Tokyo (Integrated Ocean Drilling Program Management International, Inc.).
doi:10.2204/iodp.proc.329.102.2011
²Expedition 329 Scientists' addresses.



ployed when the formation becomes too stiff or too hard for the APC system. The XCB cutting shoe (bit) extends as far as ~30.5 cm ahead of the main bit in soft sediments but retracts into the main bit if hard formations are encountered.

APC refusal is conventionally defined in two ways: (1) the piston fails to achieve a complete stroke (as determined from the pump pressure reading) because the formation is too hard or (2) excessive force (>60,000 lb; ~267 kN) is required to pull the core barrel out of the formation. When a full or partial stroke can be achieved but excessive force cannot retrieve the barrel, the core barrel can be “drilled over”; after the inner core barrel is successfully shot into the formation, the drill bit is advanced to total depth to free the APC barrel. This strategy allows a hole to be advanced much farther with the APC, the preferred coring tool. Nonmagnetic core barrels are commonly used during all conventional APC coring, but the APC drillover technique is not typically conducted in the first hole at each site if hard rock might be encountered. Standard steel core barrels are usually used for the drillover technique because they are stronger than the nonmagnetic barrels. Most APC/XCB cored intervals are ~9.5 m long, which is the length of a standard core barrel.

During Expedition 329, a pilot hole was drilled or “washed” ahead without recovering sediment at each site to identify hard lithologies (e.g., chert) and the depth of basement. Such advances were necessary to minimize potential for major operational setbacks (e.g., extra pipe trips and tool damage). Drilling without coring was also necessary to advance the drill bit to a target depth where core recovery could be resumed or to ensure that coring gaps in one hole were covered by cored intervals in adjacent holes. The amount of advance varied case by case. An alternative method to adjust the offset between holes was to raise the bit off the bottom of a hole 1–4 m before shooting the next APC core. Core operations and recovery information is given in “Operations” in each site chapter.

Some APC cores were oriented using the Flexit tool (see “[Paleomagnetism](#)”). Formation temperature measurements were usually made in Hole B of each site and repeated, if necessary for data quality, in Holes C and D (see “[Downhole measurements](#)”). Downhole logging was attempted in only one hole at two of the sites with deepest penetration.

The XCB system was used to advance the hole when APC refusal occurred in a hole before the target depth was reached and when the formation became too stiff for the APC system or when drilling hard substrate such as cemented layers and nodules or chert. The XCB is a rotary system with a small cut-

ting shoe extending below the large rotary drill bit. The smaller bit can cut a semi-indurated core with less torque and fluid circulation than the main bit and thus optimizes recovery.

The bottom-hole assembly (BHA) is the lowermost part of the drill string. The exact configuration of the BHA is reported in “Operations” in each site chapter. A typical APC/XCB BHA consists of a drill bit (outer diameter = 11 $\frac{1}{16}$ inch), a bit sub, a seal bore drill collar, a landing saver sub, a modified top sub, a modified head sub, a nonmagnetic drill collar (for APC/XCB), a number of 8 inch (~20.32 cm) drill collars, a tapered drill collar, six joints (two stands) of 5 $\frac{1}{2}$ inch (~13.97 cm) drill pipe, and one crossover sub. A lockable flapper valve was used so that we could collect downhole logs without dropping the bit when APC/XCB coring.

The RCB system was deployed to drill basaltic basement at three of the sites. The RCB is a conventional rotary drilling system and requires a dedicated RCB BHA and a dedicated RCB drilling bit (outer diameter = 9 $\frac{7}{8}$ inch). A typical BHA for RCB coring includes an RCB drill bit, a mechanical bit release (MBR), a modified head sub, an outer core barrel, a modified top sub, and a series of drill collars followed by tapered drill collar and 5 $\frac{1}{2}$ inch drill pipe.

Curatorial procedures and sample depth calculations

Numbering of sites, holes, cores, and samples followed standard IODP procedure. Drilling sites are numbered consecutively from the first site drilled by the *Glomar Challenger* in 1968. IODP Expedition 301 began using the prefix “U” to designate sites occupied by the US Implementing Organization (USIO) vessel, the R/V *JOIDES Resolution*. For all IODP drill sites, a letter suffix distinguishes each hole cored at the same site. The first hole cored is assigned the site number modified by the suffix “A,” the second hole takes the site number and the suffix “B,” and so forth. For Expedition 329, each site has three or more cored holes (A, B, C, D, etc.). With the exception of Site U1365, all pilot holes were assigned alphabetical designations (e.g., Hole U1366A) even though no cores were taken from these holes. The reason for this designation is because pilot holes provide vital drilling information that can be stored in the IODP database for use in future drilling.

A full curatorial identifier for a sample consists of the following information: expedition, site, hole, core number, core type, section number, and interval in centimeters measured from the top of the core section and also the sampling tools and volumes taken. For example, in sediment, a sample identification of

“329-U1365A-1H-2, 10–12 cm” represents a sample taken from the interval between 10 and 12 cm below the top of Section 2 of Core 1 (“H” designates that this core was taken with the APC system) of Hole A of Site U1365 during Expedition 329. For hard rocks, a sample identification of “329-U1365E-3R-8 (Piece 1, 4–7 cm)” indicates a 3 cm sample of Piece 1 removed from the interval between 4 and 7 cm below the top of Section 8 of Core 3 (“R” designates that this core was taken with the RCB) in Hole A at Site U1365. For cores taken with the XCB, the core type is indicated by an “X” after the core number. During Expedition 329, some of the sediment was drilled without coring in holes where hard chert horizons were encountered or in holes where the target recovery was underlying basement rock. Drilled intervals are assigned double-digit numbers, and the cores recovered after a drilled interval are assigned the following number in combination with the corresponding letter for drilling/coring system. For example, the drilled interval in Hole U1365E was designated 329-U1365E-11, where the first “1” indicates drilled interval 1 and the second “1” indicates the first section of that interval that was drilled. The first core recovered in Hole U1365E after the drilled interval was designated 329-U1365E-2R (“R” for rotary core barrel).

The cored interval is measured in meters below seafloor (mbsf) according to the core depth below seafloor, method A (CSF-A), depth scale (see IODP Depth Scale Terminology at www.iodp.org/program-policies/). In general, the depth below seafloor is determined by subtracting the water depth estimated from the initial drill pipe measurement to the seafloor from the total drill pipe measurement. The depth interval assigned to an individual core begins with the depth below seafloor at which coring began and extends to the depth that coring advanced. Each coring interval is generally ~9.5 m, which is the length of a core barrel; however, coring intervals may be shorter.

During Expedition 329, unless otherwise noted, all core depths below seafloor were calculated as CSF-A and all downhole wireline depths calculated as wireline depth below seafloor, method A (WSF-A). For ease of communication of shipboard results, all depths are reported in this volume as “mbsf” unless otherwise noted.

Core handling and analysis

A diverse core flow scheme was formulated for Expedition 329. Cores from the first hole at each site (typically Hole B) were dedicated for dissolved oxygen analyses (see “[Biogeochemistry](#)”), routine Core Laboratory analyses (see “[Lithostratigraphy, igneous](#)

[petrology, alteration, and structural geology](#),” “[Paleontology and biostratigraphy](#),” “[Physical properties](#),” and “[Paleomagnetism](#)”), and sampling table processing. This hole was designated for the stratigraphic backbone for the site.

As soon as cores arrived on deck, they were extracted from the core barrel in plastic liners. These liners were carried from the rig floor to the core processing area on the catwalk outside the Core Laboratory, where they were cut into ~1.5 m sections. Liner caps (blue indicating top, colorless indicating bottom) were placed onto liner sections on the catwalk by the curator. Hard rock pieces were pushed to the top of the liner sections and the total rock length was measured. The length was entered into the database using the SampleMaster application as “created” length. Created length is used to calculate recovery. Headspace samples were taken from each core catcher in Hole B using a syringe for immediate hydrocarbon analysis as part of the shipboard safety and pollution prevention program. Typically this procedure is followed in the first hole drilled at a site, but because methane was not expected at the sites drilled during Expedition 329, the Environmental Protection and Safety Panel (EPSP) and the Texas A&M University Safety Panel approved our proposal to first drill a pilot hole at each site.

The first core from each hole (i.e., Core 1H) was sampled for bottom water if a mudline was recovered and seawater was present inside the top of the core liner. The bottom seawater was used for comparative studies of microbial communities between seawater and seafloor habitats.

Cores from the first hole cored at each site were quickly processed on the catwalk, and the 1.5 m whole-round core sections were transferred immediately to the Cold Room adjacent to the Microbiology Laboratory for dissolved oxygen measurements (see “[Biogeochemistry](#)”). The whole-round cores were subsequently brought back to the Core Laboratory for routine core processing.

Cores from subsequent holes (typically Holes C and D, but sometimes E and F depending on core conditions), were processed on the catwalk and the whole-round sections were transferred immediately to the core reefer on the Hold Deck of the *JOIDES Resolution* for a wide range of geochemical and microbiological subsampling. Once the subsampling was completed, the remaining pieces of the whole-round core sections were brought back to the Core Laboratory for routine core processing. If core quality allowed, Hole C was sampled primarily for geochemistry and Hole D was sampled primarily for microbiology. When Hole D was cored by APC/XCB, it was primarily used to fill lithostratigraphic gaps of previous holes. Inter-

stitial water samples were taken with Rhizon samplers at selected intervals (see **“Biogeochemistry”** and **“Microbiology”**).

Basalt cores were processed on the catwalk and immediately taken to the core reefer on the Hold Deck for cold storage and preliminary lithostratigraphic description. The cores were visually examined by the shipboard microbiologists and petrologists, and potential samples for microbiological studies were identified, discussed by the Sample Allocation Committee, and subsequently aseptically collected by the microbiologists. Once the samples were taken, the hard rock core sections were brought to the Core Laboratory for routine core processing.

As described in **“Lithostratigraphy, igneous petrology, alteration, and structural geology,” “Physical properties,”** and **“Paleomagnetism,”** routine core processing in the Core Laboratory included whole-round logging of core sections on the Whole Round Multisensor Logger (WRMSL) and splitting into working and archive halves. Archive-half sections were imaged on the Section Half Imaging Logger (SHIL), logged with the Section Half Multisensor Logger (SHMSL), and visually described for lithologic and petrologic properties. The working halves were sampled for shipboard analyses and postexpedition research.

In the Core Laboratory, whole-round sections were split lengthwise in the core splitting room to expose the core. For hard rock cores, oriented pieces of core were marked on the bottom with a red wax pencil to preserve orientation, either before they were extracted from the core barrel or when they were removed from the split core liner. In some cases, pieces were too small to be oriented. Adjacent but broken core pieces that could be fit together along fractures were curated as single pieces. The petrologist on shift confirmed piece matches, corrected any errors, and marked the split line on the pieces, which defined how the pieces were cut in two equal halves. The aim was to maximize the expression of dipping structures on the cut face of the core while maintaining representative features in both archive and working halves. A plastic spacer was secured to the split core liner with acetone between individual pieces or reconstructed contiguous groups of subpieces. These spacers may represent a substantial interval of no recovery. The length of each section of core, including spacers, was entered into the curation database as “curated” length. Curated length commonly differs by a few to several centimeters from the created length measured on the catwalk. The database recal-

culates the assumed depth of each piece based on the curated length.

Sampling for shipboard analyses and personal research was done onboard. Both halves of the core were shrink-wrapped, put into labeled plastic tubes, sealed, and transferred to cold storage space aboard the ship. At the end of the expedition, the cores and samples were transferred from the ship to refrigerated containers and shipped to cold storage at the IODP Gulf Coast Repository in College Station, Texas (USA).

Drilling-induced core deformation

Cores may be significantly disturbed and contain extraneous material as a result of the coring and core handling process. Therefore, the top 10–50 cm of each core must be carefully examined for potential “fall-in” during description. Common coring-induced deformation includes concave-downward appearance of originally horizontal bedding. In APC cores, the motion of the piston may result in fluidization (flow-in) at the bottom of the cores. Retrieval from depth to the surface may result in elastic rebound. Observed core disturbances are described in **“Lithostratigraphy”** and other sections in each site chapter and graphically indicated on the core standard graphic reports (visual core descriptions [VCDs]; see **“Lithostratigraphy, igneous petrology, alteration, and structural geology”**).

Authorship of site chapters

The separate sections of the site chapters and methods chapter were written by the following shipboard scientists (authors are listed in alphabetical order; no seniority is implied):

Operations: C. Alvarez Zarikian, S. Midgley
 Background and objectives: S. D’Hondt, F. Inagaki
 Lithostratigraphy: B. Hoppie, F. Shiraishi, G. Uramoto
 Paleomagnetism: H. Evans, T. Shimono
 Igneous petrology: C. Smith-Duque, G. Zhang
 Paleontology and biostratigraphy: C. Alvarez Zarikian
 Biogeochemistry: N. Dubois, T. Ferdelman, B. Gribsholt, J.-H. Hyun, S. Mitsunobu, R.W. Murray, D.C. Smith, A. Spivack, M. Szipak, Y. Yamaguchi, W. Ziebis
 Microbiology: T. Engelhardt, J. Kallmeyer, J. Lynch, Y. Morono, D.C. Smith, B.O. Steinsbu, Y. Suzuki, L. Toffin, X.-H. Zhang
 Physical properties: R. Harris, J. Kim
 Downhole measurements: H. Evans

Lithostratigraphy, igneous petrology, alteration, and structural geology

This section outlines the procedures used to document the composition, texture, and structure of geologic materials recovered during Expedition 329. These procedures included visual core description, smear slide description, digital color imaging, color spectrophotometry, X-ray diffraction (XRD), and inductively coupled plasma–atomic emission spectroscopy (ICP-AES). Because many of the geologic techniques and observations used to analyze sedimentary cores are similar to those used to analyze igneous cores, the methods by which those materials were analyzed are herein presented together. However, as necessary, descriptions of the dissimilar procedures required to characterize the sedimentary and crystalline basement rocks are also provided.

All acquired data were uploaded into the IODP-USIO Laboratory Information Management System (LIMS), and observations were entered using the DESClogik application in Tabular Data Capture mode. Additional details are provided below. A glossary of common geological terms used to describe the basaltic cores is in Table T1.

Core sections available for sedimentary and igneous observation and interpretation included both working and archive halves. Sections dominated by soft sediment were split using a thin wire held in high tension. Pieces of hard rock were split with a diamond-impregnated saw so that important compositional and structural features were preserved in both the archive and working halves. The split surface of the archive half was then assessed for quality (e.g., smearing or surface unevenness) and, if necessary, scraped lightly with a glass slide or spatula. After splitting, the archive half (sediment and basement) was imaged by the SHIL and analyzed for color reflectance and magnetic susceptibility using the SHMSL systems (see “[Physical properties](#)”). The archive section half was occasionally reimaged when visibility of sedimentary structures or fabrics improved following treatment of the split core surface.

Following imaging, the archive sections of the sediment core were described for primary features macroscopically. Lithostratigraphic units were characterized by visual inspection, and smear slide samples were used to determine microfossil and sedimentary constituents and abundance to aid in lithologic classification. Core from the basement (basalt) was also described visually and subsequently with the aid of thin sections for primary igneous features, secondary features, and structural geology. All descriptive data

were entered into DESClogik (see “[Data capture software](#)” for details). Based on preliminary visual descriptions and physical property data, thin section samples and samples for XRD and ICP-AES were extracted from the working-half sections. All descriptions and sample locations were recorded using curated depths and then recorded on standard graphic report forms and documented on VCDs (Fig. F1).

Sediment visual core descriptions

Color and composition

Sediment color was determined qualitatively for core intervals using Munsell Color Charts (Munsell Color Company, Inc., 2000). Visual inspections of the archive section halves using the unaided eye and a low-power (i.e., 10×) hand lens identified compositional elements of the sediment, including concretions and nodules, porcellanites and chert, and ash.

Textures, structures, and sedimentary fabric

When visible at low magnifications, sediment grain size was determined using the Wentworth scale (Wentworth, 1922). Grain size, particle shape, and sorting were also noted; however, these textural attributes required inspection at high magnification and were only performed on smear slides and thin sections (see below).

Sedimentary structures observed in recovered cores included bedding, soft-sediment deformation, bioturbation, and displacive early diagenetic mineral authigenesis. Bed thickness was defined according to McKee and Weir (1953) and included the following units:

- Very thick bedded = >100 cm.
- Thick bedded = 30–100 cm.
- Medium bedded = 10–30 cm.
- Thin bedded = 3–10 cm.
- Very thin bedded = 1–3 cm.
- Laminae = <1 cm.

Samples were microscopically inspected for micrograded bedding (i.e., graded bedding occurring within laminations) and indications of preferential particle orientations, including lineation and imbrication of elongated detrital and biogenic material.

Syn- to postdepositional disturbances in bedding structures, including burrowing and bioturbation, displacement of beds in the layers associated with metalliferous nodules, and soft-sediment deformation, were also noted. Of these features, the semi-quantitative description of bioturbation, deemed “ichnofabrics,” warrants additional discussion. Ichnofabric description analysis included evaluation of the extent of bioturbation and notation of distinctive biogenic structures. To assess the degree of bio-

turbation semiquantitatively, a modified version of the Droser and Bottjer (1986) ichnofabric index (1–5) scheme was employed as follows:

- 1 = no apparent bioturbation.
- 2 = slight bioturbation (1%–30% of visible sectioned core half).
- 3 = moderate bioturbation (30%–60% of visible sectioned core half).
- 4 = heavy bioturbation (60%–90% of visible sectioned core half).
- 5 = complete bioturbation (no depositional structure remaining).

These indexes are illustrated using the numerical scale in the ichnofabric column of the core description sheets. It is important to note that the complete mixing of sediment by bioturbating organisms produces homogeneous sediment with an appearance similar to nonbioturbated sediment resulting from the deposition of material of homogeneous color and grain size. Therefore, a bioturbation scale cannot be applied to homogeneous sediment with confidence and would consequently fall into ichnofabric index 1, no apparent bioturbation.

Induration

The induration of sediment was described using a simple tripartite scale of poorly, moderately, and well-indurated classes. Each interval was assigned to one of these classes based on the ease or difficulty of inserting instruments or the ease or difficulty of obtaining samples of the material for other analyses prior to the lithologic description of the cores.

Lithologic classification scheme for sediments

The lithologic classification scheme employed during Expedition 329 conforms to the Ocean Drilling Program (ODP) sediment classification scheme of Mazzullo et al. (1988). Based on past sampling of sediments in the southern and southwestern Pacific Ocean (e.g., Shipboard Scientific Party, 1986, 1987; Graham et al., 1997), shipboard sedimentologists used only those methods listed in Mazzullo et al. (1988) that address pelagic sediments (i.e., sediments containing >60% particles finer than 63 μm). Consequently, lithologic names used during this expedition are based on (1) composition and (2) degree of consolidation of recovered sediments (Fig. F2).

Principal lithologic names used during Expedition 329 include clay, ooze, porcellanite, and chert. Although the principal name “clay” is not directly associated with pelagic sediments in Mazzullo et al.’s (1988) work, sedimentologists aboard the *JOIDES Resolution* use the term frequently to describe fine-grained sediments deposited in open-marine deposi-

tional environments. Our use of the term denotes the presence of clay-sized particles (i.e., <2 μm) and not specific clay-group minerals (e.g., illite, montmorillonite, or polygorskite). When calcareous or siliceous components (e.g., coccoliths or radiolarians) are dominant in sediment cores and the material is poorly consolidated, the term “ooze” was assigned to the sediment. “Porcellanite” describes fine-grained, well-indurated sediment with dull luster and bulk densities that are between clays/oozes and chert. “Chert” is used to describe compact, glassy, indurated siliceous sediments.

Principal names were modified by terms that describe compositional, textural, and structural attributes of the sediment. When sedimentary units contain a mixture of constituents, the principal name is preceded by major modifiers (in order of increasing abundance) that refer to components that make up >25% of the sediment. Examples of principal names found in the South Pacific Gyre that are modified by their compositional constituency include metalliferous pelagic clay (Shipboard Scientific Party, 1987) and siliceous microfossil ooze (Graham et al., 1997). Minor components that represent between 10% and 25% of the sediment follow the principal name in order of increasing abundance. Sedimentologists aboard Deep Sea Drilling Project (DSDP) Leg 91 demonstrated this method of adapting Mazzullo et al.’s (1988) naming schema to southwestern Pacific sediments. Their detailed sediment descriptions contain modifiers such as metalliferous clay with chert and metalliferous pelagic clay with zeolites (Shipboard Scientific Party, 1987).

Consolidation was used to further refine principal names. Oozes exist on a continuum that includes “-ites.” For example, sediments dominated by radiolarians and easily deformed by the application of light pressure are called radiolarian oozes, whereas those that are hard and compact are called radiolarites. The suffix “-stone” is used similarly and is applied to clays and silts. The names porcellanite and chert carry with them connotations that the sediment is well indurated.

Lithology, structures, and coring disturbances were recorded on standard graphic reports using a common set of symbols. A summary of the symbols and their definitions is provided in Figure F3.

Smear slide analysis

From successive sedimentary intervals with distinct color and textural characteristics, toothpick samples were taken and used to create smear slides according to the method outlined in Mazzullo et al. (1988). Individual slides were fixed by ultraviolet curing using Norland optical adhesive immersion medium. Tables

summarizing data from smear slides are available (see smear slides for each site in “[Core descriptions](#)”). These tables include information about the sample location, whether the sample represents a dominant (D) or a minor (M) lithology in the core, and the visually estimated percentage ranges of all identified components. Compositional elements noted under microscopic inspection of the slides include detrital particles (i.e., clay, feldspar, quartz, lithic fragments, and vitric particles), biogenic particles (i.e., radiolarians, ichthyoliths, discoasters, foraminifers, and coccolithophorids), and authigenic or indeterminate particles (i.e., red-brown to yellow-brown semiopaque material and metalliferous micronodules). In accord with the objectives of Expedition 329, smear slides were examined closely for zeolites and Fe-Mn authigenic minerals.

As with the inspections of prepared thin sections, particle size, shape, and sorting were observed in the smear slides and documented accordingly.

Sedimentary thin sections

Thin sections were created on board to study the composition and texture of the $>2\ \mu\text{m}$ particles in the pelagic clays, oozes, and unusual lithologies (e.g., concretions and nodules) encountered. Thin sections were also created when intervals of interest were too well indurated to permit smear slide sampling and analysis. Thin sections generally provide less biased samples of whole rock than smear slides, and they allow for more accurate identification of the minerals present. However, the limitation of selecting samples from sorted samples and indurated sediments like concretions and nodules implies that there was some bias in the types of lithology sampled, including

- Routinely excluding $>60\%$ of the recovered sediments from study under high magnification,
- Sampling concretions in one lithology over unlithified sediments from another, and
- Recovering concreted horizons at the expense of other sediments.

Lithologies were defined according to the main lithologic classification scheme described above (Fig. [F2](#)). Additionally, a thin section sample worksheet was completed before the results were added to the database.

Hard rock visual core descriptions

During the description process, lithologic units and subunits were defined by contacts, chilled margins, variations in occurrence and abundance of primary mineralogy (e.g., phenocryst abundance), color, grain size, and structural or textural variations (e.g.,

Fig. [F1B](#)). Where possible, a geologic indicator was used to define a unit boundary (e.g., volcanic cooling units); however, limited recovery resulted in arbitrary boundaries placed where the unit above and below are different. Subunit classification was used in cases where mineralogy remains similar but frequent changes in texture take place. An example of such subunit classification includes frequent glassy margins within a mineralogically similar length of core. The schemes used for visual description of recovered cores are detailed below.

A VCD was created for each section of recovered core. Symbols used on the VCD are shown in Figure [F4](#). Each form describes the following features

- Depth
- Core length scale
- Piece number
- Core image
- Orientation
- Shipboard samples taken
- Lithologic unit
- Veins
- Structure
- Structure measurement
- Phenocrysts
- Groundmass grain size
- Glass
- Alteration

Pieces orientated vertically are indicated with an upward arrow on the VCD form. All shipboard sampling is noted in terms of location and purpose (Fig. [F1B](#)). Lithologic units and subunits (increasing in number downhole) are defined by a solid and dashed horizontal line, respectively. Subunits are termed A, B, C, and so on. The structural description on the VCD contains symbols which denote the location and type of feature observed (Fig. [F4](#)). The unit summary located on the right includes

- Expedition-Hole-Core
- Unit number
- Rock name
- Summary description
- Pieces
- Contacts
- Color
- Phenocrysts
- Groundmass
- Glass
- Vesicles
- Alteration
- Veins
- Structure
- Physical properties

Igneous petrology

For each unit, the DESClogik program was used to describe groundmass, primary mineralogy, color, vesicles, and igneous contacts. Separate lithologic units within the basaltic core sections were defined by the type and abundance of phenocrysts, as well as the nature of igneous contacts and margins. The most abundant phenocryst type is named last during any written description. For example, olivine is the most abundant mineral in a plagioclase-olivine phyric basalt. Definition limits are defined as follows:

Aphyric = <1% phenocrysts.

Sparsely phyric = 1%–5% phenocrysts.

Moderately phyric = 5%–10% phenocrysts.

Highly phyric = >10% phenocrysts.

Color was determined using a Munsell color chart on a wet cut rock surface. Wetting of the rock was carried out using tap water and a sponge. Wetting was kept to a minimum because of adsorption of water onto clay minerals (particularly saponite and celadonite) that are present throughout the core.

Groundmass is characterized by grain size with the following standard notation:

G = glassy.

cx = cryptocrystalline (<0.1 mm).

µx = microcrystalline (0.1–0.2 mm).

fg = fine grained (>0.2–1 mm).

mg = medium grained (>1–2 mm).

cg = coarse grained (>2 mm).

Vesicles were recorded as nonvesicular (<1%), sparsely vesicular (1%–5%), moderately vesicular (>5%–20%), or highly vesicular (>20%). Vesicle data are graphically recorded on the VCD using the DESClogik core description software on a subunit level of detail. Within each subunit, relatively high zones of vesicularity (e.g., chilled margins) are described verbally within the VCD.

Breccia was described on the basis of clasts and matrix. Clasts were described in terms of size, shape, sorting, composition, and alteration, and the matrix was described in terms of volume, composition, structure, alteration, and cement by volume and composition. Breccia was defined as

- Bh (hydrothermal breccia that contains secondary matrix),
- Bm (magmatic breccia that contains glass, quench textures, and primary matrix minerals [e.g., hyaloclastites and pillow breccia]), or
- Bc (tectonic breccia in which the matrix is composed of the same material as the host rock [e.g., fault-gouge and cataclastite]).

Igneous units in the recovered basalt cores were defined as pillow basalt, basalt flows, or sheet flows

based on the nature of the recovered contacts and margins. Pillow basalt was characterized by the presence of curved margins that are oblique to the vertical axis of the core or by the presence of variolitic texture, curved fractures, or micro- to cryptocrystalline groundmass grain size. Basalt flow chill margins were defined as margins with no structural similarity to pillow margins (e.g., not curved or variolitic), whereas sheet flows were defined by margins that are subhorizontal and increase in grain size toward the center of the flow.

Alteration

Alteration at all sites from which basement was recovered during Expedition 329 was manifested in terms of

- Background alteration, which is pervasive throughout basement;
- Alteration halos;
- Hydrothermal veins;
- Secondary minerals filling vesicles; or
- Hydrothermal breccia and incipient brecciation.

Areas where veining is numerous are described as a vein net, and estimated volumes of mineral contents are given. These alteration types are recorded in separate logs using the DESClogik program and are later combined into an alteration summary on the VCD.

Levels of background alteration, based on rock color and visual calibration by thin section, are defined using the following scale:

Fresh = <2% alteration.

Slight = 2%–10% alteration.

Moderate = >10%–50% alteration.

High = >50%–95% alteration.

Complete = >95%–100% alteration.

Glass was also recorded in terms of total fresh and total altered, and the abundance and composition of infilling by secondary minerals was described. The order of infill for vesicles and veins was used, where possible, to ascertain mineral precipitation order. Halos surrounding veins and vesicles were described in terms of size, color, and most abundant secondary mineral(s) present within the halo. Any visible and obvious overprinting of earlier alteration phases was noted. Alteration patches may be spherical, irregular, or elongate; these represent domains of enhanced alteration and were recorded separately with drawings and annotations.

Veins are described using detailed vein logs in the DESClogik software package. The presence, location, width, crosscutting relationships, shape, composition percent, color, and width are recorded. Veins and halos are also recorded in DESClogik. Structural

measurements of the veins were recorded in the Structures portion of the VCD and in the DESClogik program.

Hard rock thin sections

Thin sections are made because they allow more accurate description than hand specimens for grain/phenocryst size, mineralogy, abundance, and the nature of secondary mineral types and abundances. Therefore, a suite of thin sections for each site was made to calibrate and build upon our hand-specimen observations of igneous and alteration features. A thin section was made from each igneous unit and from intervals with interesting alteration or igneous features. In addition, thin section description permits us to document glomerocryst types, the presence of phenocrysts within inclusions, and the presence of minor phases that are otherwise not detectable in hand specimen (e.g., spinel, primary oxides, and sulfides). In addition, thin section descriptions are used to determine the timing and method of emplacement in terms of vesicle and void fillings, vein composition, and primary mineral replacement. Information regarding crystal size (in millimeters; minimum, maximum, and average), mineral morphology, and texture was recorded for all primary phases. Where replacement of primary phases took place, the abundance, composition, and textural features were recorded. Phenocryst abundance measurements were carried out by a combination of point counting and visual inspection.

Groundmass texture was defined as

- Heterogranular (different crystal sizes),
- Seriate (continuous range in grain size),
- Porphyritic (increasing presence of phenocrysts), or
- Glomeroporphyritic (containing clusters of phenocrysts).

Groundmass may also be defined as

- Holohyaline (100% glass),
- Hypocrystalline (100% crystals),
- Variolitic (fine, radiating fibers of plagioclase or pyroxene),
- Intergranular (olivine and pyroxene grains between plagioclase laths),
- Intersertal (groundmass fills the interstices between unoriented feldspar laths),
- Ophitic (lath-shaped euhedral crystals of plagioclase, grouped radially or in an irregular mesh, with surrounding or interstitial large anhedral crystals of pyroxene), or
- Subophitic.

Glass definitions are

- Fresh glass (amber in transmitted polarized light and isotropic in transmitted cross-polarized light),
- Dark (darkness is caused by abundant crystallites; interstitial volcanic glass of basaltic composition is termed trachylytic),
- Glass with spherulites (spheroid aggregates of acicular crystals form a nucleus), and
- Altered glass (partially or completely altered to clay minerals).

Flow texture definitions are

- Trachytic (subparallel arrangement of plagioclase laths in the groundmass),
- Pilotaxitic (aligned plagioclase microlites embedded in a matrix of granular and usually smaller clinopyroxene grains), and
- Hyalopilitic (aligned plagioclase microlites with a glassy matrix).

Plagioclase habits (as adopted from Shipboard Scientific Party, 2003b) are

- Cryptocrystalline aggregates of fibrous crystals,
- Comb-shaped or sheaflike plumose crystals,
- Granular–acicular subhedral to anhedral crystals, and
- Prismatic to stubby euhedral to subhedral crystals.

In order to maintain consistency, the same terminology is used for both macroscopic and microscopic descriptions. An example of a thin section description is provided in Figure **F1B**. Digital photomicrographs of each section, together with a whole-section photograph, complement the descriptions. All thin section observations were recorded into DESClogik and are available in “**Core descriptions**” and the IODP database.

Structural geology

Structural features were observed and recorded for the basement cores at all three sites from which basement was recovered. To maintain consistency with legacy DSDP/ODP/IODP sites during Expedition 329, we used conventions that were adopted by previous Shipboard Scientific Parties (e.g., Shipboard Scientific Party, 1989, 1992, 1993a, 1993b, 1995, 2003a, 2003b). The working and archive halves were described, with all structures and orientation measurements made on the archive half. Structural features in basement cores recovered during Expedition 329 were summarized on the VCD. Important structural features or structurally complex zones were recorded on a separate structural description form. All structural data were entered into the DESClogik program. Structural features were defined according to brittle deformation parameters. These include joints, shear

veins, faults, and breccia, which were determined according to the presence of fractures, filling phases, and evidence of shear displacement. Terminology is consistent with that of previous ODP/IODP legs and expeditions, such as ODP Leg 118 and IODP Expeditions 309 and 327 (Shipboard Science Party, 1989; Teagle, Alt, Umino, Miyashita, Banerjee, Wilson, and the Expedition 309/312 Scientists, 2006; Fisher, Tsuji, Petronotis, and the Expedition 327 Scientists, 2011). This terminology also follows that of Ramsay and Huber (1987), Twiss and Moores (1992), Davis (1984), and Passchier and Trouw (1996). Brittle deformation features recorded include the following:

- f = fracture (brittle failure \pm displacement).
- J = joint (fracture with no shear displacement).
- V = vein (fracture filled with secondary minerals).
- Sv = shear vein (shear-displaced fracture filled with secondary minerals).
- F = fault (fracture with shear displacement).
- mF = microfault (fault with <1 mm of deformation).
- B = breccia (divided into Bm, Bh, and Bc as described in “[Igneous petrology](#)”).

No plastic-brittle structures were identified during Expedition 329; therefore, we do not include these features in these notes. The term “vein” is used for all fractures that have secondary mineral fill regardless of their width (note that Ramsay and Huber [1987] define veins as having >1 mm fill). Structural features that do not conform to the categories outlined above are detailed with comments and drawings.

Structural features were recorded in centimeters from the top of each section. Depth of the structure was recorded as distance from the top of the section to the top and bottom of the feature. Structures are measured according to the IODP core reference frame as used in ODP Leg 206 and Expeditions 309 and 327 (Shipboard Scientific Party, 2003b; Teagle, Alt, Umino, Miyashita, Banerjee, Wilson, and the Expedition 309/312 Scientists, 2006; Fisher, Tsuji, Petronotis, and the Expedition 327 Scientists, 2011). The plane normal to the borehole axis is given as the horizontal plane. A 360° net with a pseudosouth (180°) pointing into the archive half and a pseudo-north (0°) pointing out of the archive half and perpendicular to the cut surface of the core is used on this plane. The cut surface of the core, or cut face, is therefore a vertical plane striking 90° – 270° . The dip direction of planar features measured across the cut face was measured with 0° down the vertical axis of the core, and the dip was measured using the right-hand rule (Fig. F5). Measured orientations were rotated to the IODP reference frame using MATLAB.

Drilling disturbance

Deformation and disturbance of sediment that clearly resulted from the coring process were noted and documented. The degree of drilling disturbance is described for soft and firm sediments using the categories listed below (blank regions indicate the absence of drilling disturbance):

- Slightly disturbed: bedding contacts are slightly bent or drilling biscuits are unrotated and in stratigraphic order.
- Moderately disturbed: bedding contacts are extremely bowed or sediment biscuits are rotated but likely still in stratigraphic order.
- Very disturbed: bedding is completely disturbed or sediment biscuits are likely rotated and no longer in stratigraphic order.
- Drilling slurry or flow-in: intervals are water saturated or have otherwise lost all aspects of original bedding resulting from flow-in or the presence of drilling slurry.

The degree of fracturing in indurated sediments is categorized as follows:

- Slightly fractured: core pieces are in place and contain little drilling slurry or breccia.
- Moderately fragmented: core pieces are in place or partly displaced, but the original orientation is preserved or recognizable (drilling slurry may surround fragments).
- Highly fragmented: pieces are from the cored interval and probably in the correct stratigraphic sequence (although they may not represent the entire section), but the original orientation is completely lost.
- Drilling breccia: core pieces are no longer in their original orientation or stratigraphic position and may have mixed with drilling slurry.

Data capture software

DESClogik data capture

Information from macroscopic description of each core was recorded using IODP’s DESCinfo hierarchical database and DESClogik, a software application for capturing data derived from shipboard laboratories and downhole logging operations (Expedition 320T Scientists, 2009). Geological core descriptions and interpretive information were entered into DESClogik through the customized spreadsheet application, Tabular Data Capture. Prior to core description, shipboard sedimentologists and igneous petrologists populated the Tabular Data Capture tabs and columns with terms that represent a range of sedimentary and igneous characteristics as well as drilling-related features that they expected to encounter in recovered cores. During core descriptions,

scientists accessed this information through computer workstations suspended over the split core display tables and entered results into DESClogik accordingly.

Standard graphic report

The LIMS2Excel application was used to extract data in a format that could be used to plot descriptive as well as instrumental data in core graphic summaries using a commercial program (Strater, Golden Software). The Strater program was then used to produce a simplified, annotated, publication-quality VCD for each core.

Beginning with the leftmost column, each VCD displays the depth scale (meters below seafloor), core length, and section information. A fourth column displays the concatenated section half images adjacent to a graphic lithology column in which core lithologies are represented by the graphic patterns illustrated in Figure F3. Subsequent columns provide information on drilling disturbance, sedimentary structures, lithologic accessories, ichnofabric, and shipboard samples. Additional columns present age data (if possible); plots of core logging data such as magnetic susceptibility, natural gamma radiation (NGR), and color measurements (see “[Physical properties](#)”); and color determined using the Munsell soil color chart.

X-ray diffraction

XRD was used to (1) check the observations of the smear slide analysis and (2) identify small-scale compositional changes, potential authigenic minerals, principal mineral types in basalts, and the material filling fractures and vesicles in the basalt. For sediment and poorly consolidated samples, each sample was freeze-dried, ground, and mounted with a random orientation in an aluminum sample holder. For igneous samples, fragments and/or scrapings were crushed to successively finer particle sizes using shipboard crushers, mortars and pestles, and mills. For XRD measurements, a Bruker D4 Endeavor XRD with a $\text{CuK}\alpha$ source (40 kV and 35 mA) and Ni filter was used. The shipboard instrument also features a Vantec-1 detector. Peak intensities were converted to values appropriate for a fixed slit width. The goniometry scan was performed from 2° to $40^\circ 2\theta$ at a scan rate of $1.2^\circ/\text{min}$ (step = 0.01° ; count time = 0.5 s). Common minerals were identified based on their peak position and relative intensities in the diffractogram using an interactive software package (Bruker AXS Diffrac.EVA, version 1.2).

Inductively coupled plasma–atomic emission spectrometry

During Expedition 329, a representative suite of rock samples was analyzed for major and trace elements using ICP-AES. Targets of study included distinct basaltic units as well as alteration zones in basalt. The analyses focused on assessment of major (i.e., Al, Ca, Fe, K, Mg, Mn, Na, P, Si, and Ti) and trace (i.e., Ba, Cr, Ni, Sc, Sr, V, Y, and Zr) elements.

Sample preparation

Samples were taken at each site where basement was rotary cored (Sites U1365, U1367, and U1368) to determine primary igneous chemistry and alteration characteristics, with preference to alteration phases. These samples ($\sim 8 \text{ cm}^3$) were cut using a diamond saw blade and ground on a diamond-impregnated disk to remove contamination from cutting and drilling. The samples were placed individually into beakers containing trace metal–grade methanol and ultrasonically washed for 15 min. The methanol was decanted and the samples were washed twice in 18.2 M Ω deionized water in an ultrasonic bath for 10 min. The clean pieces were dried for 10–12 h at 110°C .

The clean, dry whole-rock samples were crushed to $<1 \text{ cm}$ chips between two disks of Delrin plastic in a hydraulic press. The chips were ground to a fine powder using tungsten carbide in a SPEX 8510 shatterbox. Once this powder was formed, the powder was prepared for ICP-AES. One gram of the resulting powder was ignited at 1025°C for 4 h. A $100 \pm 0.5 \text{ mg}$ aliquot of ignited residue was mixed with $400 \pm 0.5 \text{ mg}$ of lithium metaborate (LiBO_2) flux. The combined sample powder and flux were then fused in Pt–Au crucibles at 1050°C for 5 min in a Bead Sampler NT-2100. After cooling, the resulting glass bead was dissolved in 50 mL of 2.3 M nitric acid and shaken for 1 h. The resulting solution was filtered through $0.45 \mu\text{m}$ glass filters. A 2.5 mL subsample of this solution was isolated and diluted with 17.5 mL of 2.3 M HNO_3 . Thus, the volume of solution used for analysis was 20 mL and the original rock sample was diluted by a factor of 4000.

Analyses and data correction

Concentrations of major and trace elements were determined using a Teledyne Leeman Labs Prodigy ICP-AES instrument. To facilitate steady operation, the plasma was operated for 30 min prior to analyses and a peak profile alignment was performed. During the initial setup, standard BAS-140 was used to select an emission profile for each peak to determine peak-

to-background intensities and set the locations of background levels for each element. The Prodigy software uses these background locations to calculate the net intensity for each emission line. Photomultiplier voltage was optimized by automatically adjusting the gain for each element using the BAS-140 standard. ICP-AES results presented in the site chapters of this volume were attained by integrating the area under the curves for wavelength versus response plots.

Each sample was analyzed three times from the same dilute solution (i.e., in triplicate) within a given sample run. For elements measured at two wavelengths, we either used the wavelength giving the better calibration line in a given run or, if the calibration lines for both wavelengths were of similar quality, we used the data for both and reported the average concentration. A typical ICP-AES run (Table T2) included eight certified rock standards that were analyzed at the beginning of each run and again after every 20 samples. As many as 15 unknown samples were analyzed in triplicate. A 10% HNO₃ wash solution was run for 60 s before and after each analysis. A drift-correcting standard (BHVO-2) was analyzed twice each time the instrument was operated. Blank solutions were analyzed at the beginning and end of each run and at an intermediate point in runs of 12–15 samples. In addition, two “check” standards were run in triplicate as unknowns. Each standard was analyzed in triplicate at least twice during a run.

Following each sample run, the measured raw intensity values were corrected for instrument drift and procedural blank. Drift correction was applied to each element by linear interpolation between the drift-monitoring solutions run every fifth analysis. Following drift correction and blank subtraction, a calibration line for each element was calculated using the results for the certified rock standards. Element concentrations in the samples were then calculated from the relevant calibration lines. Estimates of accuracy and precision for major and trace element analyses were based on replicate analyses of international standards, the results of which are present in Table T3. Internal precision, from which error bars are derived, is reported from an unknown (Sample 329-U1367F-2R-3, 60–63 cm) that was run in triplicate (Table T4).

Digital color imaging

The SHIL captures continuous high-resolution images of section-half surfaces for analysis, description, and reporting of recovered core material. The system was custom built for the *JOIDES Resolution* by IODP-USIO. Adhering to the basic principles of professional photography, the SHIL creates highly detailed

images by orchestrating the proper combination of good lighting, high-quality camera and lens, and appropriately positioned camera and object relative to each other. Six light-emitting diodes containing 12 separate emitters are arranged in two fanlike banks to create lighting for the SHIL. This configuration forms a homogeneous light beam at distances >75 mm from the face of the lens. At the desired target distance of 100 mm, the optimal width of illumination is 6 mm. The SHIL image capture system consists of a commercial line-scan camera fitted with a Nikon 60 mm f/2.8 microlens. The camera lens is mounted perpendicular to the section half on a firm, smooth traveling track that is motion controlled through an integrated computer interface. When held still, producing the SHIL's maximum resolution, as much as to 20 μm of a section half can be resolved. In operation, scanning a section half at 10.5 cm/s produces an image with a resolution of 100 μm per scan line. The integrated software that operates the SHIL also promotes straightforward capture and editing of images, as well as saving and transfer of section-half images to the shipboard database.

Paleontology and biostratigraphy

The primary scientific objectives of Expedition 329 demanded a higher number of shipboard geochemists and microbiologists and a lower number of core describers (and no paleontologists) than a usual IODP expedition. Therefore, only very preliminary biostratigraphic and paleontological determinations at selected sites were carried out on board. We primarily examined planktonic and benthic foraminifers, ostracods, and, to a lesser extent, ichthyoliths (fish teeth) and radiolarians. Preliminary biostratigraphic determinations were based on fish teeth and radiolarians at Site U1365, where the dominant lithology is zeolitic metalliferous clay, and on planktonic foraminifers at Sites U1367, U1368, and U1370, where carbonate ooze was recovered. More detailed postexpedition examination will be necessary to better characterize microfossil assemblages and refine biostratigraphic assignments.

Sediment sample processing

The major biogenic components found in the sediments of the Expedition 329 sites were assessed by analyzing smear slide (see “**Lithostratigraphy, igneous petrology, alteration, and structural geology**”) and sieved core catcher samples. Core catcher samples were processed following routine methods for the study of foraminifers. Core catcher samples were dried and weighed. Dry sediment was washed with

tap/distilled water over a 63 or 38 μm wire-mesh sieve. Indurated samples were soaked in water for a short time prior to washing to promote disaggregation. Once sieved, all samples were dried on filter papers in a low-temperature oven at $\sim 50^\circ\text{C}$ and weighed and subsequently examined under a binocular light microscope. To minimize contamination of foraminifers between samples, the sieve was placed into a sonicator for several minutes and thoroughly checked between samples to enable identification of contaminants from previous samples. Planktonic foraminifer species distributions are presented for Sites U1367, U1368, and U1370. Species identification for planktonic foraminifers were generally made on the >250 , >125 , and >63 μm size fractions, with the exception of Site U1370, from which the >38 μm size fraction was also scanned for distinctive taxa. Benthic foraminifer assemblage compositions were based on counts of ~ 200 specimens from the >250 , >125 , and >63 μm size fractions, when possible. In the case of ostracods, all specimens per sample were picked and counted. Relative percentages of benthic to planktonic tests were determined by counting specimens in four adjacent quadrants in three different locations on the picking tray. Relative and absolute abundances were based on the overall counting of all the specimens found in each sample analyzed. The preservation, abundance, and zonal assignment for selected samples and for each microfossil group described were entered through DESClogik into the LIMS database. Paleontological and biostratigraphic analyses focused on the stratigraphy-dedicated hole, usually Hole B, at each site (see “[Introduction, operations, and curation](#)”).

Foraminifers

Planktonic foraminifer zonal scheme and taxonomy

The planktonic foraminifer zonal scheme for the Paleocene (P zones) follows Olsson et al. (1999). The Eocene and Oligocene (E and O zones, respectively) scheme follows Berggren and Pearson (2005) and Wade et al. (2010). The Neogene (M, PL, and PT zones) scheme follows Berggren et al. (1995) and Wade et al. (2011). The biostratigraphy is tied to the geomagnetic polarity timescale (GPTS) used for IODP Expedition 320/321, which is based upon a composite of several timescales (Cande and Kent, 1995; Lourens et al., 2004; Pälike et al., 2006b). Ages and calibration sources of planktonic foraminifer datums are presented in Table T5. The age estimates presented are adjusted to the timescale of Expedition 320/321. Planktonic foraminifer taxonomic concepts selectively follow those of Bolli and Saunders (1985), Spe-

zzaferri and Premoli Silva (1991), Chaisson and Leckie (1993), Leckie et al. (1993), Spezzaferri (1994), Chaisson and Pearson (1997), Pearson and Chaisson (1997), Olsson et al. (1999), and Pearson et al. (2006).

Benthic foraminifer taxonomy

Taxonomic assignments follow Tjalsma and Lohmann (1983), Miller and Katz (1987), Thomas (1990), Katz and Miller (1991), Jones (1994), Nomura (1995), and Holbourn and Henderson (2002). The generic classification of Loeblich and Tappan (1988) was used.

Abundance and preservation

Relative percentages of benthic to planktonic tests were determined by counting specimens in four adjacent quadrants in three different locations on the picking tray during Expedition 329. The following abundance categories were estimated from visual examination of the dried sample for planktonic and benthic foraminifers and ostracods:

- D = dominant ($>30\%$ of assemblage).
- A = abundant ($>10\%$ – 30% of assemblage).
- F = few ($>5\%$ to $<10\%$ of assemblage).
- R = rare ($>1\%$ to $<5\%$ of assemblage).
- P = present ($<1\%$ of assemblage).
- B = barren.

The preservation status of planktonic and benthic foraminifers was estimated as follows:

- VG = very good (no evidence of overgrowth, dissolution, or abrasion).
- G = good (little evidence of overgrowth, dissolution, or abrasion).
- M = moderate (calcite overgrowth, dissolution, or abrasion are common but minor).
- P = poor (substantial overgrowth, dissolution, or fragmentation).

Ostracods

Ostracods, calcareous bivalve microcrustaceans, are the only metazoan organisms commonly preserved as microfossils in deep-sea sediments. Similar to benthic foraminifers, ostracods have limited biostratigraphic use, but they can provide important environmental information and are valuable proxies in paleoceanographic studies (Dingle and Lord, 1990; Corrège 1993; Ayress et al., 1997; Didié and Bauch, 2000; Cronin et al., 2002; Alvarez Zarikian et al., 2009). Ostracod taxonomic concepts selectively follow Ayress (1995), Ayress et al. (1995), Boomer and Whatley (1995), Whatley and Boomer (1995), Boomer (1999), Zhao (2005), Alvarez Zarikian (2009), and Yasuhara et al. (2009). Ostracods were

picked and identified from the examined samples following the same methodology as for benthic foraminifers (see above).

Radiolarians

Radiolarian identification was carried out postexpedition by C. Hollis (GNS Science, New Zealand). Radiolarian taxonomic assignments follow Sanfilippo and Riedel (1985). Age assignments are based on Hollis and Kimura (2001).

Paleomagnetism

Samples, instruments, and measurements

Paleomagnetic investigations during Expedition 329 focused mainly on measuring the natural remanent magnetization (NRM) of archive-half sections before and after alternating-field (AF) demagnetization. We also collected one discrete sample per section from working-half sections for use in AF experiments. Discrete samples were taken from the first APC hole (because the cores from other holes were heavily sampled for microbiological and geochemical whole-round samples, precluding sequential discrete samples for paleomagnetic study) at every site and from the basaltic cores at sites where basement was recovered. We collected discrete sediment samples by inserting a hollow subcorer into the middle of split-core sections and then extruding the sediment into plastic cubes (2 cm × 2 cm × 2 cm, with an internal volume of 7 cm³) (Fig. F6) as described in Richter et al. (2007). For discrete basalt samples, we prepared cubic samples of the same size with a rock saw.

All remanence measurements were made using a 2G Enterprises Model-760R superconducting rock magnetometer (SRM) equipped with direct-current superconducting quantum interference devices (SQUIDs) and an in-line, automated AF demagnetizer capable of reaching a peak field of 80 mT. The coordinate system for the SRM is shown in Figure F7.

The SRM and other instruments in the Paleomagnetism Laboratory used during Expedition 329 are listed in Table T6. In the table, we also give quality assessment information (i.e., sensitivity, accuracy, and precision) of the instruments determined by experimentation or based on past experience and information provided by the vendors. For example, the noise level of the SRM is $<1 \times 10^{-10}$ Am², based on tests conducted at the beginning of Expedition 329. For split-core samples, in which the volume of material measured is ~100 cm³, this permits samples with intensities as low as $\sim 1 \times 10^{-5}$ A/m to be measured.

NRM was usually measured every 2.5 or 5 cm interval along the split-core sections. The measurement was also conducted over a 5 cm long interval before

each core section entered the SQUID sensors, as well as after each core section had passed through the sensors. These are referred to as the header and trailer measurements; they serve the dual function of monitoring the background magnetic moment and allowing for future deconvolution analysis. Typically, we measured NRM after 0 and 20 mT AF demagnetization, with an additional step at 10 mT when time and core flow allowed. Because core flow (the analysis of one core after the other) through the laboratory dictated the available time for measurements, 2 or 3 h per core, we did not always have time for the optimal number of demagnetization steps. During Expedition 329, we were able to measure at 10 mT demagnetization and occasionally at 5 and 15 mT steps. These additional demagnetization steps did not prove to be as beneficial as using the extra time to measure the core sections at higher resolution following 20 mT demagnetization, so we opted to cease the additional demagnetization steps and increase the resolution when time permitted. Measurements at 2.5 cm spacing became standard during the expedition. We did not measure sections that were entirely visibly disturbed. Similarly, in analyzing the data, we culled measurements within 7.5 cm of section ends and within intervals with drilling-related core disturbance, such as the top few to tens of centimeters of most cores.

AF demagnetization of discrete samples was conducted at peak fields of 0, 10, and 20 mT, the same as the demagnetization sequence applied to half-core sections, in order to check whether radial-inward drilling-induced magnetizations that have occasionally been reported from previous ODP/IODP expeditions are present.

A suite of discrete samples distributed evenly down-hole (typically one sample from each core) was subjected to progressive AF demagnetization and measured at 10 mT steps to peak fields of 20 mT, with basalt samples demagnetized up to 60 mT. This was done to determine whether a characteristic remanent magnetization could be resolved and, if so, what level of demagnetization was required to resolve it.

Low-field magnetic susceptibility was measured on all whole-core sections using the WRMSL (see “[Physical properties](#)”). The susceptibility meter was a Bartington loop meter (model MS2 with an MS2C sensor, coil diameter of 88 mm, and operating frequency of 0.621 kHz. The susceptibility meter has a nominal resolution of 2×10^{-6} SI (Blum, 1997). The “units” option for the meter was set on SI units, and the values were stored in the database in raw meter units. To convert to true SI volume susceptibilities, these should be multiplied by 0.68×10^{-5} .

Coring and core orientation

Cores were collected using nonmagnetic core barrels, except at depths where hard chert or porcellanite layers were expected. In addition, the bottom-hole assembly included a Monel (nonmagnetic) drill collar, which was deployed when the Flexit core orientation tool was employed. The Flexit tool uses three orthogonally mounted fluxgate magnetometers to record the orientation of the double lines scribed on the core liner with respect to magnetic north. The tool also has three orthogonally mounted accelerometers to monitor the movement of the drill assembly and help determine when the most stable and thus useful core orientation data were gathered. The tool declination, inclination, total magnetic field, and temperature are recorded internally at a regular interval until the tool's memory capacity is filled (Fig. F8).

Magnetostratigraphy

Drill sites were located between $\sim 24^\circ$ and 46°S ; typical magnetic polarity zones could be identified by distinct changes in inclination of remanence. The present-day normal field in this region, as expected by the geomagnetic axial dipole model, has a negative inclination (about -41° to -64°), so positive remanence inclinations indicate a reversed field. Magnetostratigraphies for each site were constructed by correlating obtained magnetic polarity sequences with the GPTS. Biostratigraphic age constraints significantly limit the range of possible correlations with the GPTS.

The GPTS used during Expedition 329 is based on a composite of several timescales (Table T7) (Cande and Kent, 1995; Lourens et al., 2004; Pälike et al., 2006a). Its construction follows the procedure described by Backman et al. (2008) and is excerpted here.

Global Cenozoic timescales are still under development. Orbitally tuned cyclostratigraphic data are the chronological backbone of the most recent Neogene timescale, including the Quaternary (Lourens et al., 2004). Their synthesis is considered to fairly well reflect the true progress of Neogene time. The Paleogene timescale, on the other hand, is less well defined because of the lack of a continuous Milankovitch-based Paleogene cyclostratigraphy, and it will therefore continue to develop and change over some years to come. The GPTS used during Expedition 329 was the same as that used during Expedition 320/321 and was constructed as follows:

- Interval 0.00–23.030 Ma: the Lourens et al. (2004) Neogene timescale was used, which places the Paleogene/Neogene boundary at 23.030 Ma, on

the basis of an astronomically derived age for the base of Chron C6n.2n (Shackleton et al., 2000), updated to the new astronomical solution of Laskar et al. (2004) by Pälike et al. (2006b). Pälike et al. (2006a) estimated an age of 23.026 Ma for this reversal boundary (i.e., 4 k.y. younger than the Lourens et al. [2004] estimate).

- Interval 23.278–41.510 Ma: the Pälike et al. (2006a) timescale was used from the top of Chron C6Cn.3n at 23.278 Ma to the base of Chron C19n at 41.510 Ma, implying that the 248 k.y. long Chron C6Cn.2r is artificially shortened by 4 k.y. (1.6%) when shifting from the Miocene to the Oligocene timescale.
- Interval 41.510–83.000 Ma: the Cande and Kent (1995) timescale was used from the top of Chron 20n to the top of Chron C34n, implying that the 1.026 m.y. long Chron C19r is artificially lengthened by 11 k.y. (1.1%) when shifting from the Pälike et al. (2006a) timescale to Cande and Kent's (1995) timescale.

The impact of these two artificial timescale jumps (4 k.y. with the Pälike et al. [2006a] timescale and 11 k.y. with the Cande and Kent's [1995] timescale) on the data and discussions presented here is negligible.

Biogeochemistry

Documentation of microbial processes in South Pacific Gyre sediment requires a wide range of biogeochemical analyses. Transport-reaction modeling of dissolved metabolite concentrations will allow us to quantify rates of principal net activities in the sediment (e.g., reductions of O_2 , NO_3^- , SO_4^{2-} , Mn[IV] , and Fe[III]) (Jørgensen, 2006). Chemical data (e.g., the position of the chloride maximum from the Last Glacial Maximum) and thermal data will be used to help model this transport (D'Hondt et al., 2004). Concentration data will also allow us to calculate mineral stabilities and, in anoxic sediment, to test thermodynamic models of metabolic competition (Hoehler et al., 2000; Wang et al., 2010).

The shipboard geochemistry program during Expedition 329 consisted of an ambitious campaign to characterize the geochemical environment of the seafloor of the South Pacific Gyre. We undertook key biogeochemical analyses on the ship and collected appropriate samples for critical postcruise biogeochemical studies. As described below, components targeted by shipboard analyses included headspace gases, dissolved oxygen, various species of the fixed nitrogen (nitrate, nitrite, and ammonium) and carbonate systems, chloride and sulfate, phos-

phate, dissolved silica, and a number of dissolved cations. Analyses of the organic and inorganic carbon contents, as well as of the total nitrogen contents, of the sediments were also conducted. Analytical protocols are summarized below. In many cases, these protocols are based on those of Gieskes et al. (1991), Murray et al. (2000), and the IODP user manuals for new shipboard instrumentation, with modifications as indicated. However, as described in the following subsections, in many cases the instrumentation and protocols used during Expedition 329 supersede those cited above.

Interstitial water extractions

Sedimentary interstitial waters were collected by squeezing whole-core rounds using Manheim squeezers and by sampling using Rhizon soil moisture samplers (Rhizosphere Research Products, Wageningen, The Netherlands; Gribsholt and Kristensen, 2002). Rhizon samples were taken for nitrate, nitrite, ammonium, and nitrate isotope analyses, while squeezed interstitial water samples were used for all other analyses. At Sites U1370 and U1371, interstitial waters gathered by Rhizon samplers were also acquired for shore-based metals analysis (e.g., Fe and Mn).

Rhizon sampling extracts interstitial water from sediment by suction filtering into 10 mL plastic syringes through thin tubes of hydrophilic porous polymer that has a mean pore diameter of 0.1 μm . At Sites U1365–U1367, as described further below, and prior to the squeezing of each whole-round core sample, Rhizon samplers (5 cm long filter) were inserted into one end of the whole-round core and a total volume of 2 to 11 mL of interstitial water was extracted (Fig. F9). Core sections were stored cold (9°C) during Rhizon sampling. At Sites U1368–U1371, Rhizon samples were collected from a core interval adjacent to the interstitial water sampling interval. Before deployment, new and previously used Rhizon samplers were soaked in 18.2 M Ω deionized water for several hours, followed by rinsing with 30 mL of 18.2 M Ω water that was suction-filtered through each Rhizon. After washing, Rhizon samplers were left to dry on filter paper. Care was taken to only use completely dry Rhizon samplers. Blanks consisting of 18.2 M Ω water pulled through new and recycled Rhizon samplers analyzed for nitrate onboard, as described below, were all below detection limit.

Interstitial water squeezing forces the water out of the sediment by using a titanium squeezer, modified after the stainless steel squeezer of Manheim and Sayles (1974). Gauge pressures of as much as 20,000 lb force were applied to the squeezer using a Carver laboratory hydraulic press to extract the interstitial

water. The interstitial water is passed through a pre-washed (with 18.2 M Ω water) Whatman number 1 filter fitted above a titanium screen within the squeezer and filtered through a 0.45 μm polysulfone disposable filter (Whatman Puradisc PES) fitted to the syringe that gathers the fluid sample.

Sample handling and short term storage

During this expedition, 415 whole rounds were squeezed for interstitial water analyses and 468 samples were taken by Rhizon sampling for nitrate analyses, as collectively described elsewhere in this volume. Whole rounds for microbiological studies were also often cut from the same core section. Consideration of different interstitial water extraction methods and coordination with microsensor oxygen measurements and microbiological sampling required us to develop an overall strategy to maximize sample throughput and yet preserve the integrity of the samples and analyses.

During Expedition 329, the majority of the interstitial water samples were handled in the following way. First, the cores were cut into 1.5 m (nominal) sections on the catwalk. Second, these sections were delivered to the Hold Deck refrigerator (core storage hold) where they were cut into whole rounds for interstitial water and microbiological analyses, curated, and labeled. Third, a Rhizon sampler was immediately inserted into each interstitial water whole round in the Hold Deck refrigerator (Fig. F9) and 2–11 mL of water was extracted into the Rhizon syringe. This Rhizon-extracted water was used for nitrate analysis on board, and aliquots were preserved for shore-based research. Fourth, when the Rhizon sampling was completed, which took as long as 0.1–12 h, the interstitial water whole rounds were delivered to the Biogeochemistry Laboratory. Samples were stored in a 4°C refrigerator in the Biogeochemistry Laboratory until they could be squeezed. The time samples were stored in the Biogeochemistry Laboratory varied from a few minutes to as long as >24 h in some cases, even with the use of six Manheim squeezers and three Carver presses.

At Site U1365, all samples were processed as described above. At Site U1366, some whole rounds were cut in the Hold Deck refrigerator but were not sampled using Rhizon samplers. Instead, those whole rounds were immediately delivered to the Biogeochemistry Laboratory for squeezing. The main goal for these samples was to extract interstitial water for shore-based ^{14}C research, but we also analyzed some of these waters on board for dissolved species (e.g., alkalinity, dissolved inorganic carbon [DIC], Ca, Mg, and Sr). These are referred to as the “whole round stored shorter” (WSS) samples. Starting at Site

U1367 and continuing for the rest of the expedition, a small subset of the interstitial water samples was cut on the catwalk and immediately delivered to the Biogeochemistry Laboratory for interstitial water extraction by squeezing. These are termed “catwalk” samples throughout this report. Interstitial water was not extracted from these with Rhizon samplers. Slight contrasts between the WSS samples at Site U1366, the catwalk samples at Site U1367 and afterward, and the interstitial waters extracted from whole rounds processed in the Hold Deck refrigerator are described in the individual site chapters in this volume.

Because the time that a core arrives on the rig floor is recorded by the drilling crew and because we kept time records of where each whole round was in the sample and handling process, we are able to reconstruct the amount of time it took a whole round to arrive in the Hold Deck refrigerator, the duration of Rhizon sampling, when the whole round was delivered to the Biogeochemistry Laboratory, its storage time in the laboratory refrigerator at 4°C, and the duration of the squeeze. We plotted these various storage and handling times as a function of depth for each site because the cores arrive on the rig floor and thus start in depth order and because the chemical profiles are plotted against depth. These graphs are shown in Figure F10 for all Expedition 329 sites. Graphs are also shown that document how long it took each Rhizon sample to be extracted for Sites U1369, U1370, and U1371 (Fig. F11).

Documenting of the time of day in each step of the sample storage and handling process demonstrates that there were no effects of storage on the nitrate profile or that of many other species. Dissolved species of the carbonate system showed effects in certain situations. These graphs also facilitate discussion as to whether occasional anomalous data are due to storage, spurious instrumental effects, or other factors. These effects, particularly for the carbonate system, will be further quantified by postexpedition thermodynamic calculations.

Headspace hydrocarbon gases

Routine analysis of hydrocarbon gas in sediment cores is part of the standard IODP shipboard monitoring of the cores to ensure that the sediments being drilled do not contain unsafe levels of hydrocarbons. The most common method of hydrocarbon monitoring used during IODP expeditions is analysis of gas samples obtained from either core samples (headspace analysis) or from gas expansion pockets visible through the clear plastic core liners (Vacutainer analysis). Because no gas expansion pockets were formed during Expedition 329, Vacutainer

analysis samples were not taken during the expedition.

Concentrations of hydrocarbon gases were monitored at intervals of 1 sample per core. For the required safety analysis (Kvenvolden and McDonald, 1986), a 3 cm³ bulk sediment sample from a freshly exposed end of a core section was collected immediately after retrieval on deck using an open-ended plastic syringe, extruded into a 20 mL headspace glass vial, immediately capped with a gray butyl rubber septum, and sealed with an aluminum crimp cap. When consolidated or lithified samples were encountered, chips of material were placed in the vial and sealed. The vial was then heated to 70°C for ~30 min prior to analysis.

The standard gas analysis program for safety and pollution prevention purposes was complemented by additional headspace analyses (1 per section) following a slightly different approach (Iversen and Jørgensen, 1985; Hoehler et al., 2000; Shipboard Scientific Party, 2003c; Ertefai et al., 2010) with the intent to better constrain the concentrations of adsorbed and dissolved gases. Compared to the rapid safety-oriented protocol, the latter, more time-consuming alternative is more quantitative and may yield more methane.

For samples designated for the refined headspace analysis, a 5 cm³ sediment sample was collected from a freshly exposed end of a core section using an open-ended plastic syringe. The sediment sample was collected by penetrating the sediment surface while the plunger was maintained at the sediment surface to prevent contamination from atmospheric gases or trapped air bubbles. After sampling, the syringe was extruded until 3 cm³ of sample remained and the excess was shaved off with a flat spatula flush with the end of the syringe barrel to provide an accurate estimate of the sediment volume within the syringe. The remaining 3 cm³ sediment sample in the syringe was extruded into a 20 mL vial containing 5 mL of 1N NaOH to inhibit biological activity (Iversen and Jørgensen, 1985). Beginning with Site U1368, an additional 5 mL of 1N NaOH was used to decrease headspace volume and assist in mixing the sediment plug. The vial was immediately capped with a gray butyl rubber septum and an aluminum crimp cap. After vigorous manual shaking for ~2 min, the vials were occasionally shaken to completely disperse sediment into the NaOH solution. Samples were subsequently left to stand for at least 24 h at room temperature prior to gas chromatographic analysis.

Gas chromatographic analyses of headspace samples for both safety and refined protocols were performed

identically. A 5 mL volume of headspace gas was extracted from the sealed sample vial using a standard gas syringe and directly injected into the gas chromatograph. The headspace gas samples were analyzed using an Agilent/HP 6890 Series II gas chromatograph (GC3) equipped with a 2.4 m × 3.2 mm stainless steel column packed with 100/120 mesh HayeSep R and a flame ionization detector set at 250°C. The gas chromatograph oven temperature was programmed to hold for 0.5 min at 80°C, ramp at 30°C/min to 100°C, ramp at 15°C/min to 110°C, and remain at 110°C for 4.5 min, before ramping at 50°C/min to 150°C with a final holding time of 1.8 min. Helium was used as the carrier gas. The GC3 system determines concentrations of methane (C₁), ethane (C₂), ethene (C₂₌), propane (C₃), and propylene (C₃₌).

Data were collected using the Hewlett Packard 3365 Chemstation data processing program. For both systems, chromatographic response is calibrated to nine different gas standards with variable quantities of low molecular weight hydrocarbons, N₂, O₂, CO₂, Ar, and He and checked on a daily basis.

The gas concentrations for the required safety analyses are expressed as component parts per million by volume (ppmv) relative to the analyzed gas. To the extent that sampling procedures are uniform, the differences in the headspace results reflect differences in the amount of gas remaining in the cores. The internal volumes of 15 representative headspace vials were carefully measured before any sites were occupied during Expedition 329 and were determined to average 25.41 ± 0.18 mL. This volume was taken as a constant in calculations of gas concentrations.

The volumetric units were converted to concentration units (millimolar) to facilitate comparisons with dissolved interstitial constituents using the relationship

$$\text{CH}_4 = (\chi_M \times P_{\text{atm}} \times V_H) / (R \times T \times \phi \times V_S), \quad (1)$$

where,

- V_H = volume of the sample vial headspace (cm³),
- V_S = volume of the whole sediment sample (cm³),
- χ_M = molar fraction of methane in the headspace gas (obtained from gas chromatograph analysis),
- P_{atm} = pressure in the vial headspace (obtained from the bridge) (atm),
- R = the universal gas constant (82.057 [L·atm]/[K·mM]),
- T = temperature of the vial headspace (K), and
- ϕ = sediment porosity (determined either from moisture and density measurements on ad-

jacent samples or from porosity estimates derived from gamma ray attenuation [GRA] data representative of the sampled interval).

The precision of analysis for the “B” standard was ≤1% for all gases analyzed with the GC3 and the natural gas analyzer.

Dissolved hydrogen

Dissolved hydrogen was quantified in sediment samples using a reduced gas analyzer (RGA; Trace Analytical, Inc., provided by the University of Rhode Island [USA] Geobiology Laboratory). Subcores were taken with 10 cm³ cut-off syringes either on the catwalk or in the Hold Deck core refrigerator. The 10 cm³ subcores were immediately extruded into 40 mL capacity screw-cap vials and filled with water. Care was taken to exclude any air from the vials before closing. Samples for H₂ analysis were taken next to whole-round cores used for interstitial water analysis.

A headspace was created in the vial by introducing 500 µL of N₂ gas that passed through the RGA (bypass gassiest gas was introduced through the septa using a 500 µL gas-tight syringe with a 27 gauge needle. During the injection, an equivalent amount of water was allowed to escape from the vial through a separate needle.

The samples were stored upside down for 10–20 h to allow the H₂ to partition into the headspace. Just prior sampling, the vials were centrifuged (2 min at 200× g) to move the sediment away from the septa. Afterward, 500 µL of the headspace was extracted using a needle and gas-tight syringe and injected into the RGA. The instrument was fitted with a 250 µL sample loop. The RGA was calibrated using a 102.4 ppmv H₂ gas standard (Scott-Marin, Inc.) using a gas mixer to vary the H₂ concentration.

Dissolved oxygen measurements

Capped and sealed 1.5 m core sections targeted for oxygen analysis were brought into the temperature-controlled room at near in situ temperature (10°C) within 15 min of arriving on deck. A temperature sensor (PT 1000; see optode setup below) was inserted through a hole in the core liner (4 mm) into the core center at the middle and ends (lengthwise) of the sections. Core temperature was between 7° and 12°C when cores arrived in the cold room. Core sections were left until they were at equilibrium with the cold laboratory ambient temperature (9.5°C) throughout the entire 1.5 m core section to ensure that all oxygen measurements were performed under stable temperature conditions. Temperature variation was always <0.5°C within sections and <1°C

within cores. Room temperature was continuously monitored and logged on a DICKSON SP175 temperature data logger and varied between 9° and 11°C during all measuring periods.

Whole-round sections from subsequent holes were brought to the cold laboratory after geochemical and microbiological sampling in the ship's Hold Deck core refrigerator, equilibrated to 9.5°C, and measured. Dissolved oxygen measurements were only done on whole rounds longer than 20 cm and within the lengthwise center in order to avoid edge effects.

Oxygen measurements were conducted with two independent microsensor methods: amperometric Clark-type oxygen sensors (microelectrodes) and fiber-optic oxygen microsensors (optodes). The oxygen microelectrodes (Revsbech, 1989; Unisense, Aarhus, Denmark) are made of glass with a ~5 cm long tip that is inserted and fixed within a hypodermic needle (1.1 mm diameter; 50 mm length). Electrode signals were amplified and transformed to millivolts (mV) by two-channel picoammeters (PA 2000; Unisense; provided by the University of Southern California Marine Biogeochemistry Laboratory) and directly recorded on a computer using the Profix software (Unisense). The needle-type optodes (Fischer et al., 2009; PreSens, Regensburg, Germany) are miniaturized chemical-optical sensors based on a silica fiber (140 µm diameter) with the tip mounted into a needle-type housing for robustness. Once inserted, the optical fiber is pushed out into the sediment for the measurement. Temperature was measured in each optode measuring point by inserting a temperature sensor (PT 1000) directly adjacent to the optode. The optodes and temperature sensor were connected to a MICROX TX3 (PreSens; provided by the University of Rhode Island Geobiology Laboratory) single-channel fiber-optic oxygen meter, and signals were recorded using the OxiView software (TX3, version 6.02).

Both sensor types were calibrated with a two-point calibration (0% and 100% air saturation). Electrodes were calibrated in N₂ (0%) and air-purged (100%) filtered seawater taken at the surface of each site, whereas optodes were calibrated in sodium sulfite (Na₂SO₃)-saturated filtered seawater (0%) and water-saturated air (100%). Both sensor types were calibrated using the PT 1000 temperature sensor. Calibration crosschecks between sensors showed no discrepancies.

Dissolved oxygen concentrations were calculated from percent saturation by using the oxygen solubility at in situ salinity and the temperature measured at each sampling point.

Electrode and optode measurements were conducted by inserting the sensors into the center of the intact sediment section (3 cm deep) through separate 4 mm holes drilled through the core liner. Electrode readings stabilized within 30–60 s, with a standard deviation <0.4%. Readings were logged for 1 min after stabilizing. Optode signals were left to stabilize for 3 min before being logged per second for 1 min. The standard deviation on optode measurements was <0.3%. Optodes frequently had to be replaced because of wear or breakage. When exchanged, duplicate measurements were conducted to confirm calibrations. Optode and temperature measurements were conducted at 10–20 cm intervals near the sediment surface and close to basement or oxygen depletion zones. Throughout the remaining sediment, optode measurements were taken at 2–4 depths per section (30–75 cm intervals), depending on the sediment cover. Optode measurements within each core were measured in a randomized order, except for at Site U1365. All optode measurements are shown for all sites.

Electrode measures were generally performed at 10 cm intervals for the first two sections of cores at 1–3 mbsf and at a similar resolution close to the basalt/sediment interface. At Site U1365, four electrodes that were independently calibrated and connected to separate picoammeters were used simultaneously for the downcore measurements. For the subsequent sites, two independently calibrated electrodes connected to two independent picoammeters were used. Below 3 mbsf, electrode measurements were typically attempted at 20–25 cm intervals, although for some intervals visible disturbance of core sections prevented successful measurements at those intervals. Toward the basaltic basement or near zones of oxygen depletion (when reached), electrode measurements were conducted at 10 cm intervals. For illustrative purposes, the tables and figure for Holes U1365A and U1365B include values from sections that were visibly disturbed before or during the measurement (e.g., by fluid intrusion, sediment mixing, and gas voids) (see “[Biogeochemistry](#)” in the “Site U1365” chapter [Expedition 329 Scientists, 2011]). For the remaining sites, values determined using electrodes were not recorded for intervals where attempted measurements were abandoned because of obvious physical disturbance of the core section.

Redox potential

Redox (Eh) was measured in sediments from Site U1371 using needle redox electrodes. Redox-potential sensors were connected to a portable or tabletop pH/mV meter (WTW-pH340, WTW GmbH, Weil-

heim, Germany; pH-m210 Meter Lab, Radiometer Analytical, Lyon, France; provided by the University of Southern California, Marine Biogeochemistry Laboratory).

pH and alkalinity

Alkalinity and pH in interstitial water were measured immediately after squeezing. The pH was measured with a combination glass electrode, and alkalinity was determined by Gran titration with an autotitrator (Metrohm 809 Titrando; provided by the University of Rhode Island Geobiology Laboratory). Five milliliters of interstitial water was titrated with 0.1 M HCl at 25°C. CRM 104–certified reference material obtained from the laboratory of Professor Andrew Dickson, Marine Physical Laboratory, Scripps Institution of Oceanography (California, USA), was used for calibration of the acid. Standardization was conducted at the beginning and end of a set of samples for each site and after every fifth sample.

Dissolved inorganic carbon

DIC was measured with the OI Analytical Aurora 1030C total organic carbon (TOC) analyzer, consisting of a syringe module, a sample-stripping manifold, and an infrared CO₂ analyzer. Interstitial water samples (1 mL for each injection) were acidified with 0.2 mL of 2 M HCl. The CO₂ released was stripped and flowed through the CO₂ analyzer. The CO₂ Beer-Lambert absorption law was integrated to determine the total CO₂ released from the sample.

The laboratory standard for DIC was Batch 94 (2015.92 ± 0.85 mM/kg) or Batch 104 (2020.10 ± 0.39 mM/kg) certified reference material obtained from the laboratory of Professor Andrew Dickson, Marine Physical Laboratory, Scripps Institution of Oceanography. The standard was analyzed at least three times at the start of analyses to verify instrument stability and was subsequently analyzed following every fifth sample to constrain instrument drift. No significant drift was observed during each analytical run. The average of all standard measurements was used in the concentration calculations. Concentrations were calculated using the following equation:

$$\text{DIC} = A_{\text{sample}}/A_{\text{standard}} \times C_{\text{standard}}, \quad (2)$$

where A_{sample} and A_{standard} are the integrated Beer-Lambert CO₂ absorptions of the sample and standard, respectively; C_{standard} is the DIC concentration of the standard, the molar concentration (moles/liter) which was taken as the certified molal concentration (moles/kilogram) times a density of 1.025 kg/L. A

single determination consisted of four separate injections of sample. The calculated concentrations are based on the average of the latter three absorptions because the first injection tends to show a low value.

Chloride and sulfate

Sulfate and chloride were quantified with a Metrohm 861 Advanced Compact ion chromatograph (provided by the University of Rhode Island Geobiology Laboratory). The ion chromatograph comprises an 853 CO₂ suppressor, a thermal conductivity detector, a 150 mm × 4.0 mm Metrosep A SUPP 5 150 column, and a 20 µL sample loop. A Metrohm 837 ion chromatography eluent/sample degasser was coupled to the system. The column oven was set at 32°C. The eluent solution was 3.2 mM Na₂CO₃ and 1.0 mM NaHCO₃. A 1:50 dilution of interstitial water with 18.2 MΩ deionized water was analyzed.

Aliquots of a 20 L secondary standard (~1:50 dilution) were used in all analytical runs. This standard was calibrated against International Association for the Physical Sciences of the Oceans (IAPSO) standard seawater (18 alternate analyses of the secondary standard and IAPSO standard). All samples were diluted using the same pipettes as were used in the IAPSO calibration (10 mL dispensette and 200 fixed-volume Eppendorf pipettor).

The analysis sequence in an analytical run (36 analyses) was three standards followed by a repetitive sequence of four samples and a standard. In each run, two dilutions (duplicates) of each sample were analyzed. In each run, four IAPSO samples were analyzed to quantify long-term reproducibility and as quality assurance for each run. Reproducibility was also calculated for each run based on the sample and IAPSO duplicates using the method of combined (pooled) standard deviations. If the range between two duplicates was greater than three times the standard deviation, the data were not accepted and another pair of duplicates of the same sample was prepared and analyzed. If the measured concentration of IAPSO standard in a run was not within the expected range (based on the combined standard deviation and 95% confidence interval based on student-t values), the data from the entire run were not accepted and all the samples were reanalyzed. This occurred in only one analytical run.

All quantification was based on peak areas. Chloride peak areas of the standard were examined to identify sensitivity drift in each run. If there was no significant drift, the average value within an analytical run of the Cl peak area for the standards was used in concentration calculations. If drift was detected, either a first- or second-order least-squares fit to the response

was determined and used for the calculation of concentrations.

For sulfate, calculations were based on the measured S/Cl peak area ratio, as this method removes variations caused by temperature-dependent changes in injected volume and sample dilution. Sensitivity drift was corrected in a manner similar to that used for chloride. The reported values are given as a sulfate anomaly, symbolized by \odot , which is the percent difference in the S/Cl ratio of the sample relative to the IAPSO standard,

$$\odot = [(R_{\text{sample}}/R_{\text{std}}) - 1] \times 100, \quad (3)$$

where

$$(R_{\text{sample}}/R_{\text{std}}) = [(\text{SO}_4^{2-}/\text{Cl}^-)_{\text{sample}}]/[(\text{SO}_4^{2-}/\text{Cl}^-)_{\text{std}}], \quad (4)$$

and, for any sample or standard,

$$R = [(\text{peak area})_{\text{SO}_4^{2-}}/(\text{peak area})_{\text{Cl}^-}]. \quad (5)$$

The combined standard deviation of Cl^- analyses for all duplicates is 0.13%. Because all samples were analyzed in duplicate, the standard error is given as 0.09%. The combined standard deviation of sulfate anomaly (\odot) analyses for all duplicates is 0.07% with a standard error of 0.05%.

Reported concentrations are based on a Cl^- concentration in IAPSO of 559.5 mM and a SO_4^{2-} concentration of 28.94 mM. Sulfate concentrations were calculated from sulfate anomalies and chloride concentrations with the following formula:

$$[\text{SO}_4^{2-}]_{\text{sample}} = ((\odot \times 10^{-2}) + 1) \times ([\text{SO}_4^{2-}]/[\text{Cl}^-])_{\text{IAPSO}} \times [\text{Cl}^-]_{\text{sample}}. \quad (6)$$

Nitrate measured from interstitial water collected by Rhizon sampler

During previous seafloor microbiological research expeditions, it was learned that squeezing to obtain an interstitial water sample generated a high nitrate blank corresponding to between 1 and 5 μM NO_3^- in the sample. This is an unacceptably high value for a blank. Because of this problem, nitrate concentrations in interstitial water during Expedition 329 were measured using interstitial water from Rhizon samplers. This practice allowed us to effectively quantify even the lowest concentrations of nitrate (<1 μM).

Nitrate concentrations were analyzed with a Metrohm 844 UV/VISCompact ion chromatograph (provided by the University of Rhode Island Geobiol-

ogy Laboratory). A 150 mm \times 4.0 mm Metrosep A SUPP 8 150 column was used. The column oven was set at 30°C. The eluent was a 10% NaCl solution filtered through a 0.45 μm filter. Approximately 0.8 mL of interstitial water was injected manually into a 250 μL sample loop. Absorption at the 215 nm channel was used for quantification. A 50 μM sodium nitrate/nitrite standard was run after every second, third, or fourth sample depending on instrument stability. The 50 μM standard was calibrated with CRM 104–certified reference material obtained from the laboratory of Professor Andrew Dickson, Marine Physical Laboratory, Scripps Institution of Oceanography.

Spectrophotometric analyses of phosphate and dissolved silica

Phosphate and dissolved silica concentrations in the squeezed interstitial water samples were determined using an OI Analytical discrete analyzer (DA3500) spectrophotometer unit. This is an automated system that controls sample analysis and reagent aspiration, dispensing, heating, and mixing. A 1–2 mL aliquot from the interstitial water sample was pipetted into a DA3500 sample cup. Samples were selected in random order for analysis. Phosphate and dissolved silica analyses were conducted independently, with phosphate being measured first.

In the phosphate method, orthophosphate reacts with Mo(VI) and Sb(III) in an acidic solution to form an antimony-phosphomolybdate complex. Ascorbic acid reduces this complex, forming a blue color that is measured at 880 nm. Potassium phosphate monobasic (KH_2PO_4) dissolved in 18.2 M Ω water was used to produce a calibration curve with 1, 2, 3, 4, and 5 μM concentrations through the autodilution program on the discrete analyzer to check for instrument linearity. A secondary standard (2.5 μM) was prepared from stock solution prepared from potassium phosphate monobasic (KH_2PO_4) dissolved in 18.2 M Ω water. This standard was used to test accuracy and drift during the analytical runs. An additional certified seawater sample (0.77 $\mu\text{M}/\text{kg}$), from the laboratory of Professor Andrew Dickson was also used to evaluate the accuracy and detection limits of the method. Standard additions of phosphate to pure water and to seawater were tested, and the differences were determined to be negligible. During an analytical run, phosphate was determined in triplicate and, at Site U1368, phosphate was also determined over duplicate runs. Precision was based on pooled standard deviations estimated using the equation (McNaught and Wilkinson, 1997)

$$s_p = \{[(n_1 - 1)s_1^2 + (n_2 - 1)s_2^2 + \dots + (n_k - 1)s_k^2] / (n_1 + n_2 + \dots + n_k - k)\}^{1/2}, \quad (7)$$

where

s_p = pooled standard deviation (0.66 confidence interval),

s = standard deviation of a given measurement, and

k = number of series of measurements.

Silica in solution as silicic acid or silicate is reacted with a molybdate reagent in acid media to form molybdosilicic acid. The complex is reduced by ascorbic acid to form molybdenum blue, measured at 420 nm on the discrete analyzer. A primary standard was prepared by adding a weighed amount (~0.5642 g) of sodium silicofluoride (Na_2SiF_6) to 18.2 M Ω water. This standard was used to produce a curve of calibration standards according to the instructions given in Gieskes et al. (1991). Standards between 120 and 900 μM were freshly prepared using 5% artificial seawater. We found significant differences in standard curves between those prepared in the artificial seawater as described in Gieskes et al. (1991) and those prepared in pure water. Because of what appears to be a strong dependence of the kinetics of the reaction on time, drift could be substantial. This drift was accounted for by running an independent standard at regular intervals (every five samples). Except for Site U1365 (triplicates), duplicate measurements were performed. Precision was based on pooled standard deviations for duplicate samples that are derived from Equation 7, as discussed above (McNaught and Wilkinson, 1997):

$$s_p = [(x_{i1} - x_{i2})^2 / 2k]^{1/2}, \quad (8)$$

where x_{i1} and x_{i2} are duplicate measurements.

Analysis of cations in interstitial water by suppressed ion chromatography

Concentrations of dissolved cations (Na^+ , K^+ , Ca^{2+} , and Mg^{2+}) in interstitial water were determined by means of suppressed ion chromatography. Aliquots of interstitial water were analyzed on an ICS 3000 ion chromatograph (Dionex). The ICS 3000 combines automated eluent generation and self-regenerating suppression with a conductivity detector. IAPSO primary reference material was used for standardization and quantification.

Each aliquot of interstitial water was diluted (1:200) with 18.2 M Ω water and aliquoted to a 10 mL auto-sampler vial. Dilutions were performed manually or by Hamilton autodilutor, depending on time constraints. For each analysis, 25 μL of the sample was

injected into the sample loop. Methanesulfonic acid (18 mM) was used as a mobile phase. The pump operated in isocratic mode with a 0.250 mL/min flow rate. The cation exchange IonPac-GS12A (2 mm \times 50 mm) guard column and IonPac-CS12A (2 mm \times 250 mm) analytical column were operated at ambient temperature (25°C). Suppressor current was set to 14 mA. Detector cell temperature was set at 35°C.

Calibration was based on a six-point calibration curve, a blank and five increasingly diluted standards, to bracket the concentrations expected in diluted samples to be analyzed. Diluted IAPSO standard (P145 batch, K_{15} -0.99981) was used for all calibrations. For Site U1365, a 1:200 dilution standard was used, whereas for the remaining sites a 1:180 dilution was used to further increase signal-to-noise ratio. Analytical runs consisted of repetitive sequences of IAPSO standard and four samples. With the exception of Sites U1365 and U1366, in all analytical runs three quality assurance standards per batch were analyzed to assess reproducibility. Two dilutions of each sample were analyzed. Both replicates were rejected when the relative standard deviation between them was >2% of the measured value. Quantification was based on peak area; baselines and peak integration were manually selected by the operator. If drift was observed, sample concentrations were corrected for the drift on a point-to-point basis. Accuracy was determined by triplicate analysis of IAPSO standard. Values of precision and accuracy are reported in each site chapter.

Inductively coupled plasma–emission spectrometry

Major and minor elements (Ca, Mg, K, Na, Fe, Ba, B, and Mn) in the interstitial water were determined by inductively coupled plasma–atomic emission spectrometry (ICP–AES) with a Teledyne Prodigy high-dispersion ICP spectrometer. The general method for shipboard ICP–AES analysis of samples is described in Murray et al. (2000) and the user manuals for new shipboard instrumentation with modifications as indicated. Samples and standards were diluted 1:20 using 2% HNO_3 for trace element analyses (B, Mn, Fe, Sr, and Ba) and 1:200 for major element analyses (Na, K, Ca, and Mg).

Each batch of samples run on the ICP spectrometer contains blanks and solutions of known concentrations (such as IAPSO). Samples were analyzed in batches, commonly one batch per site, to take advantage of achieved calibration and maximize intra-site precision. Each item aspirated into the ICP spectrometer was counted four times from the same dilute solution within a given sample run.

Following each run of the instrument, the measured raw-intensity values were corrected for instrument drift and procedural blank. If necessary, a drift correction was applied to each element by linear interpolation between the drift-monitoring solutions. For many of the sites, there was no unidirectional instrumental drift >1% (total through the entire run of multiple hours), and in such cases no drift correction was employed. After drift correction, where appropriate, and blank subtraction, a calibration for each element was calculated using the results from the analyses of known solutions. For the major elements and Sr, because the calibration lines were strongly linear and concentrations deviated only slightly from seawater concentrations, the final concentrations were calculated on the basis of the ratio to the analysis of IAPSO standard. IAPSO standard was measured at least four times through a run (and as many as eight times), each time as an unknown; therefore, it was straightforward to use some IAPSO samples for precise determination of the ratio and other IAPSO samples, not used in this calibration, to provide an independent check on the resultant accuracy and precision. This strategy also enhanced long-term, intersite reproducibility.

Typical relative standard deviations of the quadruplicate counts per acquisition were better than 0.5% of the measured value for each element. Precision and accuracy are reported on a site-by-site basis in each site chapter.

Sedimentary nitrogen, organic carbon, and inorganic carbon

We routinely sampled 5 cm³ of sediment from the working half of each core on the sampling table after splitting the core. Sample aliquots were freeze-dried for ~24 h and crushed to a fine powder using an agate mortar and pestle. Geochemical analyses included carbonate and elemental analyses (C, H, N, and S).

Total inorganic carbon (TIC) concentrations were determined using a UIC 5011 CO₂ coulometer. Between 10 and 150 mg of freeze-dried, ground sediment was weighed and reacted with 2N HCl. The liberated CO₂ was titrated and the end-point determined using a photodetector. Calcium carbonate content, expressed as weight percent, was calculated from the TIC content, assuming that all evolved CO₂ was derived from dissolution of CaCO₃, by the following equation:

$$\text{CaCO}_3 \text{ (wt\%)} = \text{TIC} \times 8.33 \text{ (wt\%)}. \quad (9)$$

No correction was made for the presence of other carbonate minerals. Accuracy during individual batches of analyses was determined by running a carbonate standard (100 wt% CaCO₃) every five samples. Analytical precision and accuracy for CaCO₃ based on an internal calcium carbonate standard were ±0.6% and ±1.2%, respectively. The detection limit for CaCO₃, defined here as three times the standard deviation of the blank (2N HCl), was 0.1% for 100 mg of pelagic clay.

Total carbon and nitrogen contents of sediment samples were determined with a ThermoElectron Corporation FlashEA 1112 CHNS elemental analyzer equipped with a ThermoElectron packed column CHNS/NCS and a thermal conductivity detector. About 10–40 mg of freeze-dried, ground sediment was weighed into a tin cup and combusted at 900°C in a stream of oxygen. Total carbon content of samples from Site U1365 had to be corrected for carbon contamination associated with the vanadium pentoxide reagent. Correction values are between 0.009% and 0.021%, depending on sample weight during analysis. Replicate analysis of selected samples without vanadium pentoxide shows a good correspondence with the corrected total carbon values. After Site U1365, we discontinued use of vanadium pentoxide. All measurements were calibrated to a standard, which was run every five samples. In low-carbonate sediments, cysteine was used as the calibration standard, whereas sulfanilamide was used for carbonate ooze samples. The detection limit was 0.001% for total nitrogen (instrument limit) and 0.002% for total carbon (procedural blank, measured as an empty tin cup). The average standard deviation for total carbon replicates was 0.08% in carbonate-rich samples and 0.01% in clay-rich samples. The average standard deviation for total nitrogen replicates was 0.001% in both carbonate-rich and clay-rich samples.

TOC was obtained directly from the CHNS elemental analyzer after treating subsamples (5–20 mg) with 140–200 µL 1N HCl to remove the inorganic carbon fraction. We followed the standard operating procedure for measuring TOC by elemental analysis that was adapted from Verardo et al. (1990) for shipboard use during Expedition 320/321 (Expedition 320/321 Scientists, 2010). However, we increased the amount of acid added from 10 to 20 µL steps. After the final step (i.e., when no reaction was observed after the addition of acid) samples were placed in a 50°C oven to dry overnight. The detection limit for TOC was 0.002% (procedural blank, measured as a silver cup containing HCl, dried and packed into a tin cup). Replicate analysis of selected samples showed small

standard deviation ($\leq 0.01\%$, with a few samples $\leq 0.02\%$).

Microbiology

Research conducted during scientific ocean drilling continues to reveal significant information regarding seafloor microbial habitats, the diverse microbial communities that reside in those habitats, and the biogeochemical implications of their metabolic activities. Using a combination of shipboard and shore-based analyses, we gain knowledge of the distribution of their biomass, metabolic activities, and phylogenetic relationships. Expedition 329 is dedicated to assessing the factors that control distribution, activities, and composition of microbial life in organic-poor sediment and the underlying basalt. During the expedition, microbial abundance was quantified, experiments were initiated to quantify activities using multiple stable isotope and radioisotope tracers, and samples were taken for postexpedition characterization of communities by a variety of molecular techniques targeting DNA and RNA at both single-cell and community levels. Additional information on the types of microorganisms that inhabit these seafloor environments will be obtained by examining microbes isolated by a wide suite of culturing methods. In order to ensure that we are indeed analyzing indigenous microbial life and its activities, samples were routinely taken for assessment of contamination during coring and sampling.

Core handling and sampling

Drilling

Microbiological sampling depends on careful and appropriate sample handling techniques. Because the samples were retrieved from very stable sedimentary environments, seafloor microorganisms are expected to be sensitive to chemical and physical change, in particular to changes in oxygen concentration and temperature. Consequently, all cores to be sampled for microbiological studies were transferred from the drilling platform to the Hold Deck refrigerator ($\sim 7^{\circ}\text{--}10^{\circ}\text{C}$) as quickly as possible and kept as whole-core sections until processed. As initiated during ODP Leg 201 (D'Hondt, Jørgensen, Miller, et al., 2003) in order to avoid intermittent warming of retrieved cores, the conventional core handling procedure was modified. Once a core was retrieved, it was immediately transferred to the catwalk for labeling and cutting of sections before the next core barrel was deployed. Efforts were also made to obtain advanced piston corer (APC) cores even when this led to an increase in core recovery

time, as APC cores are generally much less disturbed than extended core barrel (XCB) cores.

While drilling cores for microbiology, potential for contamination from surface-derived microbes is high. Consequently, quantification of potential contamination and avoidance of core disturbance are critical for microbiological studies. To check for potential intrusion of drill water from the periphery toward the center of cores and, thus, to confirm the suitability of core material for microbiological research, samples were routinely taken for contamination tests using solutes (perfluorocarbon tracer [PFT]) and, for basalt cores, cell-sized particles (fluorescent microspheres). Furthermore, the freshly collected cores were visually examined for cracks and other signs of disturbance by observation through the core liner. Core sections observed to be disturbed before or after subsampling were not analyzed further.

Whole-round core sampling in the core refrigerator (cold room)

It is important to emphasize that the different analyses, experiments, and cultivation attempts that fall under the rubric “microbiological methods” have widely different requirements concerning handling and storage. Keeping samples cool and processing times short and minimizing contamination were the key criteria for determining how the core sections were processed. Therefore, all core sections sampled for microbiology or geochemistry were transferred to the core refrigerator on the Hold Deck for most microbiological sampling (the only microbiological samples collected on the catwalk were for cell counts and PFT analyses). To minimize changes in microbial populations, all core processing for whole-round core microbiological samples took place in the refrigerated core room on the Hold Deck of the *JOIDES Resolution* at $\sim 7^{\circ}\text{--}10^{\circ}\text{C}$. This room was equipped with a workbench, working space for two to four persons, and all sampling tools, including core cutters, chain vises, sample containers, label maker, and so forth. Because the core liner is not sterile and the outer surface of the core is contaminated during drilling, subsampling of whole-round cores excluded the sediment next to the core liner. Where appropriate, handling and subsampling were performed under anoxic conditions using an anaerobic glove box in the cold room.

Normally, all 1.5 m sections from all cores were held in the cold room in the event section(s) intended for microbiological sampling were found during sampling to be disturbed. In cases where cores were determined to be disturbed, sections from other cores were sampled. The core liner was cut by the standard IODP core cutter and cut with an ethanol-wiped

spatula. Some whole-round core sections were immediately capped with new end caps and stored at 4°C for shore-based analysis, whereas others were immediately subsampled into sterile 5, 10, 20, or 60 cm³ tip-cut syringes. Samples (whole-round cores or syringe subcores) for molecular analysis were transferred to ultralow-temperature freezers (−80°C) on board.

Basaltic core sampling

During Expedition 329, basaltic rock of different ages was recovered from three sites using the rotary core barrel (RCB) coring system. In addition, small pieces of the uppermost altered basalt were recovered from sediment/basalt interfaces at most drilling sites using standard APC coring. Those interface samples were subsampled aseptically in the cold room for microbiological and biomineralogical investigations. The basalt cores were brought to the cold room after recovery and stored there until mineralogical and microbiological subsampling. To maintain the moisture of the cores, wet sponges were placed in the core liner. For microbiological subsampling, pieces of basalt or altered basalt were cracked with a flame-sterilized hammer and chisel and suspended in a 3% NaCl solution to remove surface contaminants and cuttings. Some portions of the “contaminated” suspension were also subsampled as a reference for subsequent analyses. If there was enough material for multiple microbiological experiments, a piece of the surface part was briefly flamed and crushed on a flame-sterilized tray for aseptic subsampling. The aseptically prepared basalt pieces were then further powdered with a flame-sterilized percussion mortar, and the powdered samples were used for cultivation, cell enumeration, and shore-based molecular analyses.

Quantifying potential contamination

To evaluate the extent to which contaminating cells may have penetrated a sample, the shipboard science party (1) continuously injected PFT into the drilling fluid (in sediment and basalt) and (2) introduced fluorescent microspheres at the drill bit (in basalt). Contamination will be further assessed by postcruise genomic comparison of the basalt or sediment sample with drilling fluid from the time of coring. The two shipboard techniques have been successfully used on multiple ODP legs and during Expedition 301 (Smith et al., 2000a, 2000b; House et al., 2003; Lever et al., 2006). The third technique is common for studies of seafloor samples, in which contamination is ubiquitous and genomic signatures of the contaminating material are subtracted from those of the seafloor sample. Previous shipboard PFT studies

have consistently shown that the interior of cores are much less contaminated than core peripheries (by factors of 3–300) and that APC cores are generally not significantly contaminated (Smith et al. 2000a; House et al., 2003). The uppermost 1.5 m section of an APC core tends to be more contaminated than deeper sections (Lever et al., 2006). Contamination tends to be much greater in RCB cores (e.g., on surfaces of cored basalt) and XCB cores than in APC cores. In all categories of core, potential contamination varies considerably from sample to sample. Consequently, to avoid contamination of microbiological results, contamination tests must be conducted on each core or hard rock sample that is used for a microbiological experiment (D’Hondt, Jørgensen, Miller, et al., 2003).

Perfluorocarbon tracer

The PFT used on the *JOIDES Resolution* during Expedition 329 was perfluoromethylcyclohexane. This compound is volatile, with a boiling point of 76°C, and is chemically inert. PFT was introduced into the drilling fluid with a high-pressure liquid chromatography (HPLC) pump at a constant concentration of 1 mg/L as a proxy for potential contamination of the core material by nonindigenous microbes. It is important to work quickly but carefully with the core material; because the PFT is volatile, it is possible to contaminate internal core material with the PFT (and microbes) from the relatively closed atmosphere of the cold room or the outside of the core section.

For PFT measurement of sediment cores, 3 cm³ subsamples were taken with a cut-off syringe and directly extruded into a gas chromatograph sample vial. During Expedition 329, we tested a new PFT measurement approach using *iso*-octane as a solvent. Fifteen milliliters of *iso*-octane (2,2,4-trimethylpentane) was added to the vial, which was then quickly sealed. Sample vials were placed on the wrist shaker (Burrell) and shaken for a minimum of 5 min. One microliter of the supernatant was injected into a gas chromatograph (Agilent 6890) with an electron capture detector (ECD). A calibration curve of PFT in the solvent was prepared from concentrations of 10^{−10} to 10^{−6} by serial dilution. Each standard was injected into the gas chromatograph, and a curve of response factors was developed.

Using the new method as described above, the sediment subcore did not break down into the *iso*-octane but remained as a solid piece. There was very little improvement after 24 h of vigorous shaking. The low efficiency hindered the release of PFT into the *iso*-octane phase and hence a reliable quantity of PFT

could not be extracted (see “**Microbiology**” in the “Site U1365” chapter [Expedition 329 Scientists, 2011]). Therefore, as an alternative method of PFT measurement, we prepared PFT samples using the previously established method (Smith et al. 2000a; House et al., 2003; Lever et al., 2006), slightly modified by taking 3 cm³ sediment samples on the catwalk immediately after core recovery and placing them into gas chromatograph vials with 2 mL of 18.2 MΩ water. Each vial was quickly sealed and stored upside down at 4°C for later analysis. The analyses will be done postexpedition.

Fluorescent microspheres for basalt contamination test

Fluorescent microspheres of a size similar to indigenous microorganisms (0.5 μm) have long been used in drilling operations to assess dispersal and transport of microbe-sized objects (Harvey et al., 1989). Yellow to green fluorescent microspheres (Fluoresbrite carboxylate microspheres; Polysciences, Inc., 15700) with a diameter of 0.52 ± 0.01 μm were used as a particulate tracer during basalt coring. These microspheres are highly fluorescent (458 nm excitation; 540 nm emission). They appear bright green when observed by epifluorescence microscopy through a blue filter set (Zeiss filter set 05 or 08) (Smith et al., 2000b).

Microspheres were only deployed on cores that recovered basalt samples for microbiological cultivation and molecular biological analyses. The concentration of microspheres was set at 10¹⁰ spheres/mL (Smith et al., 2000b; House et al., 2003). Microspheres were deployed in plastic bags containing 40 mL of microsphere suspension in 18.2 MΩ water (2 × 10¹¹ microspheres in a 40 mL bag). The bag was then heat-sealed and placed into an additional plastic bag that was open at each end. By attaching the loose plastic ends with cord, the bag was wedged into a shim above the core catcher and stretched across the throat of the core barrel. The bags were ruptured as core entered the barrel, releasing the microspheres.

Concentrations of fluorescent microspheres in core samples were quantified using a Zeiss Axiophot epifluorescence microscope fitted with a mercury lamp (HBO 100 W), a blue filter set, and a 100× Plan-NEOFLUAR oil-immersion objective. Nonfluorescent immersion oil was used for all observations.

For hard rock samples, aliquots (100 μL) of the crushed rock were suspended in 10 mL of 0.2 μm filtered Tris-buffered saline (TBS; pH 7.4) solution and filtered onto black, 25 mm diameter polycarbonate filters (0.2 μm pore size) in a filtration tower. The filters were then mounted on microscope slides with a

drop of nonfluorescent immersion oil and covered with a coverslip. The microspheres on the filter were counted using epifluorescence microscopy as described above. Microsphere abundance on the filter was determined by averaging the total number seen in at least 20 randomly selected fields of view. However, it is worth noting that we were not able to assess the contamination level quantitatively based on the number of fluorescent beads because the bag is crushed immediately at the initiation of RCB coring and the drilling fluid (i.e., seawater) subsequently dilutes the in situ concentration of fluorescent beads during drilling.

Assessment of potential contamination sources

RCB drilling requires huge amounts of surface seawater to be pumped into the borehole. This water is the major source of microbial contamination to cores collected for microbiological analyses. In order to check for this contamination (independent of the tracer tests), drilling fluid, surface seawater, and bottom seawater above the mudline were collected. Microorganisms present in these fluids were collected on 0.2 μm pore filters. The filters were frozen (−80°C) and will be analyzed postcruise for 16S rRNA. In some cases, filters were divided into pieces using a sterile scalpel for microbiological and biomineralogical investigations.

Cell detection and enumeration

Sediment

One of the fundamental objectives of subseafloor biosphere research is to understand the global distribution of microbial populations and their activities. Previous microbiological efforts of scientific ocean drilling expeditions have mainly focused on organic-rich continental-margin sediments. Hence, the distribution of organisms in organic-poor subseafloor environments, such as the subseafloor in the South Pacific Gyre, remains largely unknown. Previous study of shallow (≤9 mbsf) sediment from the South Pacific Gyre showed that cell abundance is several orders of magnitude lower than in any other marine sedimentary environment studied to date (D’Hondt et al., 2009). Even in samples from the sediment/water interface, microbial abundance was only ~10⁵ cells/cm³, decreasing with depth to values of 10³ to 10⁴ cells/cm³ by ~9 mbsf. These results suggest that microbial populations in deeper sediment realms might be extremely low, requiring very sensitive technology to obtain accurate biomass estimates.

Because extremely low cell abundances were expected in the South Pacific Gyre, cells were extracted from the sediment prior to counting according to

the protocol of Kallmeyer et al. (2008) with slight modifications as described below. The extracted cells were stained by SYBR Green I fluorescent dye and enumerated by direct counting with epifluorescence microscopy.

Samples close to the sediment/water interface may harbor cell abundances that are high enough to be counted directly without cell extraction. In order to obtain a measure of the extraction efficiency of the cell extraction, direct (nonextracted) cell counts were performed on a few samples from the upper part of the core. Because 100× to 500× less sediment can be used for counting than for cell extraction, the minimum detection limit increases accordingly from ~10³ cells/cm³ (extracted samples) to ~5 × 10⁴ cells/cm³ (nonextracted samples).

During Expedition 329, 2 cm³ sediment plug samples for cell enumeration were taken using 3 cm³ tip-cut syringes, either directly at the catwalk or in the cold room, from 5 cm whole-round core. Only the 2 cm³ syringe samples were used for the onboard analysis. The 5 cm whole-round cores were stored at -80°C for additional shore-based analyses. The 2 cm³ sediment plug was transferred into a sterile 15 mL centrifuge tube containing 8 mL of 0.2 μm filtered 2.5% (w/v) NaCl solution with 2% (v/v) formalin as a fixative and thoroughly shaken to form a homogeneous suspension. The slurried formalin-fixed samples were subjected to cell detachment and cleaning steps using the following protocol:

1. Depending on the expected cell abundance, between 50 and 500 μL of the (1:5) slurry was used for the extraction. When sample volumes were <500 μL, 2.5% NaCl solution was added to adjust the sample volume to 500 μL. Then, 50 μL each of detergent mix (100 mM disodium EDTA dihydrate, 100 mM sodium pyrophosphate decahydrate, and 1 vol% Tween 80) and methanol were added. The sample was placed on a vortex shaker for 30 min to 1 h. In cases of extremely low cell abundances, the volumes of slurry and all reagents were increased.
2. The sample was underlain by a cushion of ~500 μL Nycodenz (50% w/v) and centrifuged at 3250× g for 20 to 40 min.
3. The supernatant was carefully removed by siphoning it off with a small syringe and retained. The pellet was then resuspended in NaCl solution to a total volume of 500 μL.
4. The resuspended sample was treated as described in Step 1. After the vortex mixing, the sample was subjected to ultrasonic treatment with an ultrasonic probe (Model UH-50, SMT Co. Ltd., Tokyo, Japan) at 20 W for 5 × 10 s with 20 s breaks. The

samples were placed in a cold water bath to minimize heating.

5. The sample was underlain with Nycodenz (set to ~1.2 g/mL), centrifuged, and the second supernatant was removed as described and added to the first one.
6. A volume of 100 μL of 1% HF was added to the pooled supernatant and left for 20 min.
7. To remove HF from the supernatant, 120 μL of a solution containing 0.5 M each of CaCl₂ and sodium acetate was added. Visible precipitation of the highly insoluble CaF₂ occurred immediately. Alternatively, we added 100 μL of 1.5 M TBS solution to neutralize the solution pH without CaF₂ precipitation (see Morono et al., 2009).
8. After a vortex mix, the sample was underlain by a cushion of Nycodenz and centrifuged (10 min at 2500× g) in order to remove the CaF₂.
9. The sample was then prepared for cell enumeration. For direct cell enumeration using epifluorescence microscopy, the pooled supernatant was filtered on 0.2 μm black polycarbonate filters (Whatman), stained with SYBR Green I, and counted directly on a Zeiss Axiophot epifluorescence microscope using 63× or 100× magnification.
10. For samples that contained carbonate minerals, the slurry was first treated with 10× the sample volume of a carbonate dissolution mix containing 20 mL/L glacial acetic acid and 35 g/L sodium acetate. This solution has a high acidity but a moderate (4.6) pH, avoiding excess stress on the cells. The slurries were placed in 5 mL round-bottom culture tubes with ventilated caps in order to avoid buildup of CO₂. After all carbonate was dissolved, the samples were centrifuged and the supernatants removed and kept for cell enumeration. The pellet was washed twice with Tris-EDTA (TE) buffer and treated like a normal sample as described in Step 1.

Estimation of the blank and minimum detection limit (MDL) was very important because of the very low cell abundances. Samples were processed in batches of six plus one additional blank sample, in which sterile-filtered TE buffer replaced the sediment slurry. The blank was calculated as the average of all blanks processed during the expedition. The MDL was set to be the blank value plus three times the standard deviation of the blank.

For quality assurance and control, all glassware used for cell count was combusted at 500°C for at least 1 h to remove any remaining cells. Because of higher turnover, the filter towers were soaked in 5% sodium hypochloride solution for at least 15 min, rinsed with 18.2 MΩ water, and finally rinsed with 100%

technical-grade ethanol and flamed with a blow torch. All reagents were filtered through 0.45 or 0.2 μm pore filters. An aliquot of every batch of every reagent was placed on a filter, stained, and checked for contamination using epifluorescence microscopy.

We also experimented with flow cytometry (FCM) for cell counting. This was the first use of FCM on the *JOIDES Resolution*. Because the use of this technique for enumeration of cells in sediments is still experimental, the FCM results and methodological developments are presented in a separate chapter as a specialty paper rather than in the site reports (see [Morono et al., 2011](#)). If FCM proves to be successful for onboard cell enumeration, its advantages will be

- High sample throughput and continuous cell enumeration,
- Better counting statistics because of a much larger numbers of cells being counted from individual samples, and
- Consistency of criteria for cell identification.

Consequently, the use of a high-throughput FCM cell count technique may ultimately result in higher data resolution and more consistent results than counts using epifluorescence microscopy.

Basalt

During Expedition 329, we enumerated cell abundance for basaltic rock samples without the cell extraction steps used for sediment samples. First, the surface of basalt cores was washed twice with 25 mL of 3% NaCl solution in a sterile plastic bag. After the washing step, the rock surface was briefly flamed with a propane torch. The flamed rock was cracked using a flame-sterilized hammer and chisel, and small pieces from the interior were powdered using a flame-sterilized mortar and pestle. The powdered basalt (1–2 mL) sample was fixed with 5–10 mL of TBS solution and then fixed with 4% paraformaldehyde at 4°C overnight. The fixed basalt suspension was subjected to cell counting using the following protocol:

1. After vigorous stirring of the paraformaldehyde-fixed slurry, 100 μL of the suspension was dispensed in 10 mL of filtered 1 \times phosphate-buffered saline (PBS) buffer (pH = 7.4).
2. After vigorous stirring, 1 mL of the second suspension (made in Step 1) was diluted again in 9 mL of filtered 1 \times PBS buffer and sonicated for 30 s.
3. The sonicated suspension was filtered through a 25 mm diameter, 0.2 μm pore size black polycarbonate filter. A cellulose filter (25 mm diameter; 0.45 μm pore size) was placed beneath the polycarbonate filter as support.

4. Cells on the polycarbonate filter were stained with filtered 1 \times SYBR Green I in filtered TE buffer for 5 min.
5. The stained filter was washed twice with 5 mL of filtered TBS solution.
6. The washed filter was mounted on a slide with one drop of immersion oil and covered with a coverslip.
7. The SYBR Green I-stained cells were directly observed by using a Zeiss Axiophot epifluorescence microscope with a band-path filter slit (excitation at 470 nm, fluorescence above 515 nm) at 63 \times magnification.
8. On each filter, 300 microscopic fields of views were observed, and cell-shaped forms that produced bright green fluorescence were enumerated as cells.

The MDL was estimated by counting blank filter samples that were treated with 100 μL of filtered TBS solution with 4% paraformaldehyde as described above. Cell number in the blank filters was calculated as the average of all blanks processed at each site. The MDL was set to be the average blank value plus three times the standard deviation of the blanks. For negative control samples (i.e., cell free), crushed basalt pieces were combusted at 500°C for 3 h before preparation as described above.

Fluorescent in situ hybridization

Fluorescent in situ hybridization (FISH) is a powerful molecular ecological technique, enabling us to detect metabolically active microbial cells using a specific fluorescent-labeled oligonucleotide probe for microscopic analysis. The probe will hybridize with 16S rRNA (or mRNA of the targeted functional gene) in the metabolically active cells. Thus, appropriate sample processing (i.e., cell fixation) using freshly collected samples is necessary. During Expedition 329, we prepared fixed slurries for shore-based FISH analyses. Using sterile tip-cut syringes, 10 cm^3 plug samples were collected from the innermost part of whole-round cores and placed in four times the sample volume of paraformaldehyde solution (4% paraformaldehyde in PBS buffer). The slurry was vigorously shaken until no visible clumps were observed. It was then incubated for several hours at 4°C. Following incubation, the slurry was pelleted in a centrifuge at 2500 \times g for 10 min, washed twice with cold PBS buffer, and stored in 10 mL of 1:1 (v/v) PBS:ethanol solution at –20°C.

Enumeration of viruslike particles

During Expedition 329, the number of virus-like particles (VLPs) in sediment was evaluated on board by direct counting using epifluorescence microscope.

For each sample analysis, 1 cm³ of a sediment sample was added to a mixture of 3.5 mL of 0.02 µm filter-sterilized 18.2 MΩ H₂O and 1 mL sodium pyrophosphate (55 mM; 0.02 µm filtered). The slurry was shaken until it formed a homogeneous suspension. Samples were sonicated for 3 min with 30 s breaks after each minute and vortex mixed at maximum speed during the breaks. After centrifugation for 10 min at 3250× g, the supernatant was removed and filtered through a 0.45 µm pore size polycarbonate filter. A volume of 4 mL of TE buffer (10 mM) was added, followed by resuspension of the sediment pellet and centrifugation as described before. The second supernatant was also filtered through a 0.45 µm pore size filter. Both the extracted solutions were pooled and processed immediately or temporarily stored at 4°C until further use. Volumes of 1 to 4 mL of the extracts were filtered onto 0.02 µm pore size membrane filters (Anodisc 13, Whatman) and washed with TE buffer (Tris 10 mM; EDTA 10 mM; pH 7.7). Filters were stained with SYBR Gold (40 µL; 2.5×; Invitrogen) and stained for 1 h in the dark. Stained filters were mounted to microscope slides with 5 µL of mounting solution. VLPs were directly counted in randomly chosen fields using an epifluorescence microscope (Zeiss Axioplan 2 imaging microscope) with a blue filter set.

Preparation of fixed samples for combined microbiological and mineralogical analyses

Mineralogical, textural, and isotopic studies will be used to evaluate the extent of microbial mineral alteration (Boyd and Scott, 2001; Rouxel et al., 2003). For example, the habitability of aged subseafloor basalt is a vital factor to accurately elucidate the potential extent of Earth's subsurface biosphere (Bach and Edwards, 2003). One of the primary potential electron donors in basalt is Fe[II]. If oxidation of Fe[II] is microbially mediated, a likely result is coating of the cell periphery with Fe[III] oxyhydroxides. Understanding of microbe-mineral relationships requires characterization of (1) phylogenetic affiliations of microbial populations that mediate Fe[II] oxidation and (2) crystallographic features of nanometer-scale redox features. Especially, crystallographic evolution of oxidation products over 10–120 Ma needs to be clearly defined in order to discern the modern and past occurrence of Fe[II] oxidizers and to constrain dissolution kinetics of rock-forming minerals.

Scanning transmission X-ray microscopy analysis

Scanning transmission X-ray microscopy analysis is a powerful tool for characterization of organic mate-

rials (DNA, extracellular polysaccharide [EPS], etc.) because this method can provide nanometer-scale information on light element (e.g., C and N) distributions in environmental samples (Tsuji et al., 2010). Consequently, it is very helpful for the study of biomineralization. Because dehydration can cause serious changes in some molecular species, sampling was conducted immediately to prevent samples from drying. Samples for scanning transmission X-ray microscopy analysis were soaked in filter-sterilized artificial seawater stored at 4°C.

Electron energy-loss spectroscopy and transmission electron microscopy analysis

Biogeochemical mineral transformations associated with microbial Fe reduction-oxidation play significant roles in controlling redox balance and carbon cycling (Nealson and Saffarini, 1994), as well as in mineral dissolution and neof ormation (Kim et al., 2004). Combined use of electron energy-loss spectroscopy and transmission electron microscopy is capable of measuring mineral transformations mediated by microbial activities at micro- and nano-scales (Buatier et al., 2004). From the measured electron energy-loss spectroscopy spectra, the energy-loss ratio of Fe-L₃ to Fe-L₂ lines will be determined to estimate the Fe oxidation state using the universal curve as a function of the integral ratio of L₃/L₂ versus ferric Fe concentration as determined by van Aken et al. (1998). During Expedition 329, we stored sediment and basalt samples immediately in the freezer at –80°C for shore-based electron energy-loss spectroscopy-transmission electron microscopy investigations.

Micro X-ray absorption fine structure coupled with catalyzed reporter deposition-fluorescence in situ hybridization analysis

Micro X-ray absorption fine structure (µ-XAFS) and bulk XAFS will be used to directly characterize minerals (mineral phase, size, crystallinity, etc.) in basalt samples. Coupling of µ-XAFS with catalyzed reporter deposition-fluorescence in situ hybridization analysis is a powerful approach to study microbial associations with minerals. For this approach, basalt samples were fixed with TBS buffer (pH 7.2–7.6) containing 3.7% formaldehyde. After the fixation, samples were washed three times with 1:1 (v/v) TBS buffer:ethanol and stored at 4°C. For bulk XAFS analysis, the crushed basalt samples were immediately put in plastic bottles and stored in vacuum-sealed bags at 4°C without further treatment.

Cultivation experiments

Cultivation-dependent studies will provide particularly useful information on physiology, potential biogeochemical function, diversity, and habitat range of low-activity seafloor microorganisms. During Expedition 329, onboard microbiologists initiated cultivations with a wide range of culture media, targeting various physiological types of microbes (Table T8). Generally, the inoculum slurries used for onboard cultivation experiments were individually prepared by individual shipboard scientists using subsamples taken from whole-round cores with cut-off syringes of various sizes. In addition, some sediment samples or inoculum slurries, as well as the sample-inoculated test tube cultures, were stored at 4°C or appropriate conditions for shore-based cultivation experiments.

Inoculum and culture media

To inoculate sediment and basalt samples into the culture media, we prepared inoculum slurries with 2–10 cm³ subcore samples mixed with either sterile-culture media or artificial seawater (Suess et al., 2004). Some inoculum slurries were prepared anaerobically with continuous flushing of the headspace with N₂. The test tubes or serum bottles for anaerobic media were sealed with thick butyl rubber stoppers. No reducing reagents such as Na₂S or titanium solution were used for the inoculum slurry preparation, except for samples targeting methanogens and other types of strictly anaerobic microbes. We attempted to cultivate various types of microorganisms with various combinations of electron donors and acceptors as well as various carbon and nitrogen sources under multiple incubation conditions (e.g., psychrophilic and mesophilic microbes such as aerobic or microaerobic heterotrophs, fermenters, organotrophs, autotrophic and heterotrophic nitrate/nitrite reducers, sulfate reducers, sulfur oxidizers, autotrophic or mixotrophic ammonium oxidizers, nitrite oxidizers, aerobic and anaerobic hydrogenotrophic autotrophs, iron oxidizers/reducers, and manganese oxidizers/reducers) (Table T8). Cultivations were performed with both semisolid-plate and liquid-culture media prepared by individual shipboard microbiologists. An autoclave or oven in the Microbiology Laboratory on the *JOIDES Resolution* was used for sterilizing media and equipment. Nitrogen, N₂:CO₂ (80:20 [v/v]) and/or H₂:CO₂ (90:10 [v/v]) gas cylinders were used to prepare headspace gas for anaerobic media. Inoculations were performed using sterile needles and syringes for liquid media or a spreader for solid plates. Because in situ temperature in sediment and basalt of the South Pacific Gyre is low (a few degrees Celsius), most cultures were incubated at ~10°C.

Most probable number cultivation method

To evaluate most probable numbers for cultivable microbial populations from the South Pacific Gyre sediments, we performed parallel cultivation assays using a serial dilution method of liquid media in 96-well microtiter plates or test tubes. The most probable number media will continue to be incubated in shore-based laboratories, with the goal to quantify specific physiological types of microorganisms and subsequently to isolate pure cultures.

Experiments with stable and radioactive isotopes

A major objective of Expedition 329 is to elucidate the energy and nutrient substrates that may sustain microbial populations in seafloor environments of the South Pacific Gyre. For example, the list of potential electron donors includes photosynthetically derived organic matter, reduced metal, and hydrogen produced in situ by radiolysis (D'Hondt et al., 2009). Thus, experiments were performed to detect specific aerobic respiration pathways and to track potential routes of C-, N-, and P-fixation and their turnover. During Expedition 329, freshly collected samples were fixed for (1) determination of tracer turnover and (2) further processing in shore-based laboratories. Samples were also taken to isolate cell material for single-cell approaches, such as nanoscale secondary ion mass spectrometry (NanoSIMS) analysis combined with various types of in situ hybridization techniques.

The use of isotope-labeled compounds is a critical and sensitive tool for the analysis of microbial activities in seafloor environments. In seafloor sediment, microbial processes, such as oxic respiration, nutrient uptake, oxidation of reduced substrates, and so on, take place at rates that are subnanomolar per cubic centimeters per day or even subpicomolar per cubic centimeters per day, which is more than six orders of magnitude lower than microbial activities on Earth's surface habitats (D'Hondt et al., 2002). Interstitial water gradients of dissolved compounds, such as oxygen, nitrate, or dissolved inorganic carbon, and sediment physical properties can be used to calculate in situ rates of microbial processes. However, such calculations generally do not provide highly specific insight into physiological pathways of substrate turnover. Detailed studies of these pathways typically require incubation studies with chemical tracers. It is often not possible to detect the small concentration changes in dissolved chemical concentrations during incubations of experimentally realistic durations (days to months). Using radiotracers, however, rate determinations in incubated sediment samples may become >10,000 times more

sensitive than when measuring changes in dissolved chemicals in incubated samples. However, microbial metabolic processes in subseafloor sediments are typically so slow that even radiotracer methods operate at the limit of their detectability when studying million-year-old sediments. Consequently, the amounts of radioactivity applied must be higher than normally used in studies of near-surface sediments.

Pulse-chase experiments constitute a second application of isotope-labeling methods. In these experiments, a radioactive or stable isotope-labeled compound is added to a sample and the isotope's incorporation into cells or specific biomolecules is tracked. Also known as stable isotope probing or radioisotope probing, these methods have the potential to link microbial activities with specific organisms or communities.

It is critical for all experimental activity measurements that the sediment or rock samples remain as intact as possible; otherwise data become unrealistic. This requires

- Fast handling of cores on deck to avoid warming of cold sediments. In cold deep-sea sediment, microbes may be sensitive to warming and could be killed at temperatures above 10°–15°C. In warmer sediment, this problem is not critical;
- Aseptic subsampling by sterile and anaerobic techniques from whole-round cores in which the sediment or rock has not been exposed to atmospheric oxygen by splitting of the core; and
- Starting radiotracer experiments as soon as possible after coring because the sample's chemistry and microbiology gradually change once the sediment has been brought up on deck. Experiments started after the cruise are still very useful for some categories of study (e.g., factors regulating process rates), but the absolute rates become less trustworthy with time.

In general, procedures for rate measurements with radiotracers involve subsampling of sediment or basalt into glass vials or other small sterile containers. These still-unlabeled containers are then incubated at in situ temperature in the Isotope Isolation Van for a day until thermal equilibrium is reestablished. Only then is radiotracer or stable isotope tracer injected into the sample (few microliters) and incubation continues in the Isotope Isolation Van for up to a month or more; if necessary, cooled samples still incubating may be shipped back to the shore-based laboratories by airfreight. Incubations are stopped at different times in order to check whether process rates are constant over time. The terminated samples are fixed in a manner that kills the microorganisms

and preserves the isotope-labeled substrate and product. In this state, the samples are stable and can be handled without risk of contamination or risk of altering the incubation results. At the end of the expedition, these fixed (and frozen) samples were transported, either cooled or frozen, to shore-based laboratories for further processing.

Contamination control

Laboratory contamination was controlled through standard radiochemical safety procedures, including monitoring by wipe tests before and after sample handling. Trays and absorbent paper were used. Care was taken to restrict radionuclide use to the back end of the Isotope Isolation Van. Access to the Isotope Isolation Van was restricted to trained personnel. Laboratory outerwear (lab coats and gloves) and footwear (or shoe covers) remained in the Isotope Isolation Van. Wipe tests were performed on all material prior to their removal from the Isotope Isolation Van.

Carbon isotope-labeled compounds pose the greatest danger for long-term contamination of shipboard surfaces because of the long half-life of ^{14}C (5780 y). Bicarbonate may react with water to form volatile CO_2 compounds, but all of the procedures use seawater and alkaline-buffered solution, so degassing of radioactive $^{14}\text{CO}_2$ should be minimal (expected specific activity of the experiments is 25 MBq/mM). ^{14}C -acetate at various pH conditions encountered in seawater exists primarily as soluble acetate anion and should not form a volatile compound. The small amounts of CO_2 resulting from oxidation reactions form bicarbonate and are trapped in the alkaline seawater and buffered solutions. Likewise, the small amounts of CO_2 resulting from oxidation of ^{14}C -labeled leucine to form bicarbonate should remain in solution. ^{33}P -labeled compounds have a short half-life (25.3 days) and have no volatile forms. ^{35}S -sulfate has a relatively short half-life (87.4 days) and is not volatile. Nevertheless, opening of all radioactive tracer stock solution occurred in the hood in the Isotope Isolation Van on the *JOIDES Resolution*.

Although stable isotope tracers are not considered to pose any health hazard, they are potential sources of contamination for geological and oceanographic materials. Therefore, during Expedition 329 all activities with open stable isotope tracers were treated in the same manner as the radioactive tracers. Use of stable isotopes was restricted to the Isotope Isolation Van. Users also followed the same protocols concerning laboratory apparel and shoes as for radioisotope work.

Combined radioactive and stable isotope tracer experiments

Slurry samples of sediment from the South Pacific Gyre subseafloor environments were prepared for radioactive and stable isotope–tracer experiments. Sediment whole-round cores selected for incubation were stored either in the cold room of the Microbiology Laboratory or core refrigerator on the Hold Deck of the *JOIDES Resolution* before processing. Sediment slurry was prepared from 10 cm whole-round cores. For all steps of slurry preparation, sediment was processed in the laminar flow hood and quickly returned to the cold room. For each sediment interval, 1 L of slurry was prepared by adding 200 cm³ of sediment to 800 mL of sterile-filtered (0.2 µm) surface seawater from Site U1368. The exteriors of the sediment sections were trimmed, and the interior pieces were added to chilled (9°C) and filtered seawater. Slurries were stirred constantly for 12 h. Subsequently, 40 mL of slurry was transferred to 51 mL serum vials, closed with butyl rubber stoppers, and sealed with aluminum caps. Two replicate serum vials were prepared for each sediment sample. After tracer addition to both serum vials, one was frozen immediately as the control sample. The others were incubated at 10°C. Incubations were planned to continue beyond the duration of the expedition. Samples were prepared for refrigerated shipment to the home institutes where further incubation, processing, and analyses are to follow.

Incubation experiments were performed with radioisotope-labeled compounds, stable isotope-labeled compounds, or a combination of both. The labeled compounds were added in the hood in a compartment of the Isotope Isolation Van that was cooled to 9°–10°C. In general, autotrophy radioactive experiments were performed with ¹⁴C-labeled bicarbonate and heterotrophy experiments were performed with ¹⁴C-labeled acetate. To evaluate nitrification, ¹⁵N-labeled ammonium was added. For nitrogen fixation, ¹⁵N–double labeled molecular nitrogen (N₂) gas (1 mL) was injected into sealed containers. Samples from these experiments for isolation of cell material were taken for single-cell approaches such as halogenated in situ hybridization–secondary ion mass spectrometry analysis. Phosphorus uptake was evaluated by use of ³³P-labeled phosphate or ³³P-labeled ATP. Incubations with ¹⁴C-labeled compounds (ATP, leucine, and thymidine) for cell viability were initiated on board. Incubations with ¹⁸O-labeled water were used to quantify enzyme mediated isotopic exchange with phosphate. The incubation experiment on nitrate reduction coupled to autotrophic C uptake was performed by adding ¹⁵N-nitrate and ¹³C-bi-

carbonate. For other stable isotope incubation experiments (i.e., ¹³C- and/or ¹⁵N-labeled substrates) with sediment and basalt samples, see “[Single-cell analyses of carbon and nitrogen assimilation rates of subseafloor autotrophic and heterotrophic microbial community](#)” and “[Detection of metabolically active microorganisms in basaltic rocks](#),” respectively. Tracer amounts, specific activities, and isotope labeling percentages are listed in Table T9. Radiotracer amounts for the cell viability assays are listed in Table T10.

Stable isotope probing of subseafloor microbes with ¹³C-labeled tracers

With the ¹³C-labeled tracer approach, the objective is to cultivate marine subsurface microbes capable of utilizing benzoate, methanol, or acetate as a carbon source. The primary interest is to test for the presence of and identify aerobic and anaerobic benzoate degraders and methylotrophs. To encourage the growth of these organisms, aerobic and anaerobic microbial communities were incubated with low-nutrient conditions at close to in situ temperature. If these organisms are present and physiologically active (or even dormant in the case of anaerobes) in the South Pacific Gyre sediment, they are likely to be activated on the above-mentioned ¹³C-labeled carbon sources. Even very limited growth will yield partially or completely (minimum five generations) ¹³C-labeled DNA. This “heavy” DNA can be extracted from the microcosm, purified, and separated from nonlabeled, “light” ¹³C-DNA. The experiment will be conducted in time series, in which subsamples will be collected at selected intervals to monitor population change with time.

Crimp-sealed headspace vials (20 mL) were used to prepare the incubation samples. Sediment cores (4–5 cm³, except for Site U1365 where 3–4 cm³ was used) were subsampled from whole-round cores with cut-off syringes under sterile conditions and were immediately placed in the headspace vials in a stream of nitrogen and crimp sealed with a butyl rubber septums. All vials were baked at 450°C for minimum of 6 h to ensure complete combustion of residual organic carbon that might interfere with the postcruise analyses. Media composed of filter-sterilized (0.22 µm pore size membrane filter) surface seawater amended with specific ¹³C-stable isotope tracers were prepared for the experiment. Aliquots of these media were introduced to the respective incubation samples through the septum to ensure 50% inoculum. Overpressure in the samples was removed with a sterile needle filter that was briefly inserted through the septum. For anaerobic incubations, sample han-

dling was performed in under a stream of N₂ gas and media were additionally amended with FeCl₂ and Na₂S. Large inocula were used in all incubations to increase the concentration of viable cells. At the end of the expedition, all incubation samples were transferred to an onshore laboratory where they will be incubated in similar conditions for as long as 6 months for aerobic cultivations or 12 months for anaerobic cultivations. These shore-based incubation experiments will be subsampled periodically to monitor population change over time. In the case of aerobic cultivations, subsampling will be performed from the master slurry, whereas anaerobic cultures were quadrupled to facilitate study with four time points. ¹³C-labeled heavy DNA and nonlabeled light ¹³C-DNA will be extracted and separated by CsCl gradient ultracentrifugation.

Single-cell analyses of carbon and nitrogen assimilation rates of subseafloor autotrophic and heterotrophic microbial community

Previous studies of subseafloor microbial communities in continental margin sediments demonstrated that heterotrophs that utilize organic matter derived from photosynthesis are the predominant microbes in organic-rich sediments. Conversely, the sedimentary habitat in the South Pacific Gyre contains very little organic matter because of (1) the low primary photosynthetic production in the water column and (2) the extremely low sedimentation rates, which leave organic matter exposed at the seafloor for tens of thousands to hundreds of thousands of years. A list of potential electron donors ranged from the standard photosynthetically derived organic matter inputs such as reduced carbon and ammonium to the proposed radiolytic in situ production of hydrogen (D'Hondt et al., 2009). The rates of oxygen consumption through any of these processes may be so low as to be disguised by diffusion. Thus, experiments were performed to detect specific aerobic respiration pathways and to track potential routes of carbon and nitrogen fixation and turnover (also see “[Experiments with stable and radioactive isotopes](#)”). In using sensitive isotope tracer incubation methods on selected samples, such experimentation required immediate and proper sampling as well as access to the shipboard isotope facilities. Furthermore, we have interests in experimentally elucidating types of microbial metabolism in these ultra-oligotrophic sediments in the South Pacific Gyre.

To identify autotrophic and heterotrophic microbial populations, as well as their potential substrate uptake rates, sediment samples were incubated with various stable isotope-labeled substrates, including ¹³C-glucose, ¹³C-acetate, ¹³C-pyruvate, ¹³C-bicarbon-

ate, ¹³C-¹⁵N-amino acids mix, ¹³C-methane, and ¹⁵N-ammonia (Table T11). Given oxygen concentrations in interstitial water during Expedition 329, we set oxygen concentration in headspace of vials at ~4% (v/v) by adding filter-sterilized air. Individual samples of sediment (15 cm³) were collected with tip-cut 30 mL syringes, placed in 50 cm³ sterile glass vials sealed with rubber stoppers and screw caps, and stored at 10°C. The labeled substrates were injected (15 μM of ¹³C-labeled substrates and 1.5 μM of ¹⁵N-labeled ammonium, dissolved in 50–100 μL of sterile water) into each subcore sample and incubated at 10°C in a refrigerator in the Isotope Isolation Van and onshore after the expedition. All reagents and gas components, including air used for sample preparation, were filtered through 0.45 μm polycarbonate membranes. At each of four given time points (~2 weeks, 1 month, 6 months, and 12 months after starting incubation), vials were opened and sediment samples were fixed with 4% paraformaldehyde in PBS solution (or 2% formalin) and frozen for onshore single-cell analysis by NanoSIMS coupled with molecular ecological techniques.

Detection of metabolically active microorganisms in basaltic rocks

To detect the presence of metabolically active microorganisms in the basaltic basement and sediment/basalt interface in the South Pacific Gyre, the incorporation of stable isotope-labeled tracers (¹⁵N-labeled nitrate and ¹³C-labeled acetate and bicarbonate) into cells was investigated by incubation under microaerobic conditions, to be followed by postexpedition analysis with NanoSIMS. All experiments were duplicated, and a negative control was prepared with autoclaved samples. The experimental protocol was as follows:

1. Crushed basalt pieces (3–5 mL) and sterilized bottom seawater (20 mL) were placed in 67 mL wide-mouth glass vials for incubation under microaerobic conditions (~4% O₂). Headspace gas was replaced with N₂, and 11 mL of filtered air (0.2 μm pore diameter) was injected in the vial.
2. ¹⁵N-labeled sodium nitrate solution (100 μL; 20 mM) was added to the vial. The final concentration of ¹⁵N-nitrate was 100 μM.
3. For incubation with ¹³C-labeled sodium acetate or ¹³C-labeled sodium bicarbonate as the potential carbon substrate, 100 μL each of 20 mM substrate-stock solution was added.
4. At given time points (~4 weeks, 6 months, and 2 y after starting incubation), vials will be opened and basalt pieces will be fixed by placement in 4% paraformaldehyde in TBS solution or by freez-

ing for subsequent molecular analyses coupled with NanoSIMS.

Molecular analyses of seafloor microbial communities

Culture-independent molecular ecological techniques have shown that seafloor sediment harbors phylogenetically diverse microbial components that are generally distinct from isolates with known physiology. Previous studies of organic-rich sediments from the continental margins (e.g., offshore Peru, ODP Leg 201) suggest that geological and geochemical characteristics of seafloor microbial habitats (such as lithology, physical properties, and interstitial water chemistry) strongly impact microbial diversity and the community structure. However, microbial communities that inhabit organic-poor open-ocean sediment, which covers near 50% of the seafloor, remain uncharacterized.

During Expedition 329, sediment and basalt samples were collected for a variety of molecular ecological analyses. All of these samples for culture-independent molecular analyses were stored at -80°C after recovery. Bulk environmental DNA and RNA will be directly extracted from contaminant-free or relatively uncontaminated material. If the extracted DNA or RNA concentration is not high enough for molecular analyses, the extracted DNA may be further amplified by multiple displacement amplification with phi29 polymerase (e.g., Forschner et al., 2008).

Spatial distribution of microbial community composition and the structure will be intensively studied by statistical analysis of polymerase chain reaction (PCR)-amplified fragments of 16S rRNA gene sequences (e.g., Inagaki et al., 2006). A powerful new approach using 454 Life Sciences high-throughput sequencing technologies will allow us to determine (1) microbial diversity, (2) community structure, and (3) phylogenetic affinities based on large numbers of 16S rRNA gene-tagged PCR fragments (e.g., Sogin et al., 2006). RNA sequencing studies, such as 16S rRNA and mRNA, will document the composition and functional taxonomy of the actively growing and metabolizing fraction of the microbial community. These high-throughput molecular studies will quantify bacterial and archaeal diversity richness and evenness in this little explored seafloor environment and enable detection of rare members that cannot be sampled using conventional capillary sequencing approaches.

A functional gene survey for key metabolic pathways is a powerful molecular ecological approach for identification of the potential function of biogeochemically significant microbial metabolisms. Because the

South Pacific Gyre subsurface is very different from previously explored seafloor microbial habitats in terms of nutrient and energy constraints, physiological characteristics of its microbial communities are also expected to be different. For example, its most deeply buried microbial communities may primarily rely on inorganic nutrient and energy sources (e.g., radiolytic H_2). Given this hypothesis, sediment of the South Pacific Gyre subsurface may harbor (micro)aerobic chemolithoautotrophic or chemoorganotrophic mesophiles, including hydrogenotrophic aerobes and nitrate or nitrite reducers. Using DNA from the South Pacific Gyre, we will attempt PCR detection and quantification (if possible) of some specific 16S rRNA and functional genes, such as carbon fixation pathways and key genes for aerobic respiration in shallow to deep sediment and the underlying basalt.

Physical properties

Physical property measurements provide fundamental information required to characterize lithostratigraphic units and allow for the correlation of cored materials with downhole logging data. The primary objective of the Expedition 329 physical properties program was to collect high-resolution data to document microbial habitats in both the sedimentary and basement environments. A variety of techniques and methods were used to characterize Expedition 329 sediment and basement core samples.

In general, three holes were drilled at each site after a pilot hole was washed in. Generally the first hole (Hole B) was dedicated to physical property measurements and the other two or more holes had whole rounds removed for geochemical or microbiological sampling. The remains of these cores were also logged and measured for physical properties but often at increased measurement spacing because of the now-incomplete sections.

Recovered whole-round cores were first allowed to thermally equilibrate to ambient room temperature of $\sim 20^{\circ}\text{C}$ (3 h for hard rock and 4 h for sedimentary material). After thermal equilibration, core sections with continuous intervals longer than 8 cm were run through the WRMSL for measurement of gamma ray attenuation (GRA) density, magnetic susceptibility, and compressional wave velocity (*P*-wave logger [PWL]). The noncontact resistance logger was not functional during Expedition 329. Sections longer than 50 cm were measured with the spectral Natural Gamma Ray Logger (NGRL).

After measurements with the WRMSL and NGRL, the cores were split into archive and working halves. The archive half of the core sections was passed first

through the SHIL to quickly obtain a digital image of the core section and avoid color changes caused by sediment oxidation and drying (see “**Lithostratigraphy, igneous petrology, alteration, and structural geology**”). Subsequently, the archive half sections were run on the SHMSL for measurement of point magnetic susceptibility and spectrophotometry (sediment color reflectance, see below). The SHMSL also uses a laser to detect cracks and gaps along the core.

Thermal conductivity was measured using the Teka (Berlin, Germany) thermal conductivity instrument. For cores with un lithified sediment, thermal conductivity measurements were carried out on whole-round core sections using the needle probe technique. For lithified sediment or basement samples, thermal conductivity was measured on split core using the half-space technique. In all cases thermal conductivity was measured using the Teka thermal conductivity instrument.

Discrete samples were taken from the working half at intervals of ~1 or 2 per core. Discrete measurements were used to measure compressional wave velocity in three directions, and moisture and density (MAD) samples were taken to measure wet bulk density, dry bulk density, grain density, water content, void ratio, and porosity. A comprehensive discussion of methodologies and calculations used in the *JOIDES Resolution* Physical Properties Laboratory is presented in Blum (1997). Details about each physical property measurement are described below.

Whole-Round Multisensor Logger measurements

GRA bulk density and magnetic susceptibility were measured nondestructively with the WRMSL. To optimize WRMSL performance, sampling intervals and measurement integration times were the same for all sensors. Sampling intervals were set at 2 cm with an integration time of 5 s for each measurement. These sampling intervals are common denominators of the distances between the sensors installed on the WRMSL (30–50 cm) and allow sequential and simultaneous measurements. GRA performance was monitored by passing a single core liner filled with deionized water through the WRMSL after every core.

In general, measurements are most effective on materials that completely fill the core liner and have minimal drilling disturbance. For sediment cores, the core liner has a diameter of 66 mm and is assumed to be filled. Basement sections are cored with a maximum diameter of 58.5 mm, and recovered pieces are often smaller than the maximum diameter. Therefore, GRA bulk density and magnetic susceptibility measurements tend to underestimate true

values. This bias is minimized by multiplying basalt densities by $66/58.5 = 1.18$. Additionally, many measurements of density suffer from dropouts caused by gaps between core pieces. Dropouts were minimized by removing densities $<2 \text{ g/cm}^3$.

Gamma ray attenuation bulk density

The GRA densiometer on the WRMSL operates by passing gamma rays from a ^{137}Cs source through a whole-round core into a 75 mm \times 75 mm sodium iodide detector situated directly below the core. The gamma ray peak has a principal energy of 0.662 MeV and is attenuated as it passes through the core (Evans, 1965; Harms and Choquette, 1965). The attenuation of gamma rays, mainly by Compton scattering, is related to the material bulk density and thickness of sample. The gamma ray count is proportional to density. Bulk density, ρ , determined with this method can be expressed as

$$\rho = 1/(\mu d) \times \ln(I_0/I), \quad (10)$$

where

- μ = Compton attenuation coefficient,
- d = sample diameter,
- I_0 = gamma ray source intensity, and
- I = measured intensity of gamma rays passing through the sample.

The values μ and I_0 are treated as constants, such that ρ can be calculated from I . The gamma ray detector is calibrated with a set of aligned aluminum cylinders of various diameters surrounded by distilled water in a sealed core liner that is the same as that used during coring operations. The relationship between I and the product of μ and d can be expressed as

$$\ln(I) = A(\mu d)^2 + B(\mu d) + C, \quad (11)$$

where A , B , and C are coefficients determined during calibration. Gamma ray counts through each cylinder were determined for a period of 60 s, and the natural log of resulting intensities was plotted as a function of μd . Here, ρ of each aluminum cylinder was 2.7 g/cm^3 , and d was 1, 2, 3, 4, 5, or 6 cm. These coefficients fluctuated slightly during the time period over which the measurements were made, as indicated by repeated calibrations. The WRMSL provided the values of I and μ , and ρ was calculated with the above equation. Recalibration was performed as needed if the deionized standard after every core deviated significantly (more than a few percent) from 1 g/cm^3 . The spatial resolution of the GRA is $<1 \text{ cm}$.

Magnetic susceptibility

Magnetic susceptibility, k , is a dimensionless measure of the degree to which a material can be magnetized by an external magnetic field,

$$k = M/H, \quad (12)$$

where M is the magnetization induced in the material by an external field strength H . Magnetic susceptibility responds to variations in the magnetic composition of the sediment that commonly can be related to mineralogical composition (e.g., terrigenous versus biogenic materials) and diagenetic overprinting. Materials such as clay, possibly from alteration of igneous materials, have a magnetic susceptibility several orders of magnitude lower than magnetite and some other iron oxides that are common constituents of igneous material. Water and plastics (core liner) have a slightly negative magnetic susceptibility.

The WRMSL incorporates a Bartington Instruments MS2 meter coupled to a MS2C sensor coil with a diameter of 8.8 cm operating at a frequency of 565 Hz. The sensor output can be set to centimeter-gram-second (cgs) units or SI units, with the IODP standard being the SI setting. The core diameter is smaller than the aperture through which it passes to be measured. Therefore, a volume correction factor must be applied to the data offline. Assuming a core diameter of 66 mm and using the coil aperture of 88 mm, the correction factor simply entailed multiplying the 10^{-5} SI units by a factor of 0.68 (Blum, 1997).

The instrument is calibrated with a homogeneous mixture of magnetite and epoxy in a 40 cm long piece of core liner to an accuracy of $\pm 5\%$. However, this calibration is a factory preset. The resolution of the method is ± 4 cm; therefore, core material that is not continuous over an 8 cm interval underestimates the magnetic susceptibility.

P-wave logger measurements

P-wave velocity varies with lithology, porosity, and bulk density of material; state of stress; temperature; and fabric or degree of fracturing. In sediment and rock, velocity is controlled by degree of consolidation and lithification. Because the contact between the core liners and hard rock samples is often poor, P-wave velocity measurement was not run on basement cores.

The PWL sensor measures the ultrasonic P-wave velocity of the whole-round sample residing in the core liner. The PWL transmits a 500 kHz P-wave pulse across the core section at a specified repetition rate. This signal is coupled to the sample by the plastic

pole contacts of the transducers clamped to the sides of the core by the linear actuator. No water is used to improve coupling between the transducers and the liner. The plastic pole contacts and the pressure applied by the actuator are sufficient for reliable P-wave measurement. The transmitting and receiving ultrasonic transducers are aligned so that wave propagation is perpendicular to the long axis of the core section. Torque applied by the actuator can be set by the user to ensure good acoustic contact between the liner and the core material.

The basic relationship for sonic velocity, V , is

$$V = d/t, \quad (13)$$

where d is the path length of the wave through the core and t is the traveltime. The total traveltime between the transducers includes three components:

- t_{delay} (time delay related to transducer faces and electronic circuitry),
- t_{pulse} (delay related to the peak detection procedure), and
- t_{liner} (transit time through the core liner).

The system is calibrated using a core liner filled with pure water. For routine measurement on whole-round cores inside core liners, the corrected core velocity, V_{core} , can be expressed by

$$V_{\text{core}} = (d'_{\text{core}} - 2d_{\text{liner}})/(t_0 - t_{\text{pulse}} - t_{\text{delay}} - 2t_{\text{liner}}), \quad (14)$$

where

- d'_{core} = measured diameter of core and liner,
- d_{liner} = liner wall thickness, and
- t_0 = measured total traveltime.

Traveltime is determined by signal-processing software that automatically detects first arrival of the P-wave signal to a precision of 50 ns. It is a challenge for an automated routine to pick the first arrival of a potentially weak signal if background noise is high. The search method skips the first positive amplitude and finds the second positive amplitude using a detection threshold limit, typically set to 30% of the maximum amplitude of the signal. It then finds the preceding zero crossing and subtracts one wave period to determine the first arrival. To avoid extremely weak signals, minimum signal strength can be set (typically 0.02 V) and weaker signals are ignored. To avoid signal interference at the beginning of the record from the receiver, a delay (typically 0.01 ms) can be set to force the amplitude search to begin in the quiet interval preceding the first arrival. In addition, a trigger (typically 4 V) is selected to initiate the arrival search process, and the number of waveforms to be stacked (typically five) can also be set. A linear voltage differential transformer mea-

asures the separation of the transducer to derive a signal path length (i.e., the core diameter). After corrections for system propagation delay, liner thickness, and liner material velocity, the ultrasonic *P*-wave velocity is calculated.

Natural Gamma Radiation Logger measurements

The NGRL installed on the *JOIDES Resolution* was designed and built at the Texas A&M University (College Station, Texas, USA) IODP facility between 2006 and 2008. The NGRL measures gamma rays emitted from whole-round core sections arising primarily from the decay of ^{238}U , ^{232}Th , and ^{40}K isotopes.

The main NGR detector unit consists of 8 sodium iodide (NaI) scintillator detectors, 7 plastic scintillator detectors, 22 photomultipliers, and passive lead shielding. The NaI detectors are covered by 8 cm of lead shielding. In addition, lead separators (~7 cm of low-background lead) are positioned between the NaI detectors. Half of the lead shielding closest to the NaI detectors is composed of low-background lead, whereas the outer half is composed of regular (virgin) lead. In addition to passive lead shielding, the NGRL employs a plastic scintillator to suppress the high-energy gamma and muon components of cosmic radiation by producing a cancelling signal when these charged particles pass through the plastic scintillators. The NGRL was calibrated using a source consisting of ^{137}Cs and ^{60}Co and identifying the peaks at 662 and 1330 keV, respectively. Calibration materials are provided by Eckert and Ziegler Isotope Products, Valencia, California (USA).

For presentation purposes, the counts were summed over 100–3000 keV and are thus comparable with data collection from previous cruises and are appropriate for direct comparison with downhole logging data. Background measurements of an empty core liner counted for 20,000 s (5 h) were made upon arrival at each site. Over the 100–3000 keV integration range background counts averaged 4–5 cps and contributed <0.5% to the overall signal of the measured core.

A measurement run consisted of eight measurements offset by 20 cm each, first at one position and measured at a second position shifted 10 cm from the first (for a total of 16 measurements, each 10 cm apart, for a 150 cm long section of core). The quality of the energy spectrum measured in a core depends on the concentration of radionuclides in the sample, but also on the counting time, with higher times yielding better spectra. The available count time in each position depends on core flow through the lab.

In general, we had the opportunity to count for longer times, yielding statistically significant energy spectra. Count times ranged between 1800 and 5400 s for each position, resulting in total count times of 1–3 h per section. Shorter count times were used on holes where whole rounds had been sampled for geochemistry or microbiology. These times were ~1800 s or less. Improved spectral resolution allows qualitative identification of the main contributors to the energy spectra (i.e., products of the ^{40}K , ^{232}Th , or ^{238}U decay chains). Building a database of well-resolved spectra works toward the goal of separating ^{40}K , ^{232}Th , and ^{238}U contributions and eventual quantifying concentrations of the radionuclide daughters.

Section Half Multisensor Logger measurements

The SHMSL measures magnetic susceptibility and spectral reflectance on core-section halves. The archive half of the split core is placed on the system's core track. An electronic platform moves along a track above the core section, recording the sample height with a laser sensor. The laser establishes the location of the bottom of the section and the platform reverses the direction of movement, moving from bottom to top making measurements of point magnetic susceptibility and spectral reflectance data at 2 cm intervals.

Color reflectance spectrometry

Reflectance is measured from 171 to 1100 nm wavelength at 2 nm intervals using a halogen light source, covering wavelengths from ultraviolet through visible to near infrared. The scan of the entire wavelength range takes ~5 s per data acquisition offset. The data are generated using the L^*a^*b color system, in which L^* is luminescence, a^* is the blue + green values, and b^* is the red + green values. The color reflectance spectrometer calibrates on two spectra: pure white (reference) and pure black (dark). Color calibration was conducted approximately every 12 h.

Point magnetic susceptibility

Point magnetic susceptibility is measured using a contact probe with a flat 15 mm diameter sensor operating at a frequency of 0.580 kHz. The sensor averages three measurements at 0.1 attenuation for each offset to an accuracy of 5%. The spatial resolution of the magnetic susceptibility point instrument is 20 mm, making it advantageous over whole-round magnetic susceptibility for basement cores consist-

ing of broken pieces smaller than 8 cm (the spatial resolution of whole-round magnetic susceptibility). Units are reported in dimensionless SI units on a volume basis. The point magnetic susceptibility meter was calibrated by the manufacturer before its installation on the ship. The probe is zeroed in air before each measurement point, and a background magnetic field (i.e., influence from metal track and so on) is measured and removed from the data before being output. The instrument calibration assumes that the probe is buried in the sample. However, because the probe is only in contact with the upper, flat surface, a correction factor of 2× was applied after the data were collected. Note that the data stored in LIMS have not had this correction applied.

Thermal conductivity

Thermal conductivity is the rate at which heat flows through a material and is dependent on composition, porosity, and structure. Thermal conductivity was measured on unconsolidated sediment and rock samples using either the full-space needle probe (Von Herzen and Maxwell, 1959) or the half-space line source (Vacquier, 1985), respectively. Both the full- and half-space methods approximate the heating element as an infinite line source (Blum, 1997). These measurements produce a scalar value in a plane perpendicular to the orientation of the probe. All measurements were made after the cores had equilibrated to ambient laboratory temperature. At the beginning of each measurement, temperatures in the samples were monitored to ensure that the background thermal drift was $<0.04^{\circ}\text{C}/\text{min}$. After the background thermal drift was determined to be stable, the heater circuit was closed and the increase in the probe temperature was recorded. In most cases, the reported thermal conductivity value for full-space needle-probe measurements is the average of at least three repeated measurements. Reported half-space line-source thermal conductivity values typically represent the average of between five and ten repeated measurements. Based on these repeated measurements, individual measurements are usually within 1% of the mean for both full- and half-space measurements. Both of these values are within the stated uncertainty of 5% (Blum, 1997). All data are corrected to in situ pressure and temperature, assuming a hydrostatic pressure gradient and a background temperature gradient based on advanced piston corer temperature tool (APCT-3) measurement. The pressure correction is +1% for each 1800 m depth (Ratcliffe, 1960).

In porous rock, temperature influences thermal conductivity in two competing ways. The thermal conductivity of rock matrix is inversely related to tem-

perature (Zoth and Haenel, 1988), whereas the thermal conductivity of water increases with temperature (Keenan et al., 1978). The temperature correction is +1% for each $+20^{\circ}\text{C}$ change in temperature between the laboratory and in situ conditions, a value intermediate between the +5% suggested by Ratcliff (1960) for a high-porosity, water-saturated sediment and the mean value of -3% derived from data reported by Clark (1966) for several hard rocks. Both uncorrected and corrected values of thermal conductivity are reported.

Soft-sediment full-space measurements

A full-space, single-needle TeKa TK04 probe unit (Blum, 1997) was utilized to measure thermal conductivity of whole cores. To insert this probe, a 2 mm hole was made in the core liner at a position based on visual inspection of the core. Needle probes consist of a heater wire and a thermistor. At the beginning of each measurement, temperature in the sediment is monitored to ensure that a thermal drift of no more than $0.4\text{ mK}/\text{min}$ is present. This step normally takes a minute or two. After the temperature field is determined to be near equilibrium, a calibrated heat source is applied and the rise in temperature is recorded for $\sim 80\text{ s}$. Values of thermal conductivity are based on the observed rise in temperature for a given quantity of heat. In most cases, repeated measurements were made at the same location. For these repeated measurements, the needle probe is left in place and the sample is left to reequilibrate for 10 min prior to the next measurement. Consequently, most of the time a measurement takes is waiting for the sample to reequilibrate.

Lithified sediment and hard rock half-space measurements

Thermal conductivity on basement samples was measured on the archive half of the split core with the thermal conductivity meter in half-space mode (Vacquier, 1985). Samples must be smooth to ensure adequate contact with the heating needle. Visible saw marks were removed when necessary by grinding and polishing the split surface with 120–320 gauge silicon carbide powder. Most samples did not require polishing. Basement samples equilibrated to room temperature in a seawater vacuum saturator for 24 h, and sample and sensor needle were equilibrated together in a cooler insulated with styrofoam for at least 15 min prior to measurement. Isolation of the sample and sensor needle eliminated the effect of rapid but small temperature changes introduced by air currents in the laboratory. The instrument internally measures drift and does not begin a heating run until sufficient thermal equilibrium is attained.

Cores were measured at irregular intervals (aiming for one sample per section) depending on the availability of homogeneous and relatively vein/crack-free pieces long enough to be measured without edge effects (pieces at least 7 cm long; i.e., longer than the instrument needle).

Formation factor

Formation factor was determined from electrical conductivity measurements taken every 10 cm on split sediment cores. Formation factor may be used to quantify chemical fluxes through the sediment. For these measurements, two in-line electrodes, 1.5 cm long and spaced 1 cm apart in a block of nonconducting fluoropolymer and attached to a Metrohm 712 conductometer, were inserted into the split-core sediment. Standards were measured before and after approximately every seventh measurement. This means that a standard was measured prior to, in the middle of, and after each core section.

At each sampling location, measurements of sediment conductivity, χ_{sed} (the inverse of resistivity, R_{core}), and sediment temperature were made. Measurement of seawater conductivity, χ_{sw} , and its temperature were made regularly.

Both seawater and sediment measurements of electrical conductivity were adjusted to a standard temperature of 20°C where the correction factor is given by a fifth-order polynomial (Janz and Singer, 1975),

$$\chi = a + bT + cT^2 + dT^3 + eT^4 + fT^5, \quad (15)$$

where

$$\begin{aligned} a &= 29.05128, \\ b &= 0.88082, \\ c &= -0.000198312, \\ d &= 0.00033363, \\ e &= -0.000010776, \text{ and} \\ f &= 0.000000112518. \end{aligned}$$

The temperature corrected measurement, σ_T , is given by

$$\sigma_T = \sigma \times (\chi_{20}/\chi_{\text{obs}}), \quad (16)$$

where σ is the measurement and χ_{20} and χ_{obs} are the correction factors using 20°C and the observed temperature, respectively. Both seawater and sediment measurements of electrical conductivity are adjusted for the effects of temperature. A linear drift correction based on the seawater measurements is computed and applied to both the sediment and seawater temperature adjusted measurements and the formation factor, F , is computed as,

$$F = \chi_{\text{sw}}/\chi_{\text{sed}}. \quad (17)$$

This simple method for determining formation factor does not take into account surface conductivity effects of the sediment matrix. However, this is not of concern in high-porosity sediments where the conductive pathways depend dominantly on intergranular porosity and pore connectivity, even where the sediment matrix contains significant clay.

Discrete sample measurements

Cubic samples were cut from the working halves of split cores at an interval of ~1 sample per section for both sediment and basement cores. These ~7 cm³ samples aimed to best represent the general variation and lithologies of the core. The purpose of these samples is two-fold. First, they are used for physical property measurements of compressional wave velocity and moisture and density measurements (discussed below). Second, discrete samples were shared with paleomagnetists to minimize core depletion.

Moisture and density

Several basic quantities of interest (water content, bulk density, dry density, porosity, and void ratio) are found most accurately through mass and volume determinations on discrete samples. MAD data are also used for comparison with GRA bulk density data from the WRMSL. The shipboard MAD facility on the *JOIDES Resolution* includes a dual-balance system and a hexapycnometer. During Expedition 329, only five cells were available, transforming this system to a pentapycnometer. For hard rock samples, a vacuum water saturator is also used.

Vacuum water saturator

Basement samples were saturated in a vacuum-pump system. Samples were placed in a plastic chamber filled with seawater. A vacuum pump removed the air from the chamber, drawing seawater into the samples. The samples were saturated for at least 24 h. During this time, the vacuum was checked at 2–3 h intervals for possible leaks. After removal from the saturator, the cubes were stored in sample containers filled with seawater to help prevent evaporation of interstitial water. Next, the cube surfaces were patted dry with a paper towel and wet mass was immediately determined using the dual-balance system.

Dual-balance system

The dual-balance system was used to measure both wet and dry masses. The two analytical balances (Mettler-Toledo XS204) were used to compensate for ship motion, one acting as a reference and the other

for measurement of the unknown. A standard weight of similar value to the sample was placed on the reference balance to increase accuracy. The default setting of the balances is 300 measurements (taking ~1.5 min).

Hexapycnometer system

The hexapycnometer system measures dry sample volume using pressurized, helium-filled chambers. At the start of the expedition and whenever the helium gas tank was changed, shipboard technicians performed a calibration using stainless steel spheres of known volume. A batch of samples consisted of four cells with samples of unknown volumes and one cell with two stainless steel spheres (3 and 7 cm³). The spheres were cycled through the cells to identify any systematic error and/or instrument drift. Spheres are assumed to be within 1% of their total volume. Individual volume measurements were preceded by three purges of the sample chambers with research-grade (99.995% or better) helium heated to 28°C, followed by three data acquisition cycles.

Wet and dry mass measurements

Immediately after sediment samples were collected or basement samples were saturated, the wet sediment mass (M_{wet}) was measured. Dry sediment mass (M_{dry}) and volume (V_{dry}) were measured after drying the samples in a convection oven for >24 h at a temperature of 105° ± 5°C. Dried samples were then cooled in a desiccator for >1 h before the dry mass was measured. Dry volume was measured using a helium-displacement pycnometer with a nominal precision of ±0.04 cm³. Each reported value consists of an average of three measurements. A reference volume (calibrated sphere) was run with each group of four samples, and the sphere was rotated between cells to check for systematic error.

For calculation of sediment bulk density, dry density, grain density, porosity, and void ratio, the traditional ODP method was used (Method C). Water content, porosity, and void ratio were defined by the mass or volume of extracted water before and after removal of interstitial water through the drying process. Standard seawater density (1.024 g/cm³) was used for the density of interstitial water. For basement samples that were too vesicular to saturate, we calculated these values using “Method D,” where volume is determined by caliper rather than by saturation and helium-displacement pycnometer.

Water content

Water content (W_c) was determined using the methods of the American Society for Testing and Materials (ASTM) designation D2216 (ASTM International, 1990). Corrections are required for salt when measuring the water content of marine samples. In addition to the recommended water content calculation in ASTM D2216 (i.e., the ratio of pore-fluid mass to dry sediment mass [percent dry weight]), we also calculated the ratio of pore-fluid mass to total sample mass (percent wet weight). The equations for water content were

$$W_c (\% \text{ dry wt}) = (M_t - M_d)/(M_d - rM_t) \quad (18)$$

and

$$W_c (\% \text{ wet wt}) = (M_t - M_d) \times (1 + r)/M_t \quad (19)$$

where

- M_t = total mass of the saturated sample,
- M_d = mass of the dried sample, and
- r = salinity.

Bulk density

Bulk density (ρ) is the density of the saturated samples, with $\rho = M_t/V_t$. The mass, M_t , was measured using the balance, and V_t was determined from the pycnometer measurements of grain volume and the calculated volume of the pore fluid ($V_t = V_{\text{pore}} + V_d$). For the high-porosity samples from Expedition 329, bulk density was determined directly from $\rho = M_t/V_t$.

Porosity

Porosity (ϕ) was calculated using

$$\phi = (W_c \times \rho)/[(1 + W_c) \times \rho_w], \quad (20)$$

where

- ρ = measured bulk density,
- ρ_w = density of the pore fluid, and
- W_c = water content expressed as a decimal ratio of percent dry weight.

Grain density

The grain density (ρ_{grain}) was determined from measurements of dry mass and dry volume made in the balance and in the pycnometer, respectively. Mass and volume were corrected for salt using

$$\rho_{\text{grain}} = (M_d - s)/[V_d - (s/\rho_{\text{salt}})], \quad (21)$$

where s is the salt content (in grams) and ρ_{salt} is the density of salt (2.257 g/cm^3).

Compressional wave velocity

Discrete compressional wave (P -wave) velocity measurements were obtained on sediment cores at a frequency of one per core. For basement samples, we used the same discrete cube samples that were also used for MAD and paleomagnetism determinations. P -wave measurements were performed on seawater-saturated samples directly after wet mass determinations were made. Measurements used the x -axis caliper-type contact probe transducers on the P -wave velocity gantry. Oriented samples were rotated manually to measure y - and z - axis velocities with the same instrument. The system uses Panametrics-NDT Microscan delay line transducers, which transmit at 0.5 MHz. To maximize contact with the transducers, deionized water was applied to sample surfaces.

The signal received through the sample was recorded by the computer attached to the system, and the peak of the initial arrival was chosen with autopicking software. The complete waveform was stored with the data in case reanalysis is deemed necessary. However, visual checks of the picks made on board appeared satisfactory. The distance between transducers was measured with a built-in linear voltage displacement transformer (LDVT).

Calibration was performed each day, before measurements were made, with a series of acrylic cylinders of differing thicknesses and known P -wave velocity of $2750 \pm 20 \text{ m/s}$. The determined system time delay from calibration was subtracted from the picked arrival time to yield a traveltime of the P -wave through the sample. The thickness of the sample (calculated by LDVT in meters) was divided by the traveltime (in seconds) to calculate a P -wave velocity in meters per second.

Downhole temperature measurements

Downhole temperature measurements were made using the APCT-3. The APCT-3 is the third-generation tool of its kind and is used with advanced piston coring. The APCT-3 consists of three components: electronics, coring hardware, and computer software (Heeseman et al., 2006). In this expedition, downhole temperature measurements were made approximately every third core during APC coring when sediments were thick enough. The temperature sensors were calibrated for a working range of $0^\circ\text{--}45^\circ\text{C}$.

Before entering a hole, each instrument was held at the mudline for $\sim 5 \text{ min}$ to equilibrate with bottom

water temperature. After bottom water temperature equilibration, the tools were lowered down the hole and penetrated the formation. The penetration of the tool into the formation caused a rise in temperature because of frictional heating. Following the initial temperature rise, temperatures decreased along a decay curve to near equilibrium. During this decay phase, it is important that the temperature tool is not disturbed. A second rise in temperature was due to frictional heating as the tool was pulled out of the formation. Temperatures were measured as a time series with a sampling rate of 1 s and logged onto a microprocessor within the downhole tool. Data were retrieved when the tool was recovered. The formation equilibrium temperature was determined based on fitting the temperature decay curve using the program TP-Fit, which runs on MATLAB (M. Heeseman et al., pers. comm., 2008).

Downhole measurements

The main objectives of the Expedition 329 downhole measurement program are to document crustal physical properties, define structural and lithologic boundaries as a function of depth, and identify alteration in the basaltic basement from the passage of fluids. In addition, wireline logging data allow us to delineate alteration patterns, fracture densities, and structural orientations and determine how these correlate with current and paleostress environments. Comparison of wireline logging data to laboratory analyses of discrete samples helped to document the physical and chemical nature of the drilled environments. In this way, they document important constraints on subseafloor habitability. For example, the wireline logs complement core measurements by documenting the thickness of lithologic units in intervals where core recovery is poor.

Downhole logs are used to determine physical, chemical, and structural properties of the formation penetrated by a borehole. The data are rapidly collected, continuous with depth, and measured in situ; they can be interpreted in terms of the stratigraphy, lithology, mineralogy, and geochemical composition of the penetrated formation. Where core recovery is incomplete or disturbed, log data may provide the only way to characterize the borehole section; where core recovery is good, log and core data complement one another and may be interpreted jointly. Borehole logging and core-log integration are invaluable for reconstructing recovery gaps and estimating bulk geochemical and structural characteristics of deep basement drill sites.

Downhole logs are sensitive to formation properties on a scale that is intermediate between the scale of

data obtained from laboratory measurements on core samples and the scale of data obtained from geophysical surveys. They are useful in calibrating the interpretation of geophysical survey data (e.g., through the use of synthetic seismograms) and they provide a necessary link for the integrated understanding of physical properties on all scales.

Wireline logging

During wireline logging, logs were made with a variety of Schlumberger logging tools combined into several tool strings, which were run down the hole after coring operations were completed. Two wireline tool strings were used during Expedition 329 (Fig. F12; Table T12), the triple combination (triple combo; gamma radiation, density, and electrical resistivity) and the Formation MicroScanner (FMS)-gamma (gamma radiation, and microresistivity image of the borehole wall).

In preparation for logging, the boreholes were flushed of debris by circulating with seawater through the drill pipe to the bottom of the hole. The BHA was pulled up. The tool strings were then lowered downhole by a seven-conductor wireline cable during sequential runs. A wireline heave compensator was employed to minimize the effect of ship's heave on the tool position in the borehole. During each logging run, incoming data were recorded and monitored in real time on the MCM MAXIS logging computer. The tool strings were then pulled up at constant speed, typically 250–300 m/h, to provide continuous measurements as a function of depth of several properties simultaneously.

Logged sediment properties and tool measurement principles

The logged properties, and the methods that the tools use to measure them, are briefly described below. The main logs taken by the tools are listed in Table T13. More detailed information on individual tools and their geological applications may be found in Ellis and Singer (2007), Goldberg (1997), Lovell et al. (1998), Rider (1996), Schlumberger (1989, 1994), and Serra (1984, 1986, 1989).

Natural radioactivity

The Hostile Environment Natural Gamma Ray Sonde (HNGS) uses two bismuth germanate scintillation detectors and five-window spectroscopy to determine concentrations of ^{40}K , ^{232}Th , and ^{238}U . The isotopes of these three elements dominate the natural radiation spectrum. The HNGS filters out gamma ray energies below 500 keV, eliminating sensitivity to bentonite or KCl in the drilling mud and improving

measurement accuracy. The computation of the elemental abundances uses a least-squares method of extracting thorium, uranium, and potassium elemental concentrations from the spectral measurements.

Density and photoelectric effect

Formation density was determined with the Hostile Environment Litho-Density Sonde (HLDS). The sonde contains a radioactive cesium (^{137}Cs) gamma ray source (622 keV) and far and near gamma ray detectors mounted on a shielded skid, which is pressed against the borehole wall by a hydraulically activated eccentricizing arm. Gamma rays emitted by the source undergo Compton scattering, which involves the transfer of energy from gamma rays to the electrons in the formation through elastic collision. The number of scattered gamma rays that reach the detectors is directly related to the density of electrons in the formation, which is in turn related to bulk density. Porosity may also be derived from this bulk density if the matrix (grain) density is known.

The HLDS also measures photoelectric absorption as the photoelectric effect (PEF). Photoelectric absorption of the gamma rays occurs when their energy is reduced below 150 keV after being repeatedly scattered by electrons in the formation. Because PEF depends on the atomic number of the elements in the formation, it also varies according to the chemical composition of the minerals present. Good contact between the tool and borehole wall is essential for good HLDS logs; poor contact results in underestimation of density values.

Electrical resistivity

The phasor dual induction–spherically focused resistivity tool (DITE-SFL) was used to measure electrical resistivity. The DITE-SFL provides three measures of electrical resistivity, each with a different depth of investigation into the formation. The two induction devices (deep and medium depths of penetration) transmit high-frequency alternating currents through transmitter coils, creating magnetic fields that induce secondary currents in the formation. These currents produce a new inductive signal, proportional to the conductivity of the formation, which is measured by the receiving coils. The measured conductivities are then converted to resistivity (in units of ohm-meters). For the shallow penetration resistivity, the current necessary to maintain a constant drop in voltage across a fixed interval is measured; this is a direct measurement of resistivity. Typically, igneous minerals found in crustal rocks are electrical insulators, whereas sulfide and oxide minerals as well as ionic solutions like interstitial water

are conductors. Electrical resistivity, therefore, can be used to evaluate porosity (with Archie's law) and fluid salinity.

Formation MicroScanner

The FMS provides high-resolution electrical resistivity-based images of borehole walls. The tool has four orthogonal arms and pads, each containing 16 button electrodes that are pressed against the borehole wall during recording. The electrodes are arranged in two diagonally offset rows of eight electrodes each. A focused current is emitted from the button electrodes into the formation, with a return electrode near the top of the tool. Resistivity of the formation at the button electrodes is derived from the intensity of current passing through the button electrodes. Processing transforms these measurements into oriented high-resolution images that reveal the geologic structures of the borehole wall. Further analysis can provide measurements of dip and direction (azimuth) of planar features in the formation.

The development of the FMS tool has added a new dimension to wireline logging (Luthi, 1990; Lovell et al., 1998; Salimullah and Stow, 1992). Features such as bedding, fracturing, slump folding, and bioturbation can be resolved; the fact that the images are oriented means that fabric analysis can be carried out and bed orientations can be measured.

The maximum extension of the caliper arms is 38.1 cm (15 inches). In holes with a diameter >38.1 cm, the pad contact will be inconsistent and the FMS images may appear out of focus and too conductive. Irregular (rough) borehole walls will also adversely affect the images if contact with the wall is poor.

Log data quality

The principal influence on log data quality is the condition of the borehole wall. If the borehole diameter is variable over short intervals resulting from washouts during drilling or ledges caused by layers of harder material, the logs from those tools that require good contact with the borehole wall (i.e., FMS and density) may be degraded. Deep investigation measurements such as resistivity and sonic velocity, which do not require contact with the borehole wall, are generally less sensitive to borehole conditions. Very narrow ("bridged") sections will also cause irregular log results. The quality of the borehole is improved by minimizing the circulation of drilling fluid while drilling, flushing the borehole to remove debris, and logging as soon as possible after drilling and conditioning are completed.

The quality of the depth determination depends on a series of factors. The depth of the wireline-logged

measurement is determined from the length of the logging cable played out at the winch on the ship. The seafloor is identified on the natural gamma log by the abrupt reduction in gamma ray count at the water/sediment boundary (mudline). Discrepancies between the drillers depth and the wireline log depth occur because of core expansion, incomplete core recovery, incomplete heave compensation, and drill pipe stretch in the case of drillers depth. In the case of log depth, discrepancies occur because of incomplete heave compensation, incomplete correction for cable stretch, and cable slip. Tidal changes in sea level also have an effect. To minimize the wireline tool motion caused by ship heave, a new hydraulic wireline heave compensator adjusts for rig motion during wireline logging operations.

Logging data flow and log depth scales

Data for each wireline logging run were monitored in real time and recorded using the Schlumberger MAXIS 500 system. The initial logging data are referenced to the rig floor (wireline depth below rig floor). After logging was completed, the data were shifted to a seafloor reference (wireline depth below seafloor).

The data were transferred onshore to Lamont-Doherty Earth Observatory, where standardized data processing took place. The main part of the processing is depth matching to remove depth offsets between data from different logging runs, which results in a new depth scale, wireline matched depth below seafloor. Also, corrections are made to certain tools and logs, documentation for the logs (with an assessment of log quality) is prepared, and the data are converted to ASCII for the conventional logs and GIF for the FMS images. Schlumberger Geo-Quest's GeoFrame software package is used for most of the processing. The data were transferred back to the ship within a few days of logging and were made available (in ASCII and digital log information standard [DLIS] formats) through the shipboard IODP logging database.

References

- Alvarez Zarikian, C.A., 2009. Data report: late Quaternary ostracodes at IODP Site U1314 (North Atlantic Ocean). In Channell, J.E.T., Kanamatsu, T., Sato, T., Stein, R., Alvarez Zarikian, C.A., Malone, M.J., and the Expedition 303/306 Scientists, *Proc. IODP*, 303/306: College Station, TX (Integrated Ocean Drilling Program Management International, Inc.). doi:10.2204/iodp.proc.303306.213.2009
- Alvarez Zarikian, C.A., Stepanova, A.Y., and Grütznér, J., 2009. Glacial-interglacial variability in deep sea ostracod assemblage composition at IODP Site U1314 in the

- subpolar North Atlantic. *Mar. Geol.*, 258(1–4):69–87. doi:10.1016/j.margeo.2008.11.009
- ASTM International, 1990. Standard method for laboratory determination of water (moisture) content of soil and rock (Standard D2216–90). In *Annual Book of ASTM Standards for Soil and Rock* (Vol. 04.08): Philadelphia (Am. Soc. Testing Mater.). [revision of D2216-63, D2216-80]
- Ayress, M., Neil, H., Passlow, V., and Swanson, K., 1997. Benthonic ostracods and deep watermasses: a qualitative comparison of southwest Pacific, Southern and Atlantic Oceans. *Palaeogeogr., Palaeoclimatol., Palaeoecol.*, 131(3–4):287–302. doi:10.1016/S0031-0182(97)00007-2
- Ayress, M., Whatley, R., Downing, S.E., and Millson, K.J., 1995. Cainozoic and Recent deep sea Cytherurid Ostracoda from the south western Pacific and Eastern Indian Oceans, Part I. *Cytherurinae. Rec. Aust. Mus.*, 47:203–223.
- Ayress, M.A., 1995. Late Eocene Ostracoda (crustacea) from the Waihao District, South Canterbury, New Zealand. *J. Paleontol.*, 69(5):897–921.
- Bach, W., and Edwards, K.J., 2003. Iron and sulfide oxidation within the basaltic ocean crust: implications for chemolithoautotrophic microbial biomass production. *Geochim. Cosmochim. Acta*, 67(20):3871–3887. doi:10.1016/S0016-7037(03)00304-1
- Backman, J., Jakobsson, M., Frank, M., Sangiorgi, F., Brinkhuis, H., Stickley, C., O'Regan, M., Løvlie, R., Pälike, H., Spofforth, D., Gattacecca, J., Moran, K., King, J., and Heil, C., 2008. Age model and core-seismic integration for the Cenozoic Arctic Coring Expedition sediments from the Lomonosov Ridge. *Paleoceanography*, 23(1):PA1S03–PA1S17. doi:10.1029/2007PA001476
- Berggren, W.A., Kent, D.V., Swisher, C.C., III, and Aubry, M.-P., 1995. A revised Cenozoic geochronology and chronostratigraphy. In Berggren, W.A., Kent, D.V., Aubry, M.-P., and Hardenbol, J. (Eds.), *Geochronology, Time Scales and Global Stratigraphic Correlation*. Spec. Publ.—SEPM (Soc. Sediment. Geol.), 54:129–212.
- Berggren, W.A., Kent, D.V., Flynn, J.J., and van Couvering, J.A., 1985. Cenozoic geochronology. *Geol. Soc. Am. Bull.*, 96(11):1407–1418. doi:10.1130/0016-7606(1985)96<1407:CG>2.0.CO;2
- Berggren, W.A., and Pearson, P.N., 2005. A revised tropical to subtropical Paleogene planktonic foraminiferal zonation. *J. Foraminiferal Res.*, 35(4):279–298. doi:10.2113/35.4.279
- Blum, P., 1997. Physical properties handbook: a guide to the shipboard measurement of physical properties of deep-sea cores. *ODP Tech. Note*, 26. doi:10.2973/odp.tn.26.1997
- Bolli, H.M., and Saunders, J.B., 1985. Oligocene to Holocene low latitude planktic foraminifera. In Bolli, H.M., Saunders, J.B., and Perch-Nielsen, K. (Eds.), *Plankton Stratigraphy* (Vol. 1): *Planktic Foraminifera, Calcareous Nannofossils and Calpionellids*: Cambridge (Cambridge Univ. Press), 155–262.
- Boomer, I., 1999. Late Cretaceous and Cainozoic bathyal Ostracoda from the Central Pacific (DSDP Site 463). *Mar. Micropaleontol.*, 37(2):131–147. doi:10.1016/S0377-8398(99)00015-8
- Boomer, I., and Whatley, R., 1995. Cenozoic ostracoda from guyots in the western Pacific: Holes 865B and 866B (Leg 143). In Winterer, E.L., Sager, W.W., Firth, J.V., and Sinton, J.M. (Eds.), *Proc. ODP, Sci. Results*, 143: College Station, TX (Ocean Drilling Program), 75–86. doi:10.2973/odp.proc.sr.143.249.1995
- Boyd, T.D., and Scott, S.D., 2001. Microbial and hydrothermal aspects of ferric oxyhydroxides and ferrosic hydroxides: the example of Franklin Seamount, Western Woodlark Basin, Papua New Guinea. *Geochem. Trans.*, 2:45. doi:10.1186/1467-4866-2-45
- Buatier, M.D., Guillaume, D., Wheat, C.G., Hervé, L., and Adatte, T., 2004. Mineralogical characterization and genesis of hydrothermal Mn oxides from the flank of the Juan de Fuca Ridge. *Am. Mineral.*, 89:1807–1815.
- Cande, S.C., and Kent, D.V., 1995. Revised calibration of the geomagnetic polarity timescale for the Late Cretaceous and Cenozoic. *J. Geophys. Res., [Solid Earth]*, 100(B4):6093–6095. doi:10.1029/94JB03098
- Chaisson, W.P., and Leckie, R.M., 1993. High-resolution Neogene planktonic foraminifer biostratigraphy of Site 806, Ontong Java Plateau (western equatorial Pacific). In Berger, W.H., Kroenke, L.W., Mayer, L.A., et al., *Proc. ODP, Sci. Results*, 130: College Station, TX (Ocean Drilling Program), 137–178. doi:10.2973/odp.proc.sr.130.010.1993
- Chaisson, W.P., and Pearson, P.N., 1997. Planktonic foraminifer biostratigraphy at Site 925: middle Miocene–Pleistocene. In Shackleton, N.J., Curry, W.B., Richter, C., and Bralower, T.J. (Eds.), *Proc. ODP, Sci. Results*, 154: College Station, TX (Ocean Drilling Program), 3–31. doi:10.2973/odp.proc.sr.154.104.1997
- Clark, S.P. (Ed.), 1966. *Handbook of Physical Constants*. Mem.—Geol. Soc. Am., 97.
- Corrège, T., 1993. The relationship between water masses and benthic ostracod assemblages in the western Coral Sea, Southwest Pacific. *Palaeogeogr., Palaeoclimatol., Palaeoecol.*, 105(3–4):245–266. doi:10.1016/0031-0182(93)90086-X
- Cronin, T.M., Boomer, I., Dwyer, G.S., and Rodriguez-Lázaro, J., 2002. Ostracoda and paleoceanography. In Holmes, J.A., and Chivas, A.R. (Eds.), *The Ostracoda: Applications in Quaternary Research*: Washington, DC (Am. Geophys. Union), 99–119.
- Davis, G.H., 1984. *Structural Geology of Rocks and Regions*: New York (John Wiley and Sons, Inc.).
- D'Hondt, S., Jørgensen, B.B., Miller, D.J., Batzke, A., Blake, R., Cragg, B.A., Cypionka, H., Dickens, G.R., Ferdelman, T., Hinrichs, K.-U., Holm, N.G., Mitterer, R., Spivack, A., Wang, G., Bekins, B., Engelen, B., Ford, K., Gettemy, G., Rutherford, S.D., Sass, H., Skilbeck, C.G., Aiello, I.W., Guerin, G., House, C.H., Inagaki, F., Meister, P., Naehr, T., Niitsuma, S., Parkes, R.J., Schippers, A., Smith, D.C., Teske, A., Wiegel, J., Naranjo Padillo, C., and Solis Acosta, J.L., 2004. Distributions of microbial activities in deep subseafloor sediments. *Science*, 306(5705):2216–2221. doi:10.1126/science.1101155

- D'Hondt, S., Rutherford, S., and Spivack, A.J., 2002. Metabolic activity of the subsurface life in deep-sea sediments. *Science*, 295(5562):2067–2070. doi:10.1126/science.1064878
- D'Hondt, S., Spivack, A.J., Pockalny, R., Ferdelman, T.G., Fischer, J.P., Kallmeyer, J., Abrams, L.J., Smith, D.C., Graham, D., Hasiuk, F., Schrum, H., and Stancin, A.M., 2009. Subseafloor sedimentary life in the South Pacific Gyre. *Proc. Nat. Acad. Sci., U. S. A.*, 106(28):11651–11656. doi:10.1073/pnas.0811793106
- D'Hondt, S.L., Jørgensen, B.B., Miller, D.J., et al., 2003. *Proc. ODP, Init. Repts.*, 201: College Station, TX (Ocean Drilling Program). doi:10.2973/odp.proc.ir.201.2003
- Didié, C., and Bauch, H.A., 2000. Species composition and glacial–interglacial variations in the ostracode fauna of the northeast Atlantic during the past 200,000 years. *Mar. Micropaleontol.*, 40(1–2):105–129. doi:10.1016/S0377-8398(00)00034-7
- Dingle, R.V., and Lord, A.R., 1990. Benthic ostracods and deep water-masses in the Atlantic Ocean. *Palaeogeogr., Palaeoclimatol., Palaeoecol.*, 80(3–4):213–235. doi:10.1016/0031-0182(90)90133-R
- Droser, M.L., and Bottjer, D.J., 1986. A semiquantitative field classification of ichnofabric. *J. Sediment. Res.*, 56(4):558–559. <http://jsedres.sepmonline.org/cgi/content/abstract/56/4/558>
- Ellis, D.V., and Singer, J.M., 2007. *Well Logging for Earth Scientists*, (2nd ed.): Dordrecht, The Netherlands (Springer).
- Ertefai, T.F., Heuer, V.B., Prieto-Mollar, X., Vogt, C., Sylva, S.P., Seewald, J., and Hinrichs, K.-U., 2010. The biogeochemistry of sorbed methane in marine sediments. *Geochim. Cosmochim. Acta*, 74(1):6033–6048. doi:10.1016/j.gca.2010.08.006
- Evans, H.B., 1965. GRAPE—a device for continuous determination of material density and porosity. *Trans. SPWLA Annu. Logging Symp.*: 6(2):B1–B25.
- Expedition 302 Scientists, 2005. Arctic Coring Expedition (ACEX): paleoceanographic and tectonic evolution of the central Arctic Ocean. *IODP Prel. Rept.*, 302. doi:10.2204/iodp.pr.302.2005
- Expedition 320T Scientists, 2009. USIO Sea Trials and Assessment of Readiness Transit (START): Ontong Java Plateau. *IODP Prel. Rept.*, 320T. doi:10.2204/iodp.pr.320T.2009
- Expedition 320/321 Scientists, 2010. Methods. In Pälke, H., Lyle, M., Nishi, H., Raffi, I., Gamage, K., Klaus, A., and the Expedition 320/321 Scientists, *Proc. IODP, 320/321*: Tokyo (Integrated Ocean Drilling Program Management International, Inc.). doi:10.2204/iodp.proc.320321.102.2010
- Expedition 329 Scientists, 2011. Site U1365. In D'Hondt, S., Inagaki, F., Alvarez Zarikian, C.A., and the Expedition 329 Scientists, *Proc. IODP, 329*: Tokyo (Integrated Ocean Drilling Program Management International, Inc.). doi:10.2204/iodp.proc.329.103.2011
- Fischer, J.P., Ferdelman, T.G., D'Hondt, S., Røy, H., and Wenzhöfer, F., 2009. Oxygen penetration deep into the sediment of the South Pacific gyre. *Biogeosciences*, 6(8):1467–1478. doi:10.5194/bg-6-1467-2009
- Fisher, A.T., Tsuji, T., Petronotis, K., and the Expedition 327 Scientists, 2011. *Proc. IODP, 327*: Tokyo (Integrated Ocean Drilling Management International, Inc.). doi:10.2204/iodp.proc.327.2011
- Forschner, S., Sheffer, R., Rowley, D.C., and Smith, D.C., 2008. Microbial diversity in Cenozoic sediments recovered from the Lomonosov Ridge in the Central Arctic Basin. *Environ. Microbiol.*, 11(3):630–639. doi:10.1111/j.1462-2920.2008.01834.x
- Gieskes, J.M., Gamo, T., and Brumsack, H., 1991. Chemical methods for interstitial water analysis aboard *JOIDES Resolution*. *ODP Tech. Note*, 15. doi:10.2973/odp.tn.15.1991
- Goldberg, D., 1997. The role of downhole measurements in marine geology and geophysics. *Rev. Geophys.*, 35(3):315–342. doi:10.1029/97RG00221
- Graber, K.K., Pollard, E., Jonasson, B., and Schulte, E. (Eds.), 2002. Overview of Ocean Drilling Program engineering tools and hardware. *ODP Tech. Note*, 31. doi:10.2973/odp.tn.31.2002
- Graham, I.J., Glasby, G.P., and Churchman, G.J., 1997. Provenance of the detrital component of deep-sea sediments from the SW Pacific Ocean based on mineralogy, geochemistry and Sr isotopic composition. *Mar. Geol.*, 140(1–2):75–96. doi:10.1016/S0025-3227(97)00006-6
- Gribsholt, B., and Kristensen, E., 2002. Impact of sampling methods on sulfate reduction rates and dissolved organic carbon (DOC) concentrations in vegetated salt marsh sediments. *Wetlands Ecol. Manage.*, 10(5):371–379. doi:10.1023/A:1020940314010
- Hancock, H.J.L., Chaproniere, G.C., Dickens, G.R., and Henderson, R.A., 2002. Early Palaeogene planktonic foraminifer and carbon isotope stratigraphy, Hole 762C, Exmouth Plateau, northwest Australian margin. *J. Micropalaeontol.*, 21(1):29–42.
- Harms, J.C., and Choquette, P.W., 1965. Geologic evaluation of a gamma-ray porosity device. *Trans. SPWLA Annu. Logging Symp.*: 6(2):C1–C37.
- Harvey, R.W., George, L.H., Smith, R.L., and LeBlanc, D.R., 1989. Transport of microspheres and indigenous bacteria through a sandy aquifer: results of natural- and forced-gradient tracer experiments. *Environ. Sci. Technol.*, 23(1):51–56. doi:10.1021/es00178a005
- Heesemann, M., Villinger, H., Fisher, A.T., Tréhu, A.M., and White, S., 2006. Data report: testing and deployment of the new APCT-3 tool to determine in situ temperatures while piston coring. In Riedel, M., Collett, T.S., Malone, M.J., and the Expedition 311 Scientists. *Proc. IODP, 311*: Washington, DC (Integrated Ocean Drilling Program Management International, Inc.). doi:10.2204/iodp.proc.311.108.2006
- Hoehler, T.M., Borowski, W.S., Alperin, M.J., Rodriguez, N.M., and Paull, C.K., 2000. Model, stable isotope, and radiotracer characterization of anaerobic methane oxidation in gas hydrate-bearing sediments of the Blake Ridge. In Paull, C.K., Matsumoto, R., Wallace, P.J., and Dillon, W.P. (Eds.), *Proc. ODP, Sci. Results*, 164: College Station, TX (Ocean Drilling Program), 79–85. doi:10.2973/odp.proc.sr.164.242.2000

- Holbourn, A.E., and Henderson, A.S., 2002. Re-illustration and revised taxonomy for selected deep-sea benthic foraminifers. *Paleontol. Electron.*, 4(2):1–34. http://palaeo-electronica.org/2001_2/foram/issue2_01.htm
- Hollis, C.J., and Kimura, K., 2001. A unified radiolarian zonation for the Late Cretaceous and Paleocene of Japan. *Micropaleontology*, 47(3):235–255. doi:10.2113/47.3.235
- House, C.H., Cragg, B.A., Teske, A., and the Leg 201 Scientific Party, 2003. Drilling contamination tests during ODP Leg 201 using chemical and particulate tracers. In D'Hondt, S.L., Jørgensen, B.B., Miller, D.J., et al., *Proc. ODP, Init. Repts.*, 201: College Station, TX (Ocean Drilling Program), 1–19. doi:10.2973/odp.proc.ir.201.102.2003
- Inagaki, F., Nunoura, T., Nakagawa, S., Teske, A., Lever, M., Lauer, A., Suzuki, M., Takai, K., Delwiche, M., Colwell, F.S., Nealson, K.H., Horikoshi, K., D'Hondt, S., and Jørgensen, B.B., 2006. Biogeographical distribution and diversity of microbes in methane hydrate-bearing deep marine sediments on the Pacific Ocean margin. *Proc. Natl. Acad. Sci. U. S. A.*, 103(8):2815–2820. doi:10.1073/pnas.0511033103
- Iversen, N., and Jørgensen, B.B., 1985. Anaerobic methane oxidation rates at the sulfate–methane transition in marine sediments from Kattegat and Skagerrak (Denmark). *Limnol. Oceanogr.*, 30(5):944–955. doi:10.4319/lo.1985.30.5.0944
- Janz, G.J., and Singer, S.K., 1975. Copenhagen Standard Sea Water: conductivity and salinity. *J. Soln. Chem.*, 4(12):995–1003. doi:10.1007/BF01074741
- Jones, R.W., 1994. *The Challenger Foraminifera*: New York (Oxford).
- Jørgensen, B.B., 2006. Bacteria and marine biogeochemistry. In Schulz, H.D., and Zabel, M. (Eds.), *Marine Geochemistry* (2nd ed.): Berlin (Springer-Verlag), 169–206. doi:10.1007/3-540-32144-6_5
- Kallmeyer, J., Smith, D.C., Spivack, A.J., and D'Hondt, S., 2008. New cell extraction procedure applied to deep subsurface sediments. *Limnol. Oceanogr.: Methods*, 6:236–245. <http://www.aslo.org/lomethods/free/2008/0236.pdf>
- Katz, M.E., and Miller, K.G., 1991. Early Paleogene benthic foraminiferal assemblages and stable isotopes in the Southern Ocean. In Ciesielski, P.F., Kristoffersen, Y., et al., *Proc. ODP, Sci. Results*, 114: College Station, TX (Ocean Drilling Program), 481–512. doi:10.2973/odp.proc.sr.114.147.1991
- Keenan, J.H., Keyes, F.G., Hill, P.G., and Moore, J.G., 1978. *Steam Tables: Thermodynamic Properties of Water Including Vapor, Liquid, and Solid Phases (international system of units; S.I.)*: New York (John Wiley & Sons).
- Kim, J., Dong, H., Seabaugh, J., Newell, S.W., and Eberl, D.D., 2004. Role of microbes in the smectite-to-illite reaction. *Science*, 303(5659):830–832. doi:10.1126/science.1093245
- Kvenvolden, K.A., and McDonald, T.J., 1986. Organic geochemistry on the *JOIDES Resolution*—an assay. *ODP Tech. Note*, 6: College Station, TX (Ocean Drilling Program). doi:10.2973/odp.tn.6.1986
- Laskar, J., Robutel, P., Joutel, F., Gastineau, M., Correia, A.C.M., and Levrard, B., 2004. A long-term numerical solution for the insolation quantities of the Earth. *Astron. Astrophys.*, 428(1):261–285. doi:10.1051/0004-6361:20041335
- Leckie, R.M., Farnham, C., and Schmidt, M.G., 1993. Oligocene planktonic foraminifer biostratigraphy of Hole 803D (Ontong Java Plateau) and Hole 628A (Little Bahama Bank), and comparison with the southern high latitudes. In Berger, W.H., Kroenke, L.W., Mayer, L.A., et al., *Proc. ODP, Sci. Results*, 130: College Station, TX (Ocean Drilling Program), 113–136. doi:10.2973/odp.proc.sr.130.012.1993
- Lever, M.A., Alperin, M., Engelen, B., Inagaki, F., Nakagawa, S., Steinsbu, B.O., Teske, A., and IODP Expedition Scientists, 2006. Trends in basalt and sediment core contamination during IODP Expedition 301. *Geomicrobiol. J.*, 23(7):517–530. doi:10.1080/01490450600897245
- Loeblich, A.R., and Tappan, H., 1988. *Foraminiferal Genera and Their Classification* (Vol. 2): New York (Van Nostrand Reinhold Co.).
- Lourens, L.J., Hilgen, F.J., Shackleton, N.J., Laskar, J., and Wilson, D., 2004. The Neogene period. In Gradstein, F.M., Ogg, J.G., and Smith, A.G. (Eds.), *A Geological Time Scale 2004*. Cambridge (Cambridge Univ. Press), 409–440.
- Lovell, M.A., Harvey, P.K., Brewer, T.S., Williams, C., Jackson, P.D., and Williamson, G., 1998. Application of FMS images in the Ocean Drilling Program: an overview. In Cramp, A., MacLeod, C.J., Lee, S.V., and Jones, E.J.W. (Eds.), *Geological Evolution of Ocean Basins: Results from the Ocean Drilling Program*. Geol. Soc. Spec. Publ., 131(1):287–303. doi:10.1144/GSL.SP.1998.131.01.18
- Luthi, S.M., 1990. Sedimentary structures of clastic rocks identified from electrical borehole images. In Hurst, A., Lovell, M.A., and Morton, A.C. (Eds.), *Geological Applications of Wireline Logs*. Geol. Soc. Spec. Publ., 48(1):3–10. doi:10.1144/GSL.SP.1990.048.01.02
- Manheim, F.T., and Sayles, F.L., 1974. Composition and origin of interstitial waters of marine sediments, based on deep sea drill cores. In Goldberg, E.D. (Ed.), *The Sea* (Vol. 5): *Marine Chemistry: The Sedimentary Cycle*: New York (Wiley), 527–568.
- Mazzullo, J.M., Meyer, A., and Kidd, R.B., 1988. New sediment classification scheme for the Ocean Drilling Program. In Mazzullo, J.M., and Graham, A.G. (Eds.), *Handbook for shipboard sedimentologists*. ODP Tech. Note, 8:45–67. doi:10.2973/odp.tn.8.1988
- McKee, E.D., and Weir, G.W., 1953. Terminology for stratification and cross-stratification in sedimentary rocks. *Geol. Soc. Am. Bull.*, 64(4):381–390. doi:10.1130/0016-7606(1953)64[381:TFSACI]2.0.CO;2
- McNaught, A.D., and Wilkinson, A. (Eds.), 1997. *IUPAC Compendium of Chemical Terminology* (2nd ed.): Cambridge (R. Soc. Chem.).
- Miller, K.G., and Katz, M.E., 1987. Oligocene to Miocene benthic foraminiferal and abyssal circulation changes in the North Atlantic. *Micropaleontology*, 33(2):97–149. doi:10.2307/1485489

- Morono, U., Kallmeyer, J., Inagaki, F., and the Expedition 329 Scientists, 2011. Preliminary experiment for cell count using flow cytometry. In D'Hondt, S., Inagaki, F., Alvarez Zarikian, C.A., and the Expedition 329 Scientists, *Proc. IODP, 329*: Tokyo (Integrated Ocean Drilling Program Management International, Inc.). doi:10.2204/iodp.proc.329.110.2011
- Morono, Y., Terada, T., Masui, N., and Inagaki, F., 2009. Discriminative detection and enumeration of microbial life in marine subsurface sediments. *ISME J.*, 3(5):503–511. doi:10.1038/ismej.2009.1
- Munsell Color Company, Inc., 2000. *Munsell Soil Color Chart*: New York (Gretag-Macbeth).
- Murray, R.W., Miller, D.J., and Kryc, K.A., 2000. Analysis of major and trace elements in rocks, sediments, and interstitial waters by inductively coupled plasma–atomic emission spectrometry (ICP–AES). *ODP Tech. Note*, 29. doi:10.2973/odp.tn.29.2000
- Nealson, K.H., and Saffarini, D., 1994. Iron and manganese in anaerobic respiration: environmental significance, physiology, and regulation. *Annu. Rev. Microbiol.*, 48(1):311–343. doi:10.1146/annurev.mi.48.100194.001523
- Nomura, R., 1995. Paleogene to Neogene deep-sea paleoceanography in the eastern Indian Ocean: benthic foraminifera from ODP Sites 747, 757 and 758. *Micropaleontology*, 41(3):251–290. doi:10.2307/1485862
- Olsson, R.K., Hemleben, C., Berggren, W.A., and Huber, B.T. (Eds.), 1999. *Atlas of Paleocene Planktonic Foraminifera*. Smithsonian. Contrib. Paleobiol., Vol. 85.
- Pälike, H., Frazier, J., and Zachos, J.C., 2006a. Extended orbitally forced palaeoclimatic records from the equatorial Atlantic Ceara Rise. *Quat. Sci. Rev.*, 25(23–24):3138–3149. doi:10.1016/j.quascirev.2006.02.011
- Pälike, H., Norris, R.D., Herrle, J.O., Wilson, P.A., Coxall, H.K., Lear, C.H., Shackleton, N.J., Tripathi, A.K., and Wade, B.S., 2006b. The heartbeat of the Oligocene climate system. *Science*, 314(5807):1894–1898. doi:10.1126/science.1133822
- Passchier, C.W., and Trouw, R.A.J., 1996. *Microtectonics*: Berlin (Springer-Verlag).
- Pearson, P.N., and Chaisson, W.P., 1997. Late Paleocene to middle Miocene planktonic foraminifer biostratigraphy of the Ceara Rise. In Shackleton, N.J., Curry, W.B., Richter, C., and Bralower, T.J. (Eds.), *Proc. ODP, Sci. Results*, 154: College Station, TX (Ocean Drilling Program), 33–68. doi:10.2973/odp.proc.sr.154.106.1997
- Pearson, P.N., Olsson, R.K., Huber, B.T., Hemleben, C., and Berggren, W.A. (Eds.), 2006. *Atlas of Eocene Planktonic Foraminifera*. Spec. Publ.—Cushman Found. Foraminiferal Res., 41.
- Ramsay, J.G., and Huber, M.I., 1987. *The Techniques of Modern Structural Geology* (Vol. 2): *Folds and Fractures*: New York (Acad. Press).
- Ratcliffe, E.H., 1960. The thermal conductivities of ocean sediments. *J. Geophys. Res.*, 65(5):1535–1541. doi:10.1029/JZ065i005p01535
- Revsbech, N.P., 1989. An oxygen microsensor with a guard cathode. *Limnol. Oceanogr.*, 34(2):472–476. doi:10.4319/lo.1989.34.2.0474
- Richter, C., Acton, G., Endris, C., and Radsted, M., 2007. Handbook for shipboard paleomagnetists. *ODP Tech. Note*, 34. doi:10.2973/odp.tn.34.2007
- Rider, M.H., 1996. *The Geological Interpretation of Well Logs* (2nd ed.): Caithness (Whittles Publ.).
- Rouxel, O., Dobbek, N., Ludden, J., and Fouquet, Y., 2003. Iron isotope fractionation during oceanic crust alteration. *Chem. Geol.*, 202(1–2):155–182. doi:10.1016/j.chemgeo.2003.08.011
- Salimullah, A.R.M., and Stow, D.A.V., 1992. Application of FMS images in poorly recovered coring intervals: examples from ODP Leg 129. In Hurst, A., Griffiths, C.M., and Worthington, P.F. (Eds.), *Geological Application of Wireline Logs II*. Geol. Soc. Spec. Publ., 65(1):71–86. doi:10.1144/GSL.SP.1992.065.01.06
- Sanfilippo, A., and Riedel, W.R., 1985. Cretaceous radiolaria. In Bolli, H.M., Saunders, J.B., and Perch-Nielsen, K. (Eds.), *Plankton Stratigraphy*: Cambridge (Cambridge Univ. Press), 573–630.
- Schlumberger, 1989. *Log Interpretation Principles/Applications*: Houston (Schlumberger Educ. Serv.), SMP-7017.
- Schlumberger, 1994. *IPL Integrated Porosity Lithology*: Houston (Schlumberger Wireline Testing), SMP-9270.
- Serra, O., 1984. *Fundamentals of Well-Log Interpretation* (Vol. 1): *The Acquisition of Logging Data*: Amsterdam (Elsevier).
- Serra, O., 1986. *Fundamentals of Well-Log Interpretation* (Vol. 2): *The Interpretation of Logging Data*. Amsterdam (Elsevier).
- Serra, O., 1989. *Formation MicroScanner Image Interpretation*: Houston (Schlumberger Educ. Serv.), SMP-7028.
- Shackleton, N.J., Berger, A., and Peltier, W.A., 1990. An alternative astronomical calibration of the lower Pleistocene timescale based on ODP Site 677. *Trans. R. Soc. Edinburgh: Earth Sci.*, 81:251–261.
- Shackleton, N.J., Crowhurst, S., Hagemberg, T., Pisias, N.G., and Schneider, D.A., 1995. A new late Neogene time scale: application to Leg 138 sites. In Pisias, N.G., Mayer, L.A., Janecek, T.R., Palmer-Julson, A., and van Andel, T.H. (Eds.), *Proc. ODP, Sci. Results*, 138: College Station, TX (Ocean Drilling Program), 73–101. doi:10.2973/odp.proc.sr.138.106.1995
- Shackleton, N.J., Crowhurst, S.J., Weedon, G.P., and Laskar, J., 1999. Astronomical calibration of Oligocene–Miocene time. In Shackleton N.J., McCave, I.N., and Graham, P.W. (Eds.), *Astronomical (Milankovitch) Calibration of the Geological Time-Scale*. Philos. Trans. R. Soc., Ser. A., 357(1757):1907–1929. doi:10.1098/rsta.1999.0407
- Shackleton, N.J., Hall, M.A., Raffi, I., Tauxe, L., and Zachos, J., 2000. Astronomical calibration age for the Oligocene–Miocene boundary. *Geology*, 28(5):447–450. doi:10.1130/0091-7613(2000)28<447:ACAFTO>2.0.CO;2
- Shipboard Scientific Party, 1986. Site 597. In Leinen, M., Rea, D.K., et al., *Init. Repts. DSDP, 92*: Washington, DC (U.S. Govt. Printing Office), 25–96. doi:10.2973/dsdp.proc.92.102.1986
- Shipboard Scientific Party, 1987. Site 596: hydraulic piston coring in an area of low surface productivity in the

- southwest Pacific. In Menard, H.W., Natland, J.H., Jordan, T.H., Orcutt, J.A., et al., *Init. Repts. DSDP*, 91: Washington, DC (U.S. Govt. Printing Office), 245–270. doi:10.2973/dsdp.proc.91.103.1987
- Shipboard Scientific Party, 1989. Introduction and explanatory notes. In Robinson, P.T., Von Herzen, R., et al., *Proc. ODP, Init. Repts.*, 118: College Station, TX (Ocean Drilling Program), 3–23. doi:10.2973/odp.proc.ir.118.101.1989
- Shipboard Scientific Party, 1992. Explanatory notes. In Behrmann, J.H., Lewis, S.D., Musgrave, R.J., et al., *Proc. ODP, Init. Repts.*, 141: College Station, TX (Ocean Drilling Program), 37–71. doi:10.2973/odp.proc.ir.141.105.1992
- Shipboard Scientific Party, 1993a. Explanatory notes. In Alt, J.C., Kinoshita, H., Stokking, L.B., et al., *Proc. ODP, Init. Repts.*, 148: College Station, TX (Ocean Drilling Program), 5–24. doi:10.2973/odp.proc.ir.148.101.1993
- Shipboard Scientific Party, 1993b. Explanatory notes. In Gillis, K., Mével, C., Allan, J., et al., *Proc. ODP, Init. Repts.*, 147: College Station, TX (Ocean Drilling Program), 15–42. doi:10.2973/odp.proc.ir.147.102.1993
- Shipboard Scientific Party, 1995. Explanatory notes. In Cannat, M., Karson, J.A., Miller, D.J., et al., *Proc. ODP, Init. Repts.*, 153: College Station, TX (Ocean Drilling Program), 15–42. doi:10.2973/odp.proc.ir.153.10X.1995
- Shipboard Scientific Party, 2003a. Explanatory notes. In Stephen, R.A., Kasahara, J., Acton, G.D., et al., *Proc. ODP, Init. Repts.*, 200: College Station, TX (Ocean Drilling Program), 1–66. doi:10.2973/odp.proc.ir.200.102.2003
- Shipboard Scientific Party, 2003b. Explanatory notes. In Wilson, D.S., Teagle, D.A.H., Acton, G.D., *Proc. ODP, Init. Repts.*, 206: College Station, TX (Ocean Drilling Program), 1–94. doi:10.2973/odp.proc.ir.206.102.2003
- Shipboard Scientific Party, 2003c. Site 1231. In D'Hondt, S.L., Jørgensen, B.B., Miller, D.J., et al., *Proc. ODP, Init. Repts.*, 201: College Station, TX (Ocean Drilling Program), 1–64. doi:10.2973/odp.proc.ir.201.112.2003
- Smith, D.C., Spivack, A.J., Fisk, M.R., Haveman, S.A., and Staudigel, H., 2000a. Tracer-based estimates of drilling-induced microbial contamination of deep sea crust. *Geomicrobiol. J.*, 17(3):207–219. doi:10.1080/01490450050121170
- Smith, D.C., Spivack, A.J., Fisk, M.R., Haveman, S.A., Staudigel, H., and the Leg 185 Shipboard Scientific Party, 2000b. Methods for quantifying potential microbial contamination during deep ocean coring. *ODP Tech. Note*, 28. doi:10.2973/odp.tn.28.2000
- Sogin, M.L., Morrison, H.G., Huber, J.A., Welch, D.M., Huse, S.M., Neal, P.R., Arrieta, J.M., and Herndl, G.J., 2006. Microbial diversity in the deep sea and the underexplored “rare biosphere.” *Proc. Natl. Acad. Sci. U. S. A.*, 103(32):12115–12120. doi:10.1073/pnas.0605127103
- Spezzaferri, S., 1994. Planktonic foraminiferal biostratigraphy and taxonomy of the Oligocene and lower Miocene in the oceanic record: an overview. *Palaeontographica Ital.*, 81:1–187.
- Spezzaferri, S., and Premoli Silva, I., 1991. Oligocene planktonic foraminiferal biostratigraphy and paleoclimatic interpretation from Hole 538A, DSDP Leg 77, Gulf of Mexico. *Palaeogeogr., Palaeoclimatol., Palaeoecol.*, 83(1–3):217–263. doi:10.1016/0031-0182(91)90080-B
- Srinivasan, M.S., and Sinha, D.K., 1992. Late Neogene planktonic foraminiferal events of the southwest Pacific and Indian Ocean: a comparison. In Tsuchi, R., and Ingle, J.C., Jr. (Eds.), *Pacific Neogene: Environment, Evolution and Events*: Tokyo (Univ. Tokyo Press), 203–220.
- Suess, J., Engelen, B., Cypionka, H., and Sass, H., 2004. Quantitative analysis of bacterial communities from Mediterranean sapropels based on cultivation-dependent methods. *FEMS Microbiol. Ecol.*, 51(1):109–121. doi:10.1016/j.femsec.2004.07.010
- Teagle, D.A.H., Alt, J.C., Umino, S., Miyashita, S., Banerjee, N.R., Wilson, D.S., and Expedition 309/312 Scientists, 2006. *Proc. IODP*, 309/312: Washington, DC (Integrated Ocean Drilling Program Management International, Inc.). doi:10.2204/iodp.proc.309312.2006
- Thomas, E., 1990. Late Cretaceous through Neogene deep-sea benthic foraminifers (Maud Rise, Weddell Sea, Antarctica). In Barker, P.F., Kennett, J.P., et al., *Proc. ODP, Sci. Results*, 113: College Station, TX (Ocean Drilling Program), 571–594. doi:10.2973/odp.proc.sr.113.123.1990
- Tjalsma, R.C., and Lohmann, P., 1983. *Paleocene–Eocene Bathyal and Abyssal Benthic Foraminifera from the Atlantic Ocean*. Micropaleontology, Spec. Publ., 4.
- Tsuji, Y., Nakano, K., Takahashi, Y., Hayashi, K., and Ro, C.-U., 2010. X-ray spectrometry. *Anal. Chem.*, 82(12):4950–4987. doi:10.1021/ac101069d
- Turco, E., Bambini, A.M., Foresi, L., Iaccarino, S., Lirer, F., Mazzei, R., and Salvatorini, G., 2002. Middle Miocene high-resolution calcareous plankton biostratigraphy at Site 926 (Leg 154, equatorial Atlantic Ocean): palaeoecological and palaeobiogeographical implications. *Geobios*, 35(1):257–276. doi:10.1016/S0016-6995(02)00064-5
- Twiss, R.J., and Moores, E.M., 1992. *Structural Geology*: New York (Freeman).
- Vacquier, V., 1985. The measurement of thermal conductivity of solids with a transient linear heat source on the plane surface of a poorly conducting body. *Earth Planet. Sci. Lett.*, 74(2–3):275–279. doi:10.1016/0012-821X(85)90027-5
- van Aken, P.A., Liebscher, B., and Styrsa, V.J., 1998. Quantitative determination of iron oxidation states in minerals using Fe-L_{2,3}-edge electron energy-loss near-edge structure spectroscopy. *Phys. Chem. Miner.*, 25(5):323–327. doi:10.1007/s002690050122
- Verardo, D.J., Froelich, P.N., and McIntyre, A., 1990. Determination of organic carbon and nitrogen in marine sediments using the Carlo Erba NA-1500 analyzer. *Deep-Sea Res., Part A*, 37(1):157–165. doi:10.1016/0198-0149(90)90034-S
- Von Herzen, R., and Maxwell, A.E., 1959. The measurement of thermal conductivity of deep-sea sediments by a needle-probe method. *J. Geophys. Res.*, 64(10):1557–1563. doi:10.1029/JZ064i010p01557
- Wade, B.S., 2004. Planktonic foraminiferal biostratigraphy and mechanisms in the extinction of *Morozovella* in the

- late middle Eocene. *Mar. Micropaleontol.*, 51(1–2):23–38. doi:10.1016/j.marmicro.2003.09.001
- Wade, B.S., Berggren, W.A., and Olsson, R.K., 2007. The biostratigraphy and paleobiology of Oligocene planktonic foraminifera from the equatorial Pacific Ocean (ODP Site 1218). *Mar. Micropaleontol.*, 62(3):167–179. doi:10.1016/j.marmicro.2006.08.005
- Wade, B.S., Pearson, P.N., Berggren, W.A., and Pälike, H., 2011. Review and revision of Cenozoic tropical planktonic foraminiferal biostratigraphy and calibration to the geomagnetic polarity and astronomical time scale. *Earth-Sci. Rev.*, 104(1–3):111–142. doi:10.1016/j.earsci-rev.2010.09.003
- Wang, G., Spivack, A.J., and D’Hondt, S., 2010. Gibbs energies of reaction and microbial mutualism in anaerobic deep seafloor sediments of ODP Site 1226. *Geochim. Cosmochim. Acta*, 74(14):3938–3947. doi:10.1016/j.gca.2010.03.034
- Wentworth, C.K., 1922. A scale of grade and class terms for clastic sediments. *J. Geol.*, 30(5):377–392. doi:10.1086/622910
- Whatley, R., and Boomer, I., 1995. Upper Oligocene to Pleistocene ostracoda from guyots in the western Pacific: Holes 871A, 872C, and 873B. In Haggerty, J.A., Premoli Silva, I., Rack, F., and McNutt, M.K. (Eds.), *Proc. ODP, Sci. Results*, 144: College Station (Ocean Drilling Program), 87–96. doi:10.2973/odp.proc.sr.144.072.1995
- Yasuhara, M., Okahashi, H., and Cronin, T.M., 2009. Taxonomy of Quaternary deep-sea ostracods from the western North Atlantic Ocean. *Palaeontology*, 52(4):879–931. doi:10.1111/j.1475-4983.2009.00888.x
- Zhao, Q., 2005. Late Cainozoic ostracod faunas and paleoenvironmental changes at ODP Site 1148, South China Sea. In Wang, P., and Lipps, J. (Eds.), *Marine Micropaleontology of the South China Sea*. *Mar. Micropaleontol.*, 54(1–2):27–47. doi:10.1016/j.marmicro.2004.09.002
- Zoth, G., and Haenel, R., 1988. Appendix: 1. In Haenel, R., Rybach, L., and Stegena, L. (Eds.), *Handbook of Terrestrial Heat-Flow Density Determination: with Guidelines and Recommendations of the International Heat Flow Commission*. Dordrecht (Kluwer Acad. Publ.), 449–4668.

Publication: 13 December 2011
MS 329-102

Figure F1. Visual core description graphic report examples, Expedition 329. A. Sediment. (Continued on next page.)

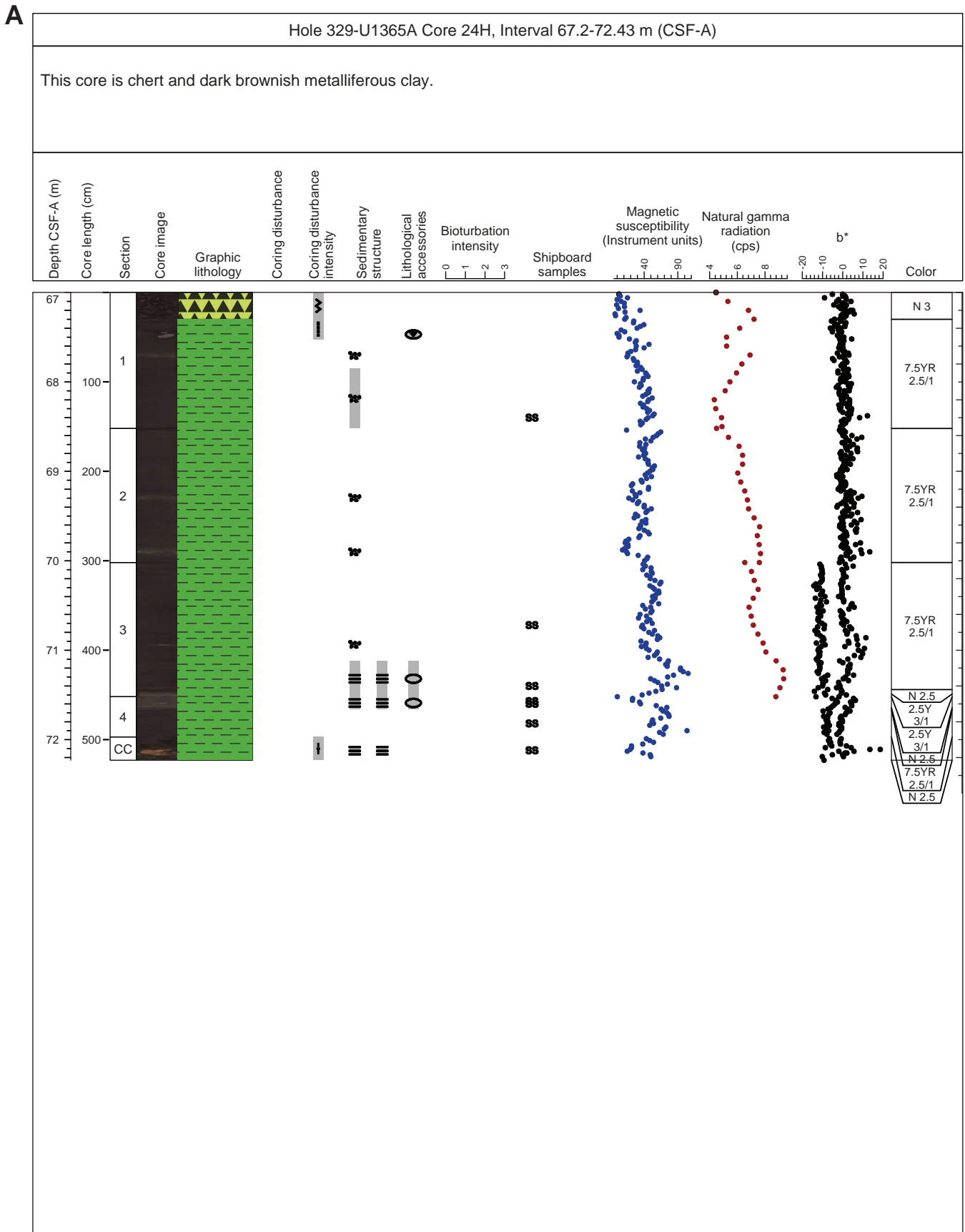


Figure F1 (continued). B. Hard rock.

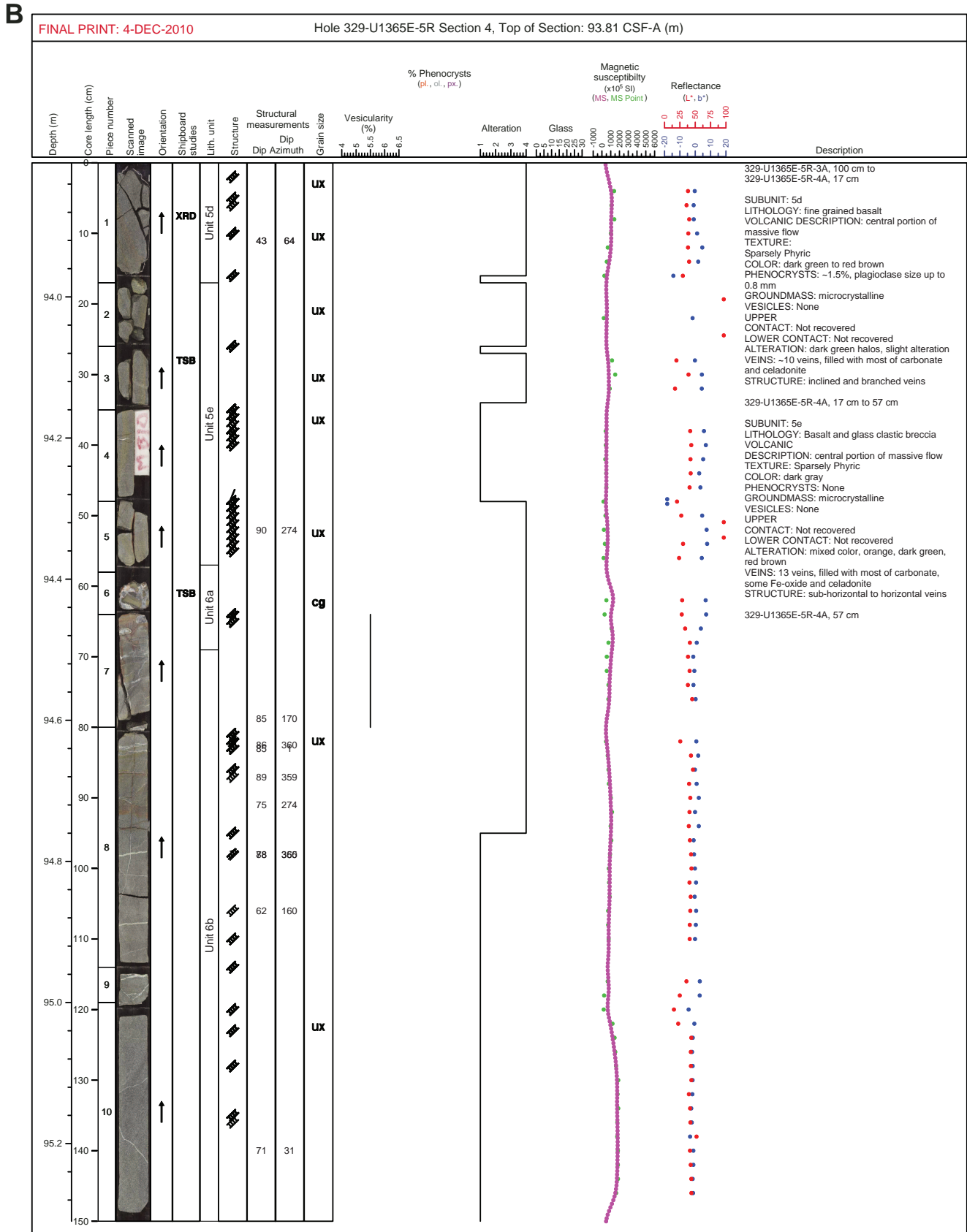


Figure F2. Ternary plot of lithology naming scheme for Expedition 329 sediment. Simplified after Expedition 302 Scientists (2005).

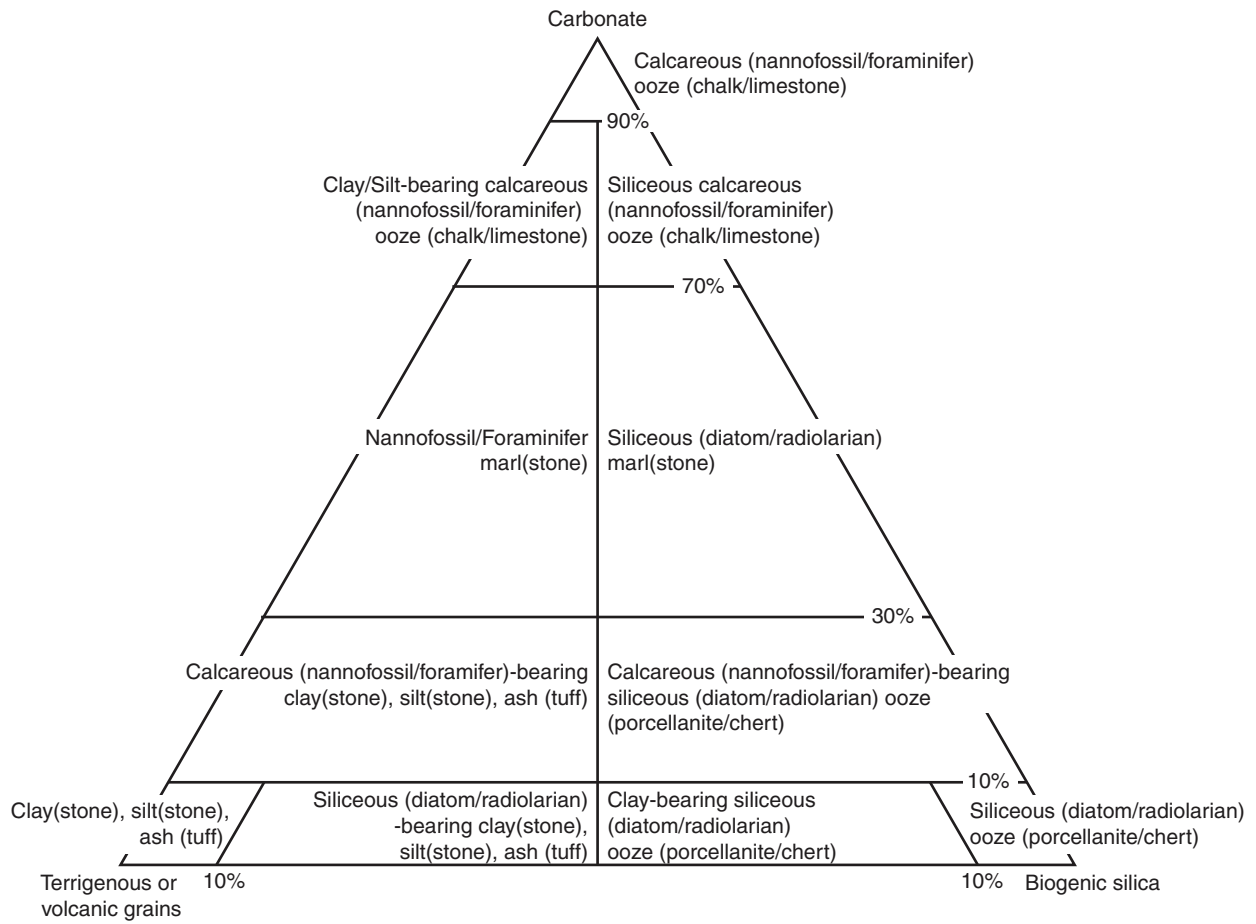
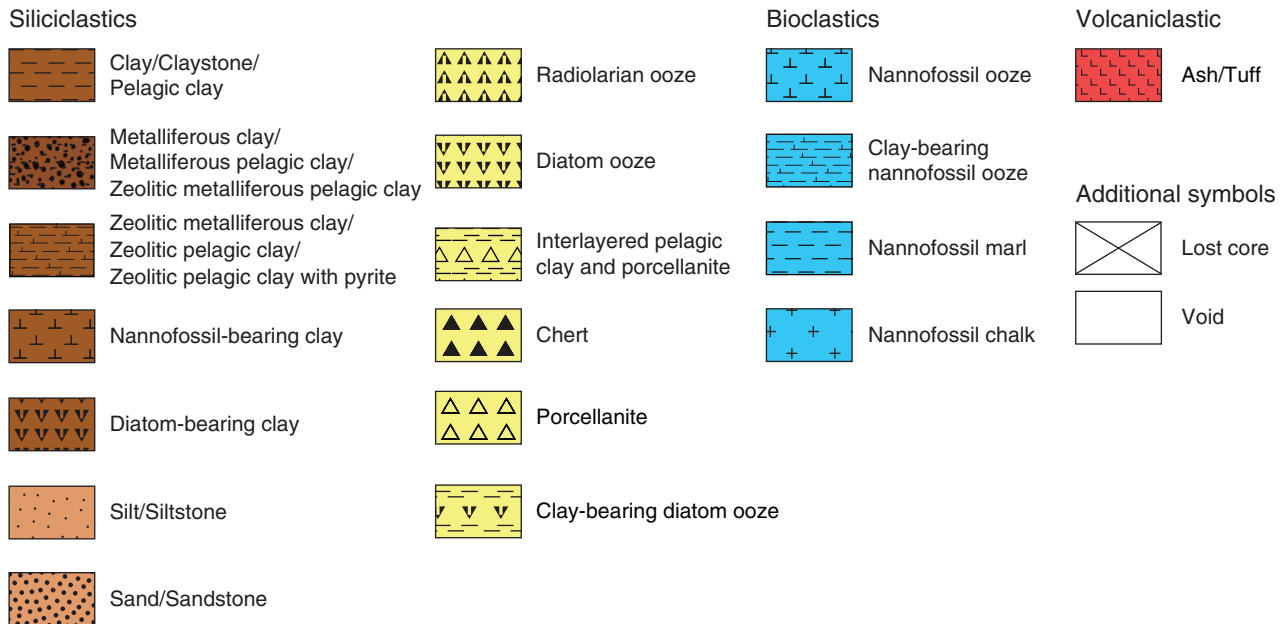
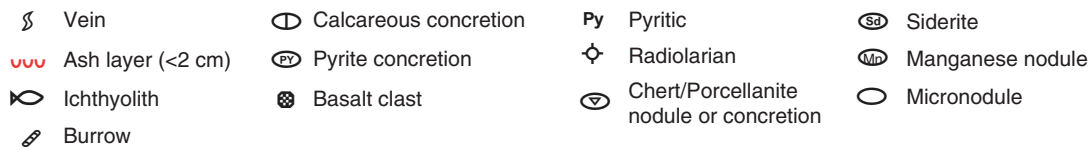


Figure F3. Core standard graphic report legend for Expedition 329 sediment, including lithology, sedimentary structure, drilling disturbance, and sampling types.

Lithology



Lithologic accessories



Coring disturbances



Sedimentary structures



Shipboard sampling

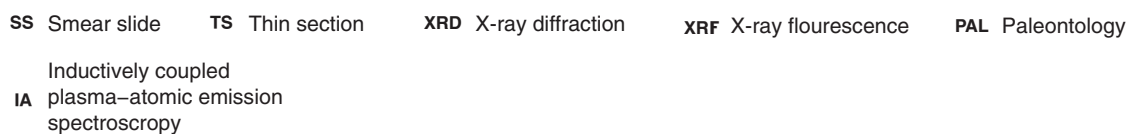















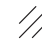


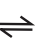


Figure F4. Thin section description legend for Expedition 329 hard rock.

Shipboard studies

ICP	Ph	PMAG	PP	TSB	XRD
ICP-AES analysis	Close-up photo	Paleomagnetic analysis	Physical property analysis	Petrographic thin section	X-ray diffraction analysis

Structure

 Chilled margin (ticks on quenched side)	 Metamorphic foliation	 Conjugate veins	 Cataclastic zone
 Igneous contact	 Breccia	 Joint	 Primary ductile deformation (e.g., folded flow tops or bottoms)
 Dike contact	 Vein	 Conjugate joints	 Magmatic and textural banding and patches
 Vesicles	 Shear vein	 Microfault	 Fractures
 Pipe vesicles	 Vein network	 Apparent sense of shear	

Structural measurements

IC	L	M	Sv	Vh	f	J	F
Igneous contact	Lineation	Magmatic fabric	Shear vein	Hydrothermal vein	Fracture	Joint	Fault

Phenocryst

a = Aphyric (<1%)	sp = Sparsely phyric (1%-5%)	mp = Moderately phyric (5%-10%)	hp = Highly phyric (>10%)
-------------------	------------------------------	---------------------------------	---------------------------

Constituent minerals

OI = Olivine	Pl = Plagioclase	Cpx = Clinopyroxene	Opx = Orthopyroxene
Amp = Amphibole	Ox = Oxide	Sp = Spinel	

Grain size

G	CX	UX	fg	mg	cg	VC
Glassy	Cryptocrystalline (<0.1 mm)	Microcrystalline (0.1-0.2 mm)	Fine grained (0.2-1 mm)	Medium grained (1-2 mm)	Coarse grained (2-5 mm)	Very coarse grained (>5 mm)



Gray rectangles or triangles schematically indicate uniform grain size or gradual increase/decrease in grain size, respectively.

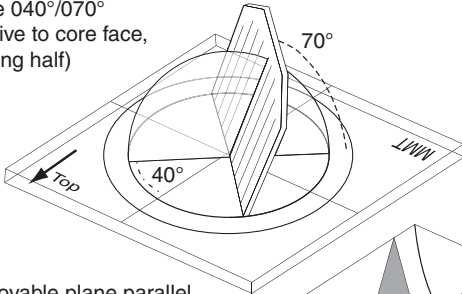
Alteration

1	2	3	4	5
Fresh (<2%)	Slight (2%-10%)	Moderate (10%-50%)	High (50%-95%)	Complete (95%-100%)

Figure F5. Diagram of conventions used for measuring orientations of structural features on the archive half, Expedition 329. **A.** Plane. **B.** Lineation. **C.** Rotation into core reference frame. Examples of orientation measurements with a protractor-based device are shown (modified from Teagle, Alt, Umino, Miyashita, Banerjee, Wilson, and the Expedition 309/312 Scientists, 2006).

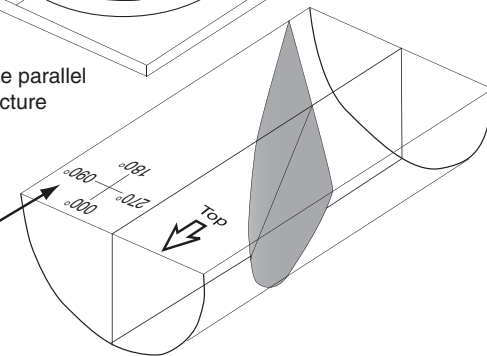
A Measuring a plane

Plane $040^{\circ}/070^{\circ}$
(relative to core face,
working half)



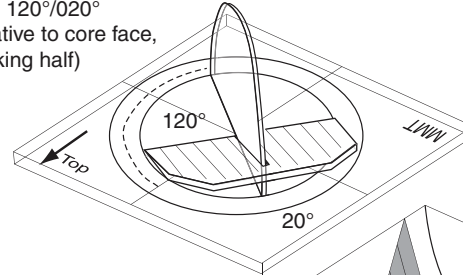
Movable plane parallel
to planar structure

Core face
coordinates



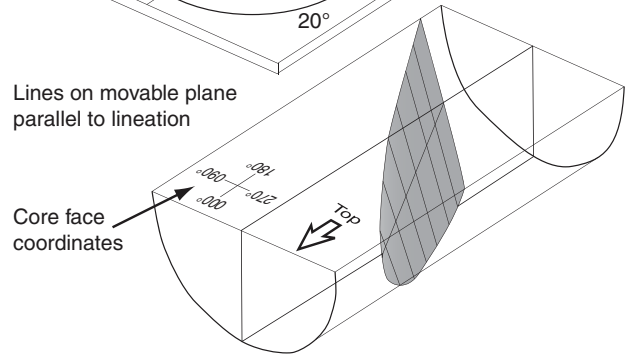
B Measuring a lineation

Line $120^{\circ}/020^{\circ}$
(relative to core face,
working half)



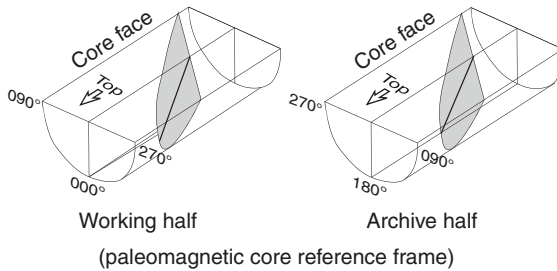
Lines on movable plane
parallel to lineation

Core face
coordinates



C Rotate into core reference frame

Plane $120^{\circ}/044^{\circ}$
Line $067^{\circ}/028^{\circ}$



Working half Archive half
(paleomagnetic core reference frame)

Figure F6. Diagrams of preparation of discrete cubic samples for paleomagnetic study, Expedition 329. **A.** Discrete sediment samples are first collected by inserting a subcorer into the split core (i.e., working-half core). The subcorer is then removed with sediment inside. Excess sediment from the base of the subcorer is trimmed with a spatula, and the rest of the sediment is extruded into the plastic sample box. **B.** Cubic sediment collected by the subcorer shown in A is placed in a plastic box with an arrow molded into its base. The internal volume of the cubic sample is 7 cm³. For hard rock samples (e.g., basalt), 8 cm³ of cubic sample is prepared by a cutting machine on the *JOIDES Resolution*.

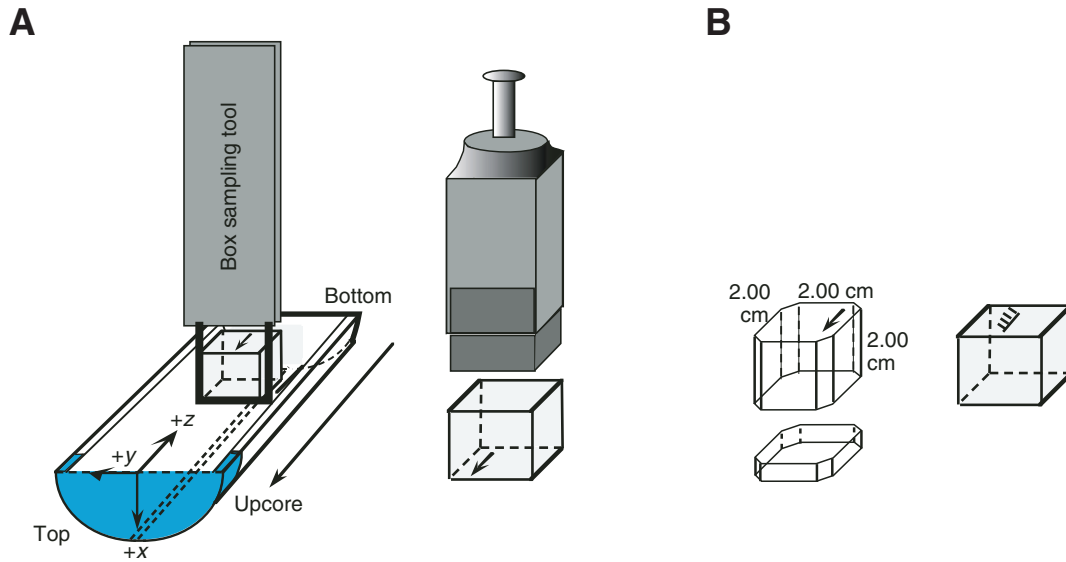


Figure F7. Diagrams of coordinate systems used for archive-half and working-half sections and for the superconducting rock magnetometer, Expedition 329. SQUID = superconducting quantum interference device.

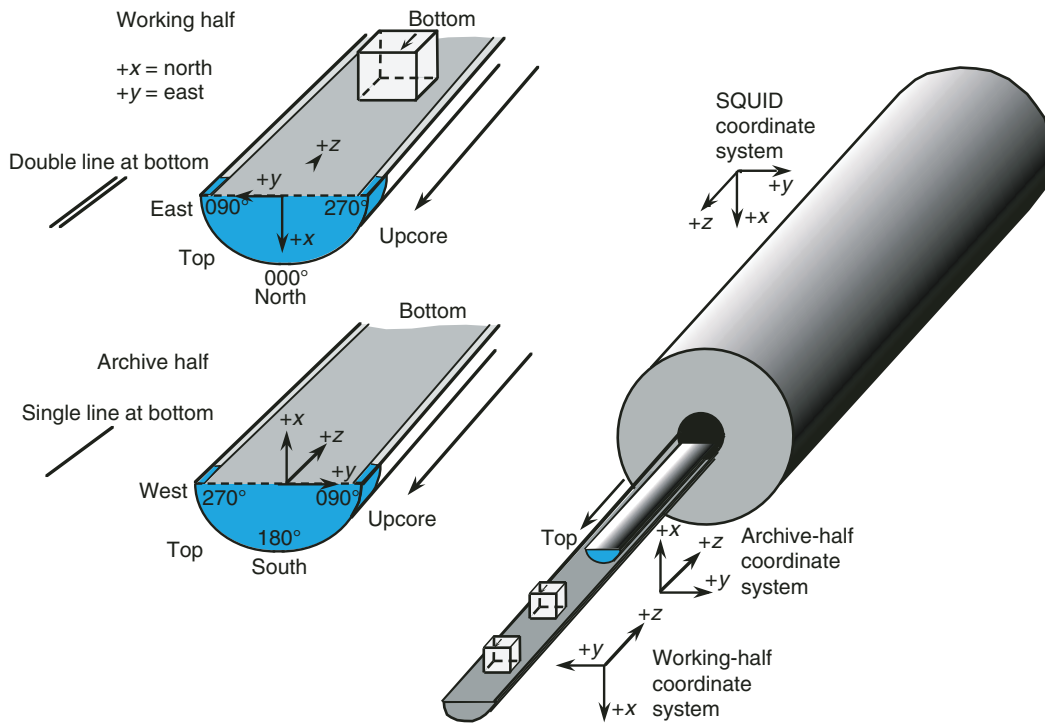


Figure F8. Plot of magnetic toolface (MTF) angle and standpipe pressure from the Flexit tool during the first tool use in Hole U1365A.

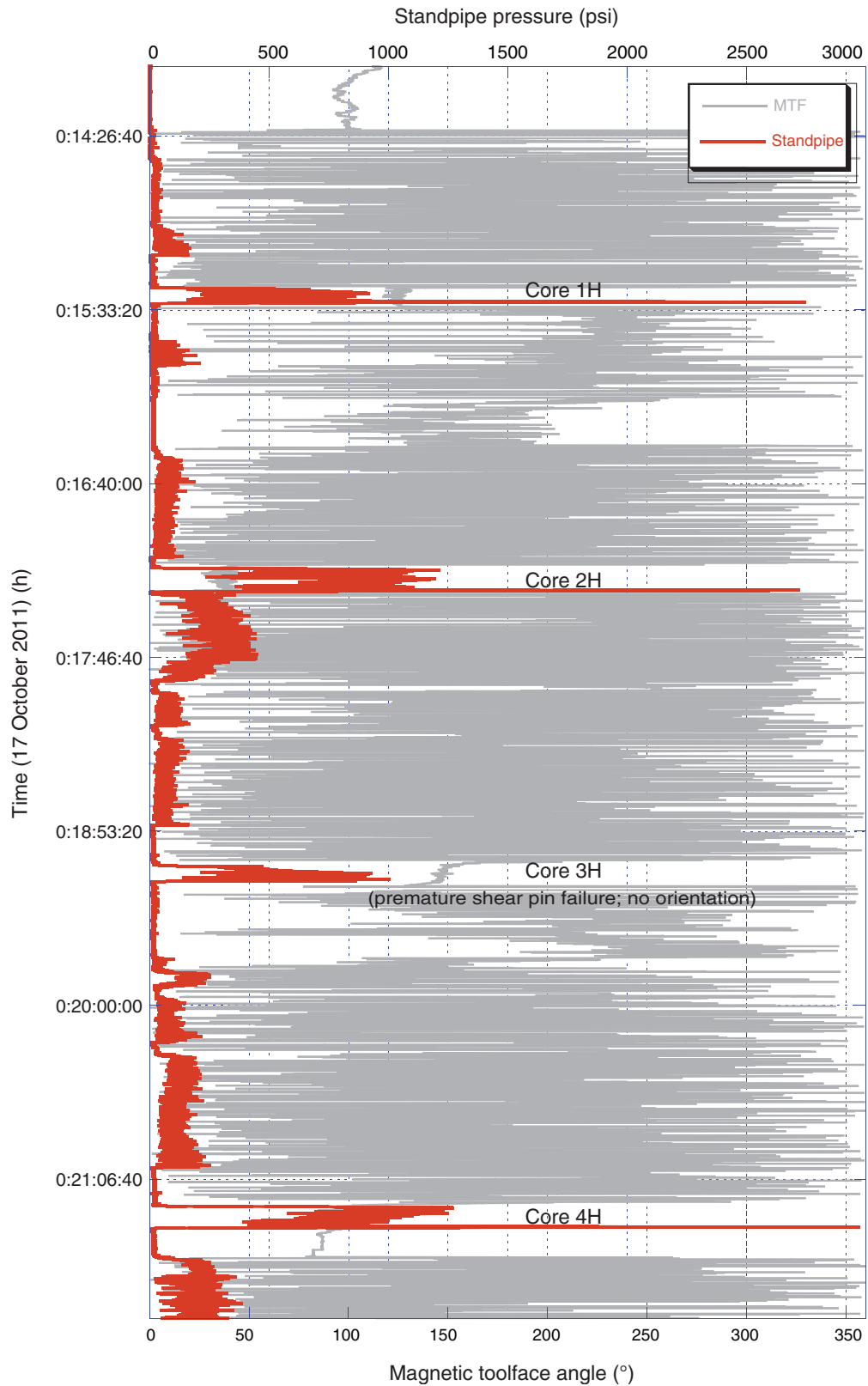


Figure F9. Image of Rhizon sampling of whole-rounds in the core refrigerator in the Hold Deck. Plastic wrap was placed over the ends of the whole-rounds and the Rhizon inserted through the plastic.





Figure F10. Plots of sample storage and handling times for all sites cored during Expedition 329. See individual site chapters for the implications of these handling times on a case-by-case basis. **A.** Site U1365. (Continued on next six pages.)

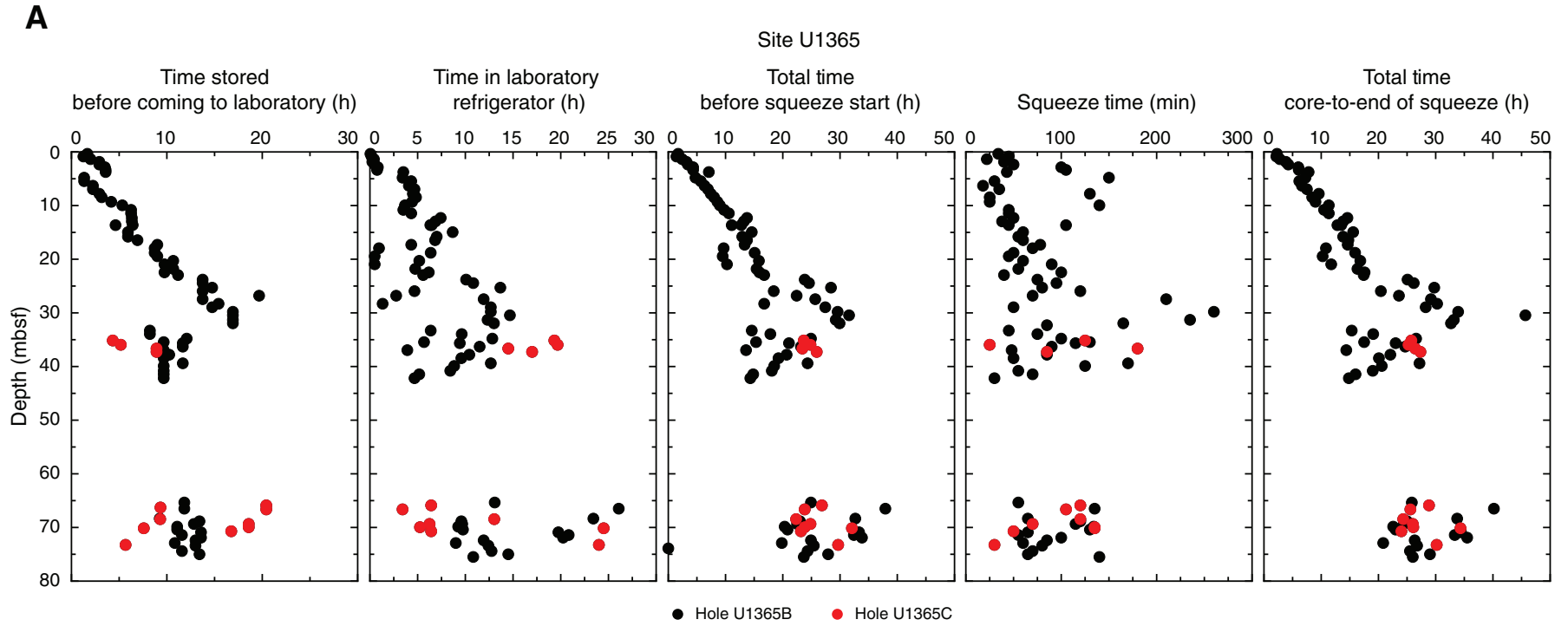




Figure F10 (continued). B. Site U1366. WSS = whole round stored shorter. (Continued on next page.)

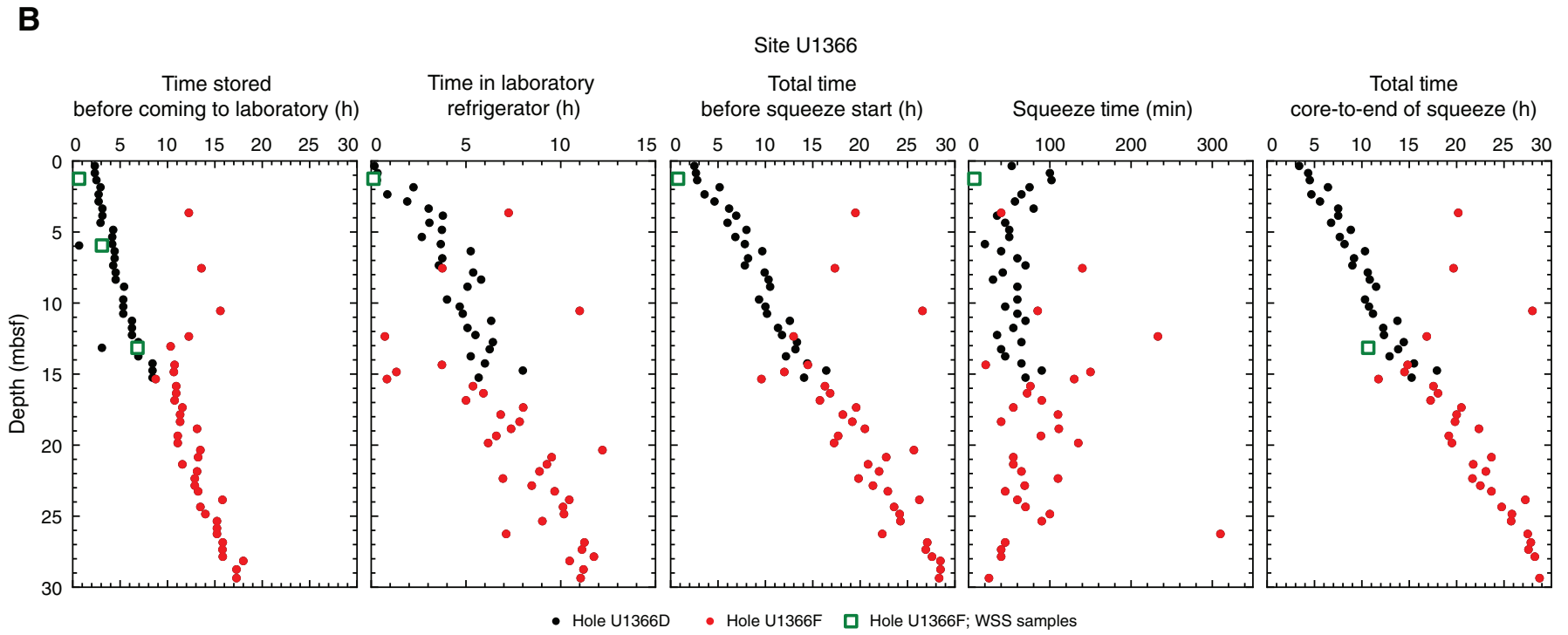




Figure F10 (continued). C. Site U1367. (Continued on next page.)

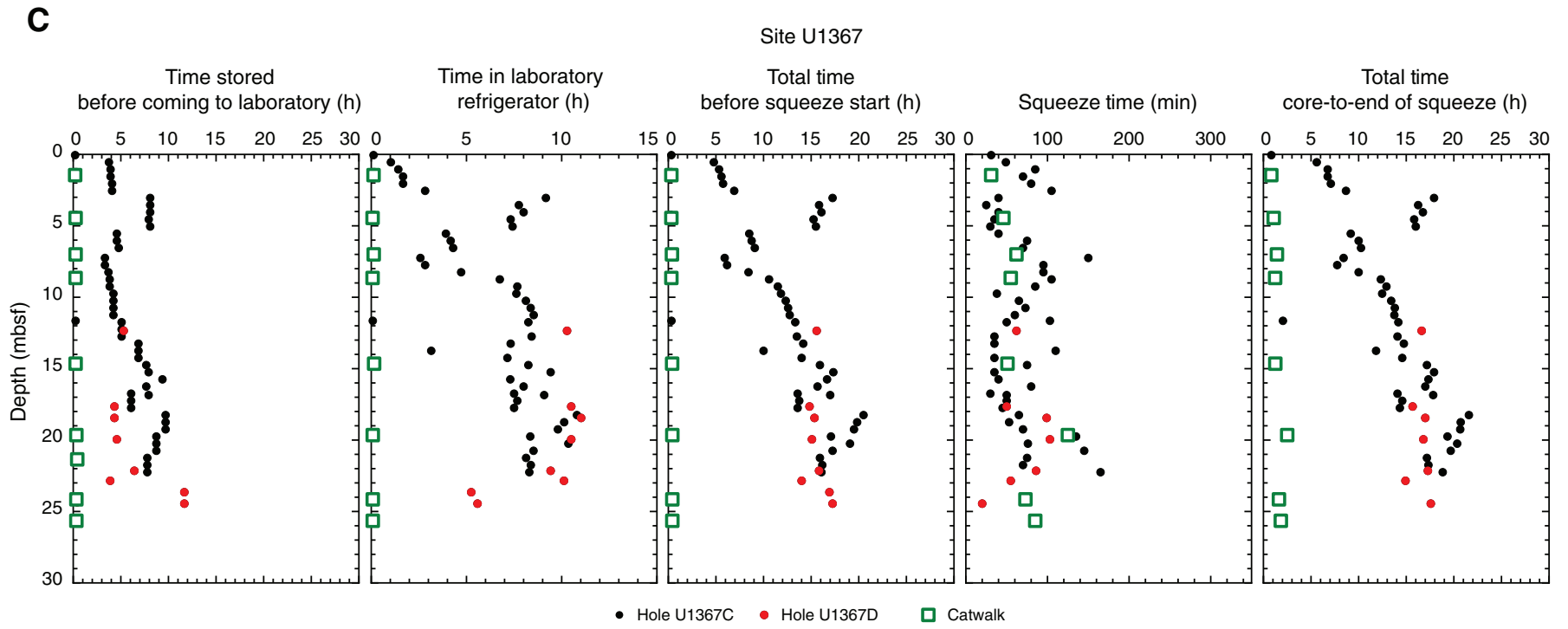




Figure F10 (continued). D. Site U1368. (Continued on next page.)

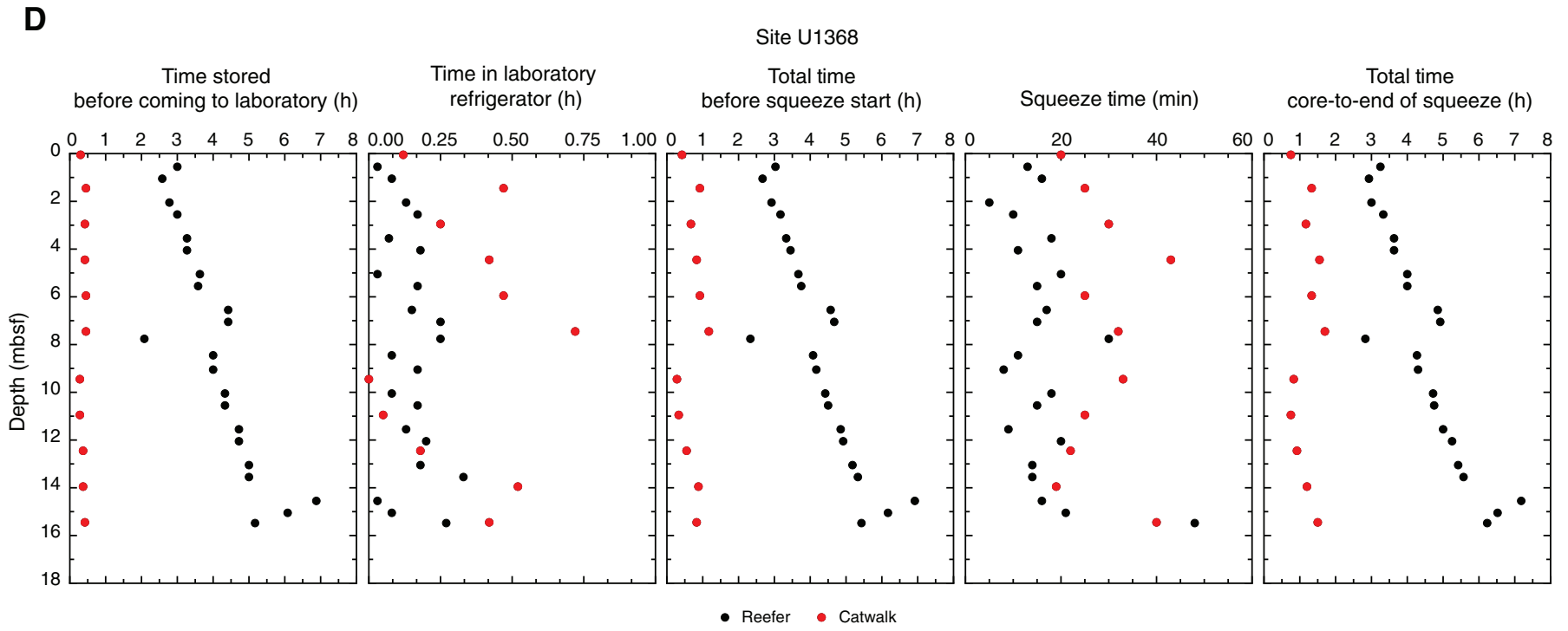




Figure F10 (continued). E. Site U1369. IW = interstitial water. (Continued on next page.)

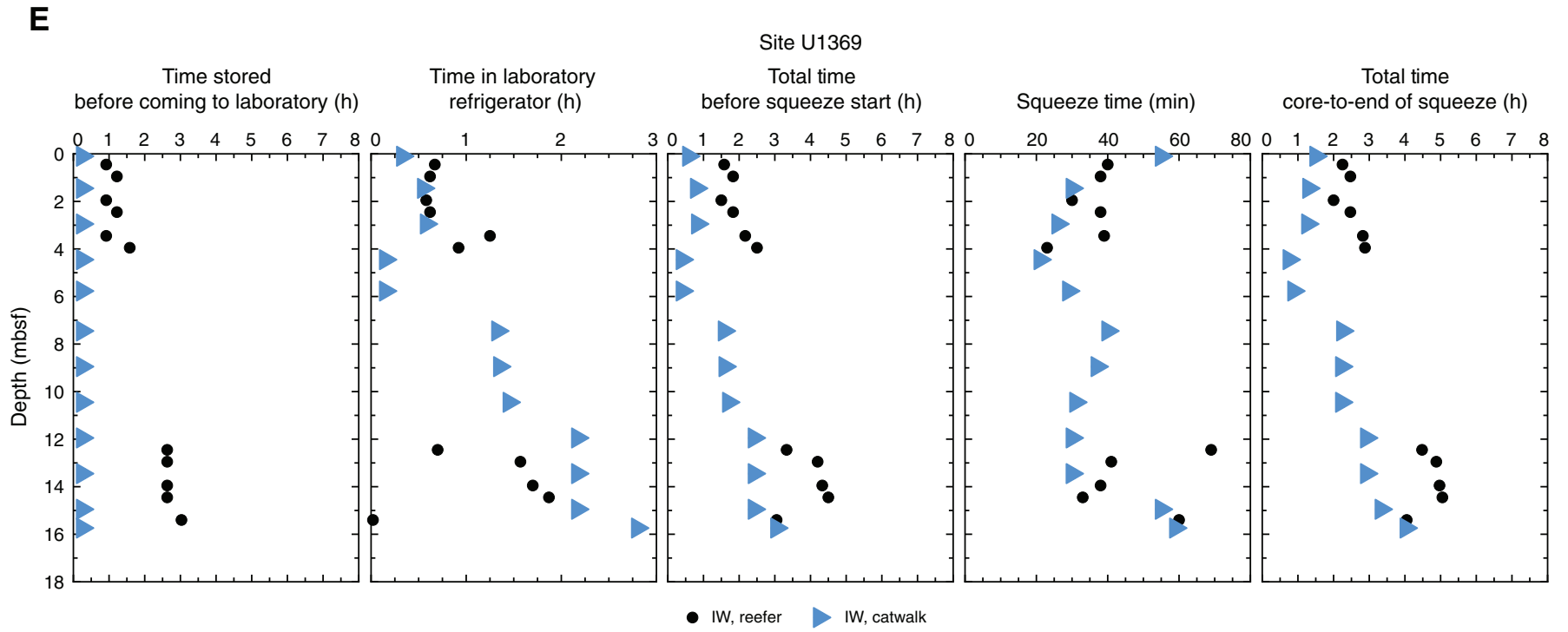




Figure F10 (continued). F. Site U1370. IW = interstitial water. (Continued on next page.)

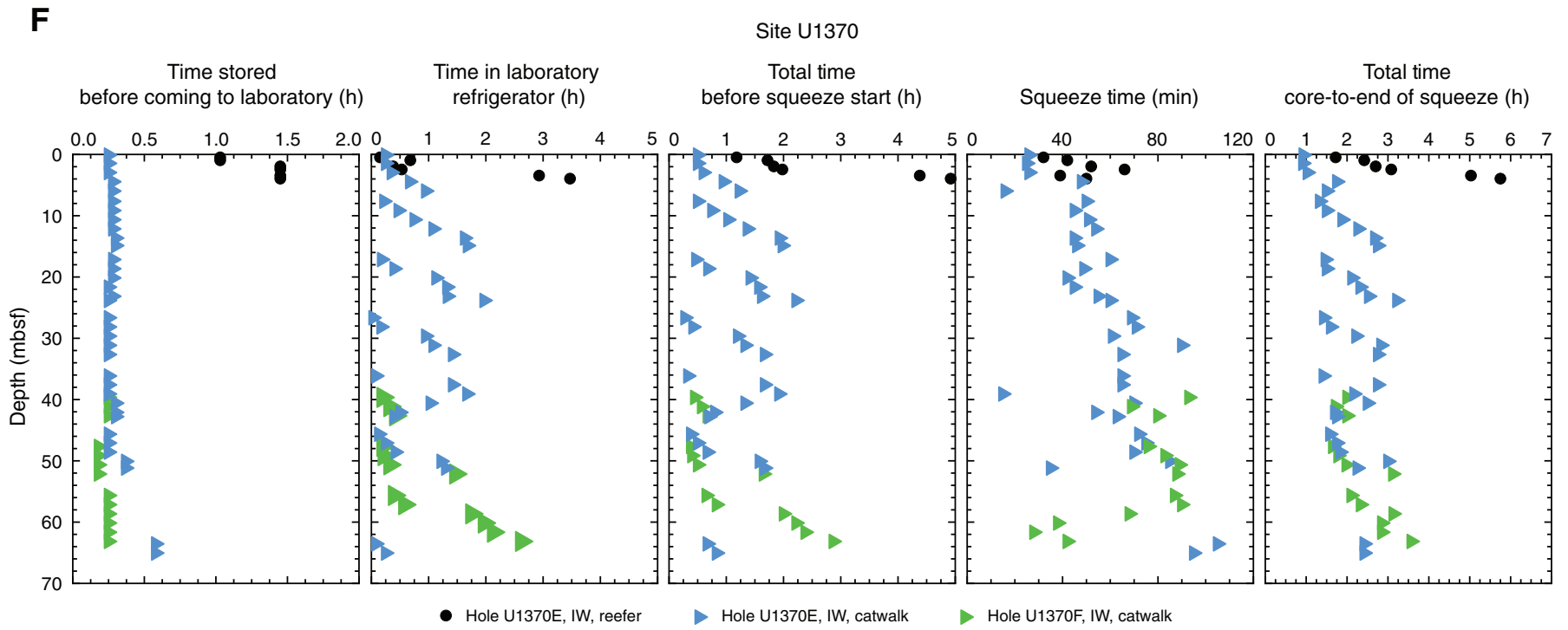




Figure F10 (continued). G. Site U1371. IW = interstitial water.

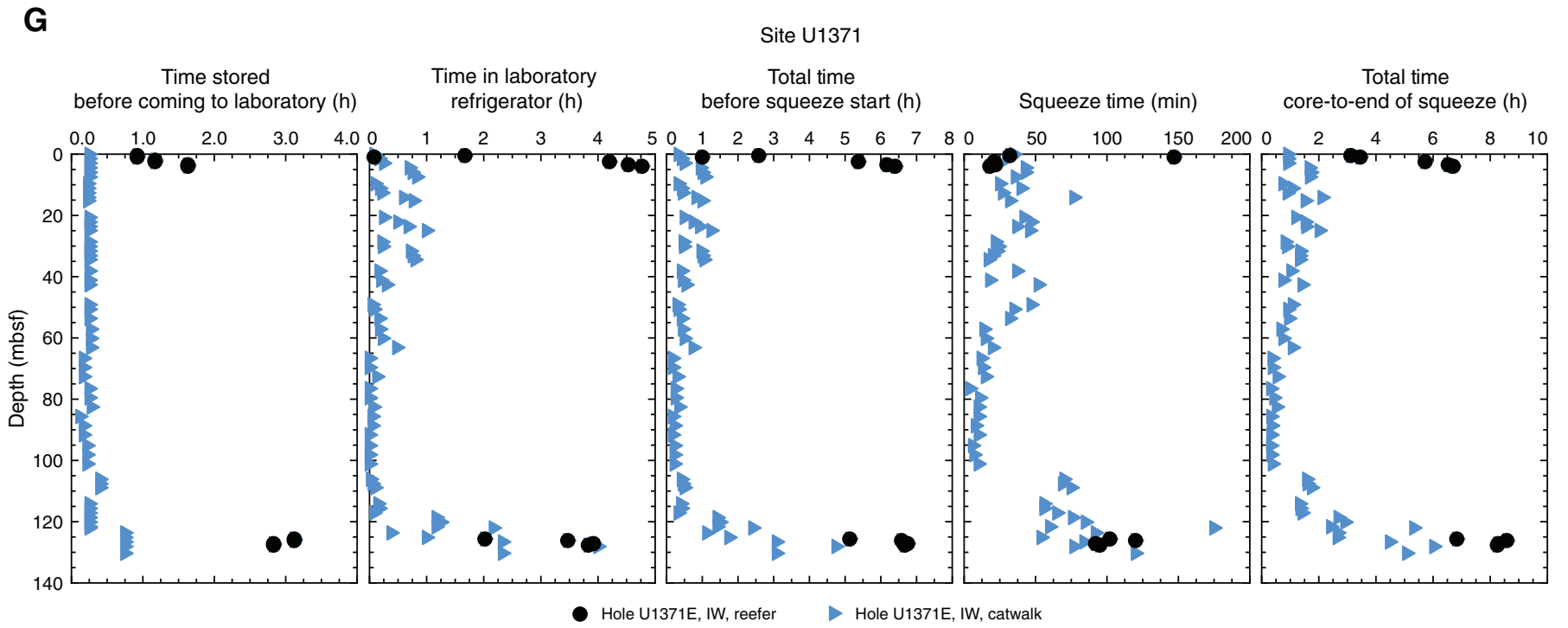




Figure F11. Plots of Rhizon sampling time, Expedition 329.

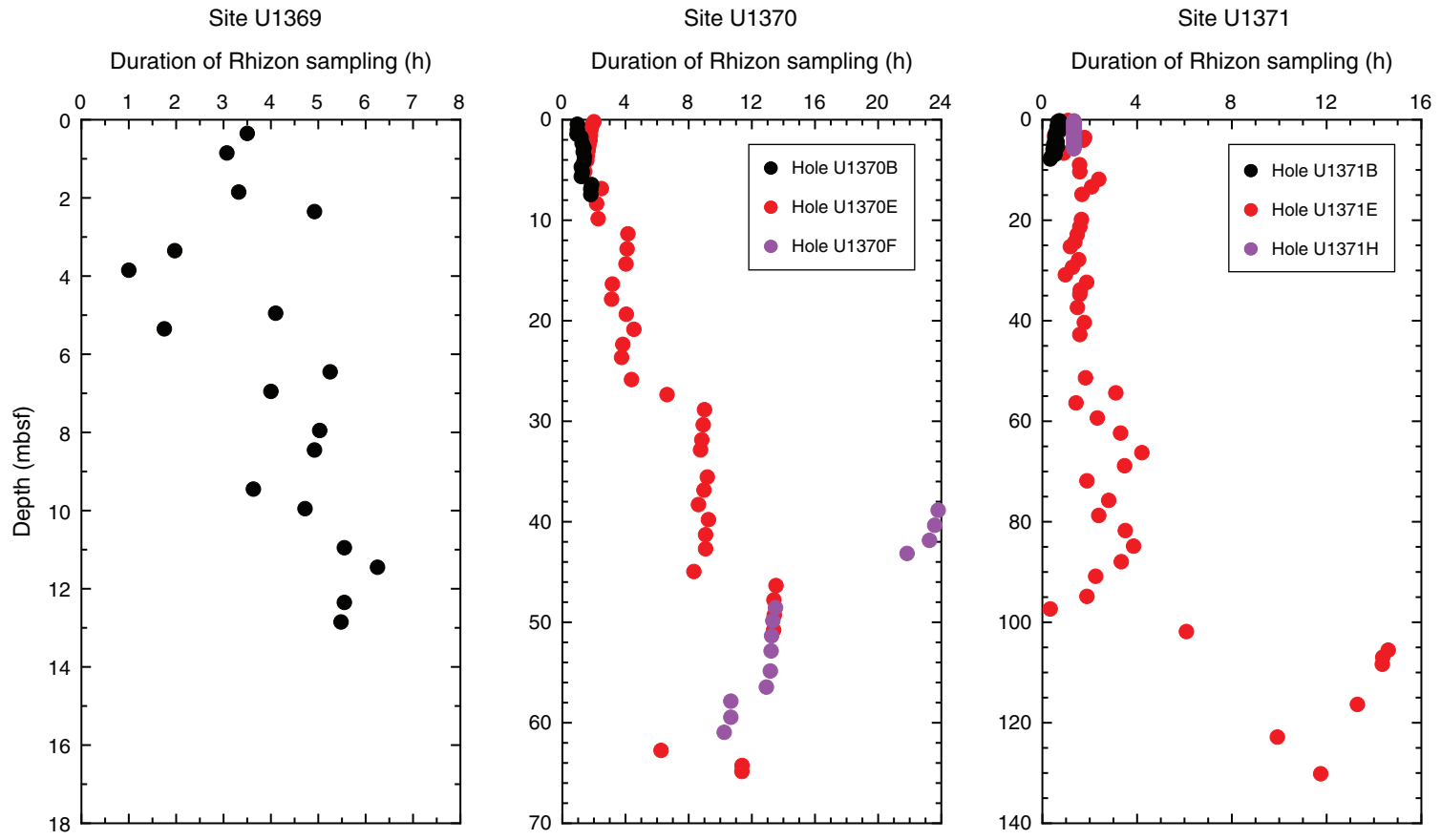


Figure F12. Diagram of wireline tool strings used during Expedition 329. HNGS = Hostile Environment Natural Gamma Ray Sonde, HLDS = Hostile Environment Litho-Density Sonde, GPIT = General Purpose Inclinometry Tool, DIT = Dual Induction Tool, FMS = Formation MicroScanner.

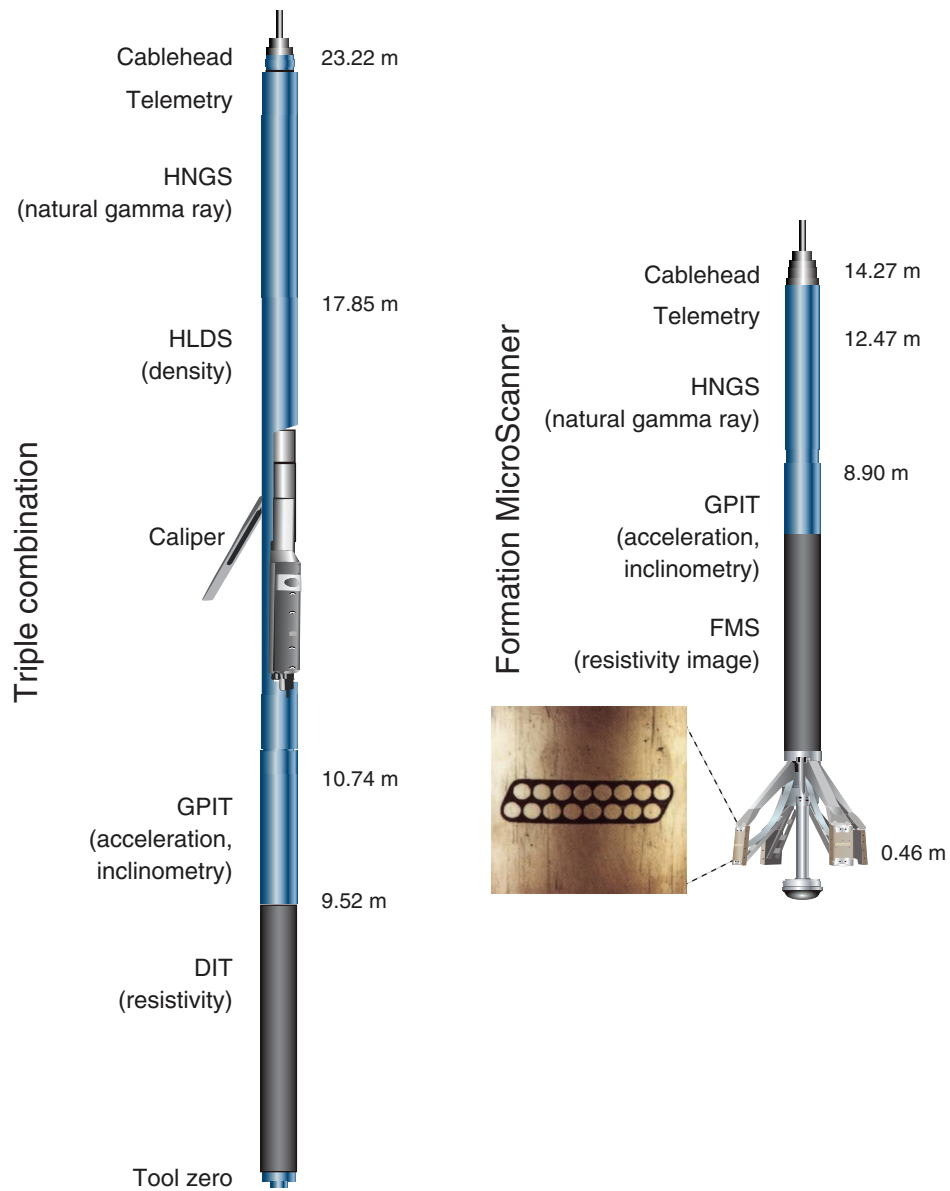


Table T1. Glossary of common geological terms used to describe basement rocks, Expedition 329.

Term	Explanation
Breccia (Br)	
Type of breccia	Hydrothermal (Bh), magmatic (Bm), tectonic (Bc)
Volume percent	Percent clasts vs. bulk rock
Size range	Maximum–minimum average size
Shape	Angular, subangular, subrounded, rounded, etc.
Composition	Monomictic, polymictic
Structure	Internal crushing, veining, fracturing, etc.; preferred orientation
Alteration	Alteration halos in the clasts
Sorting	Well sorted, moderately sorted, poorly sorted
Volume percent	Percent matrix vs. bulk rock
Grain size	Coarse, medium, fine
Composition	Lithology and/or mineralogy compared with clasts
Structure	Veining, fracturing, preferred orientation, shearing
Alteration	Alteration in the matrix
Volume percent	Percent cement vs. bulk rock
Composition	Mineralogy
Veins (V)	
Vein type	Magmatic/late magmatic (Vm), hydrothermal (Vh)
Orientation of vein	Vertical, horizontal
Depth of vein	Interval in the core
Morphology	Planar (Pl), curved (Cv), irregular (Ir), sigmoidal (Sg), stepped (St), T-shaped (T), Y-shaped (Y), splayed (S)
Vein array geometry	Conjugate, network, en echelon, anastomosing, riedel
Vein density (N/10 cm)	No vein, slight, moderate, high, complete
Fabric of the filling minerals	Fibrous (Fb), vermicular (Vr), blocky (Bl)
Vein mineralogy	Carbonate, quartz, Fe oxide, celadonite, etc.
Average width and length	Measured in millimeters
Joints (J)	
Orientation of joint	Direction of joint
Depth of joint	Interval within the core
Morphology	Planar (Pl), curvilinear (Cv), anastomosing (An), T-shaped (T), Y-shaped (Y), splayed (Spl), stepped (St)
Joint array	Conjugate, network, en echelon
Joint density	Number of joints in an igneous unit or per core/site
Faults (F)	
Orientation of fault	Direction of fault
Depth of fault	Interval within the core
Magnitude of the apparent offset	Measured offset (on the cut face of the core and side wall)
Apparent sense of shear	Dextral (dx), sinistral (sx), reversed (r), normal (n)
Crosscutting relationships	Relative timing from one feature to another
Average thickness of fault zone	Fault zone thickness measured in millimeters
Occurrence of alteration halos	Halos associated with fluid flow through the fault zone
Occurrence and type of fault rocks	Rocks formed by faulting (e.g., cataclasite)
Other	
Composite vein	Compositionally and texturally zoned vein containing different mineral assemblages that may or may not represent different generations.
Fabric	Relative orientation of parts of a rock mass. Preferred linear orientation of part of a rock is termed linear fabric, preferred planar orientation is termed planar fabric, and lack of a preferred orientation is referred to as random fabric.
Fault	Fractures with kinematic evidence for shear displacement across the discontinuity or with an associated cataclasite.
Foliation	Any repetitively occurring penetrative planar feature in a rock body.
Joint	Fractures in which the two sides show no differential displacement (relative to the naked eye or 10× hand lens) and have no filling material.
Shear vein	Obliquely opening veins with minor shear displacement, filled with slickenfibers or overlapping fibers.
Texture	Relative size, shape, and spatial interrelationship between grains and internal features of grains in a rock.
Vein	Extensional or oblique open fractures filled with epigenic minerals.

Table T2. Typical shipboard ICP-AES analyses run, Expedition 329.

Analysis number	Rock sample	Analysis type
1	DRIFT-1	Drift
2	JR-2	Standard analysis
3	Unknown-1	Sample analysis
4	BLANK (1)-2	Blank analysis
5	BCR-2 (1)	Standard analysis
6	DRIFT-2	Drift
7	Unknown-2	Sample analysis
8	Unknown-3	Sample analysis
9	NBS-1C (1)	Standard analysis
10	Unknown-4	Sample analysis
11	DRIFT-3	Drift
12	Unknown-5	Sample analysis
13	Unknown-6	Sample analysis
14	JA-3	Standard analysis
15	Unknown-7	Sample analysis
16	DRIFT-4	Drift
17	Unknown-8	Sample analysis
18	Unknown-9	Sample analysis
19	BAS-206 (1)	Standard analysis
20	Unknown-10	Sample analysis
21	DRIFT-5	Drift
22	BLANK (2)	Blank analysis

Table T3. Precision and accuracy for major and trace element analyses by ICP-AES, Expedition 329.

Wavelength accepted	BCR-2 (<i>n</i> = 24)				BAS-206 (<i>n</i> = 8)				
	Accepted international	Shipboard average	Uncertainty	SD (%)	Accepted average*	Shipboard average	Uncertainty	SD (%)	
Major element oxide (wt%):									
SiO ₂	251.611	54.1	54.6	0.65	1.19	49.29	49.4	0.86	1.75
Al ₂ O ₃	396.152	13.6	13.5	0.39	2.92	14.46	13.8	0.15	1.06
Fe ₂ O ₃ ^(T)	239.563	13.4	14.0	0.26	1.87	15.48	14.5	0.13	0.89
MnO ₂	257.61	0.2	0.2	0.01	5.15	0.26	0.2	0.02	6.54
MgO	285.213	3.4	3.9	0.18	4.51	6.94	6.8	0.10	1.54
CaO	317.933	7.0	7.4	0.30	4.05	9.63	9.8	0.29	2.99
Na ₂ O	589.592	3.3	3.4	0.25	7.33	2.72	2.8	0.05	1.79
K ₂ O	766.491	1.7	1.8	0.09	4.69	0.16	0.2	0.06	25.75
TiO ₂	337.28	2.3	2.2	0.10	4.51	2.12	1.9	0.07	3.40
P ₂ O ₅	214.914	0.4	0.4	0.06	13.25	0.20	0.2	0.05	19.92
Trace element (ppm):									
Ba	493.409	683	540	98.37	18.22	44.7	14.3	36.97	258.73
Co	228.615	42	51	2.64	5.22	53.8	59.8	3.47	5.80
Cu	324.754	19	NR	—	—	67.9	58.6	8.61	14.68
Ni	231.604	12	11	3.62	32.79	51.2	49.2	2.32	4.72
Sc	361.383	33	33	1.08	3.29	46.9	50.2	0.54	1.08
Sr	407.771	346	342	13.24	3.87	100.1	99.5	2.48	2.50
V	421.552								
V	292.401	416	411	8.18	1.99	469.0	455.0	6.04	1.33
Zn	213.856	127	132	5.93	4.49	192.3	125.6	3.49	2.78
Zr	343.823	188	179	12.89	7.19	124.5	112.6	2.90	2.58

* = based on multiple repeat runs of BAS-206 standard against known internationally accepted standards carried out at the National Oceanography Centre, Southampton, United Kingdom. *n* = number of replicates, SD = standard deviation. NR = not reported, — = not analyzed.

Table T4. Results and standard deviations for selected standard samples run by ICP-AES, Expedition 329.

	A	B	C	Average	Uncertainty	SD (%)
Internal precision:	2.00	2.00	2.00			
	R 3	R 3	R 3			
	60-63	60-63	60-63			
	18.95	18.95	18.95			
	A	B	C	Average	Uncertainty	SD (%)
Major element oxide (wt%):						
SiO ₂	49.70	49.82	49.16	49.56	0.35	0.71
Al ₂ O ₃	13.03	13.28	13.18	13.17	0.12	0.94
Fe ₂ O ₃ ^(T)	14.60	14.86	14.77	14.74	0.13	0.90
MnO ₂	0.22	0.22	0.22	0.22	0.00	0.41
MgO	5.85	5.86	5.80	5.84	0.03	0.55
CaO	10.07	10.21	10.08	10.12	0.08	0.79
Na ₂ O	2.74	2.80	2.79	2.78	0.03	1.24
K ₂ O	0.37	0.37	0.37	0.37	0.00	0.37
TiO ₂	2.31	2.31	2.28	2.30	0.02	0.84
P ₂ O ₅	0.27	0.25	0.25	0.25	0.01	4.56
Trace element (ppm):						
Ba	22	14	—	17.93	5.21	29.06
Co	61	61	63	61.68	0.91	1.47
Cu	36	29	34	32.93	3.63	11.02
Ni	28	27	31	28.77	2.46	8.54
Sc	46	46	46	45.77	0.30	0.66
Sr	120	120	119	119.75	0.67	0.56
V	463	468	462	464.36	3.21	0.69
Zn	107	108	102	105.68	3.50	3.31
Zr	163	162	159	161.38	2.25	1.40
LOI (wt%):	0.43	0.62	0.24	0.43	0.19	44.19

Internal precision used for error bars. SD = standard deviation, — = not analyzed.

Table T5. Age estimates of planktonic foraminifer datum events, Expedition 329. (Continued on next page.)

Species event	Age (Ma)	Zone/Subzone base	Reference
T <i>Globorotalia (Truncorotalia) tosaensis</i>	0.61	PT1b	Srinivasan and Sinha, 1992
T <i>Globigerinoides fistulosus</i>	1.77	PT1a	Shackleton et al., 1990
Pliocene/Pleistocene boundary	1.81		Lourens et al., 2004
B <i>Globorotalia (Truncorotalia) truncatulinoides</i>	1.92		Chaisson and Pearson, 1997
T <i>Globigerinoides extremus</i>	1.98		Chaisson and Pearson, 1997
T <i>Globorotalia pseudomiocenica</i>	2.3	PL6	Berggren et al., 1995
T <i>Globoturborotalita woodi</i>	2.3		Chaisson and Pearson, 1997
T <i>Globorotalia (Menardella) multicamerata</i>	2.98		Berggren et al., 1995
T <i>Dentoglobigerina altispira</i>	3.47	PL5	Shackleton et al., 1995
T <i>Sphaeroidinellopsis seminulina</i>	3.59	PL4	Shackleton et al., 1995
T <i>Globorotalia (Hirsutella) margaritae</i>	3.85	PL3	Chaisson and Pearson, 1997
X <i>Pulleniatina sinistral</i> → dextral	4.08		Chaisson and Pearson, 1997
T <i>Globoturborotalita nepenthes</i>	4.37	PL2	Chaisson and Pearson, 1997
B <i>Globorotalia (Menardella) exilis</i>	4.45		Chaisson and Pearson, 1997
T <i>Globorotalia (Hirsutella) cibaoensis</i>	4.61	PL1b	Berggren et al., 1995
Miocene/Pliocene boundary	5.33		Lourens et al., 2004
B <i>Sphaeroidinella dehisces</i> s.l.	5.54		Chaisson and Pearson, 1997
B <i>Globorotalia tumida</i>	5.57	PL1a	Shackleton et al., 1995
B <i>Turborotalita humilis</i>	5.81		Chaisson and Pearson, 1997
B <i>Globorotalia (Hirsutella) margaritae</i>	6.08		Chaisson and Pearson, 1997
T <i>Globorotalia languaensis</i>	6.13	M14	Berggren et al., 1995
B <i>Globorotalia plesiotumida</i>	8.58	M13b	Chaisson and Pearson, 1997
B <i>Neogloboquadrina acostaensis</i>	9.83	M13a	Chaisson and Pearson, 1997
T <i>Paragloborotalia mayeri</i>	10.46	M12	Chaisson and Pearson, 1997
B <i>Globoturborotalita decoraperta</i>	11.49		Chaisson and Pearson, 1997
B <i>Globoturborotalita nepenthes</i>	11.63	M11	Turco et al., 2002
T <i>Globorotalia (Fohsella) fohsi</i> s.l. (including <i>lobata</i> and <i>robusta</i>)	11.79	M10/N13	Chaisson and Pearson, 1997
B <i>Globorotalia (Fohsella) fohsi robusta</i>	13.13	M9b	Chaisson and Pearson, 1997
B <i>Globorotalia (Fohsella) fohsi</i> s.l.	13.41	M8/M9a/N12	Chaisson and Pearson, 1997
T <i>Globorotalia praescitula</i>	13.73		Turco et al., 2002
B <i>Globorotalia (Fohsella) "praefohsi"</i>	13.77	N11	Turco et al., 2002
T <i>Globorotalia (Fohsella) peripheroronda</i>	13.8		Turco et al., 2002
T <i>Clavatorella bermudezi</i>	13.82		Shackleton et al., 1999
B <i>Globorotalia (Fohsella) peripheroacuta</i>	14.24	M7/N10	Pearson and Chaisson, 1997
B <i>Globorotalia (Menardella) praemenardii</i>	14.38		Lourens et al., 2004
T <i>Globigerinatella insueta</i>	14.66		Pearson and Chaisson, 1997
B <i>Orbulina</i> spp.	14.74	M6/N9	Shackleton et al., 1999
B <i>Clavatorella bermudezi</i>	14.89		Pearson and Chaisson, 1997
B <i>Globorotalia (Menardella) archeomenardii</i>	16.26		Pearson and Chaisson, 1997
B <i>Praeorbulina glomerosa</i>	16.27	M5b	Berggren et al., 1995
B <i>Praeorbulina sicana</i>	16.97	M5a	Berggren et al., 1995
B <i>Globorotalia birnageae</i> *	16.69		Berggren et al., 1995
T <i>Catapsydrax dissimilis</i>	17.54	M4	Berggren et al., 1995
B <i>Globigerinatella insueta</i>	17.59	M3	Pearson and Chaisson, 1997
T <i>Globoquadrina binaiensis</i>	19.09		Pearson and Chaisson, 1997
T <i>Paragloborotalia kugleri</i>	21.12	M2	Berggren et al., 1995
T <i>Paragloborotalia pseudokugleri</i>	21.31		Berggren et al., 1995
B <i>Globoquadrina dehisces</i>	22.44	M1b	Berggren et al., 1995
T <i>Globigerina ciperoensis</i>	22.9		Pearson and Chaisson, 1997
B <i>Paragloborotalia kugleri</i>	22.96	M1a	Berggren et al., 1995
Oligocene/Miocene boundary	23.03		Lourens et al., 2004
B <i>Paragloborotalia pseudokugleri</i>	25.2		Berggren et al., 1995
T <i>Paragloborotalia opima</i>	26.9	O6	Wade et al., 2007
Tc <i>Chiloguembelina cubensis</i>	28	O5	Wade et al., 2007
B <i>Globigerina angulisuturalis</i>	29.2	O4	Berggren et al., 1995
T <i>Subbotina angiporoides</i>	29.8		Berggren et al., 1995
T <i>Turborotalia ampliapertura</i>	30.3	O3	Berggren et al., 1995
B <i>Paragloborotalia opima</i>	30.8		Berggren et al., 1995
T <i>Pseudohastigerina nagewichiensis</i>	32	O2	Berggren et al., 1995
T <i>Hantkenina</i> spp.	33.8	O1	Berggren and Pearson, 2005
Eocene/Oligocene boundary	33.8		Pälike et al., 2006a
T <i>Turborotalia cerroazulensis</i>	33.9		Berggren and Pearson, 2005
T <i>Globigerinatheka index</i>	34.5	E16	Berggren and Pearson, 2005
T <i>Globigerinatheka semiinvoluta</i>	35.8	E15	Berggren and Pearson, 2005
T <i>Morozovelloides crassatus</i>	38.1	E14	Wade, 2004

Table T5 (continued).

Species event	Age (Ma)	Zone/Subzone base	Reference
T <i>Acarinina mcgowrani</i>	38.1		Wade, 2004
T <i>Orbulinoides beckmanni</i>	40	E13	Wade, 2004
B <i>Orbulinoides beckmanni</i>	40.8	E12	Berggren et al., 1995
T <i>Acarinina bullbrookii</i>	40.8		Berggren et al., 1995
T <i>Guembelitrinoides nuttalli</i>	42.3	E11	Berggren and Pearson, 2005
B <i>Turborotalia pomeroli</i>	42.4		Berggren et al., 1995
B <i>Morozovelloides lehneri</i>	43.5		Berggren et al., 1995
T <i>Morozovella aragonensis</i>	43.6	E10	Berggren et al., 1995
B <i>Globigerinatheka kugleri</i>	45.8	E9	Berggren et al., 1995
B <i>Guembelitrinoides nuttalli</i>	46.4	E8	Wade et al., 2011
B <i>Acarinina cuneicamerata</i>	50.4	E7	Hancock et al., 2002
B <i>Astrorotalia palmerae</i>	50.4		Berggren et al., 1985
T <i>Morozovella subbotinae</i>	50.8	E6	Berggren and Pearson, 2005
B <i>Acarinina pentacamerata</i>	50.8		Berggren and Pearson, 2005
B <i>Morozovella aragonensis</i>	52.3	E5	Berggren et al., 1995
T <i>Subbotina velascoensis</i>	53.5		Berggren et al., 1995
T <i>Morozovella aequa</i>	53.6		Berggren et al., 1995
B <i>Morozovella lensiformis</i>	54	E4	Berggren et al., 1995
T <i>Morozovella velascoensis</i>	54.5	E3	Berggren and Pearson, 2005
B <i>Morozovella gracilis</i>	54.7		Berggren et al., 1995
B <i>Pseudohastigerina wilcoxensis</i>	55.4	E2	Berggren and Pearson, 2005
Paleocene/Eocene boundary	55		Berggren et al., 1995
B <i>Globanomalina australiformis</i>	55.5		Berggren et al., 1995
B <i>Acarinina sibaiyaensis</i>	55.5	E1	Berggren and Pearson, 2005
T <i>Morozovella acuta</i>	55.7		Berggren et al., 1995
B <i>Morozovella subbotinae</i>	55.9		Berggren et al., 1995
T <i>Globanomalina pseudomenardii</i>	55.9	P5	Berggren et al., 1995
T <i>Acarinina mckannai</i>	56.3		Berggren et al., 1995
B <i>Acarinina soldadoensis</i>	56.5	P4c	Berggren et al., 1995
T <i>Acarinina subsphaerica</i>	57.1	P4b	Berggren et al., 1995
B <i>Acarinina mckannai</i>	59.1		Berggren et al., 1995
B <i>Globanomalina pseudomenardii</i>	59.2	P4a	Berggren et al., 1995
B <i>Igorina albeari</i>	60	P3b	Berggren et al., 1995
B <i>Morozovella angulata</i>	61	P3a	Berggren et al., 1995
B <i>Globanomalina imitata</i>	(61.3)		Berggren et al., 1995
B <i>Praemurica uncinata</i>	61.4	P2	Berggren and Pearson, 2005
B <i>Globorotalia compressa</i>	62.9	P1c	Berggren and Pearson, 2005
B <i>Praemurica inconstans</i>	62.9		Berggren and Pearson, 2005
B <i>Parasubbotina varianta</i>	63		Berggren et al., 1995
B <i>Subbotina triloculinoides</i>	64.3	P1b	Berggren et al., 1995
T <i>Parvularugoglobigerina eugubina</i>	64.8	P1a	Berggren and Pearson, 2005
B <i>Parvularugoglobigerina extensa</i>	64.9		Olsson et al., 1999
B <i>Parvularugoglobigerina eugubina</i>	64.97	P α	Berggren et al., 1995
T <i>Globotruncana</i>	65	P0	Berggren et al., 1995

* = Zone M4 is not divided into Subzones M4a and M4b because the base of Zone M5, as defined by *B. Praeorbulina sicana*, has been recalibrated to 16.97 Ma (Lourens et al., 2004), which is older than *B. Globorotalia birnageae*, previously used to define the base of Subzone M4b. B = base, T = top, Tc = top common, X = coiling change. (61.3) = estimated age.

Table T6. Onboard laboratory equipment for paleomagnetic study, Expedition 329.

Equipment	Status	Quality assessment
2G Enterprises 760R superconducting rock magnetometer	Used and functional	Average magnetic moment for a 150 cm blank (air) is $<1 \times 10^{-10}$ Am ² after correction of the tray background.
AGICO KappaBridge KLY-4S susceptibility meter	Used and functional	Used to measure bulk susceptibilities
DTECH D-2000 alternating-field demagnetizer	Not used	Undetermined
Schonstedt TSD-1 thermal demagnetizer	Not used	Thermal demagnetization experiments were conducted at each site with a sequence of discrete samples.
ASC IM-10 impulse magnetizer (Serial 01971)	Not used	Undetermined
Applied Physics portable fluxgate magnetometer (Model 520)	Not used	Undetermined
AGICO JR6/JR6A dual-speed spinner magnetometer	Used	Undetermined

Table T7. Geomagnetic polarity timescale normal polarity intervals, Expedition 329. (Continued on next page.)

Normal polarity interval age (Ma)		Polarity chron	Cryptochron	Reference
Top	Bottom			
0.000	0.781	C1n Brunhes	C1n-1n	Lourens et al., 2005
0.988	1.072	C1r.1n Jaramillo		Lourens et al., 2005
1.173	1.185	C1r.2n Cobb Mountain		Lourens et al., 2005
			C1r. 2r-1n	Lourens et al., 2005
1.778	1.945	C2n Olduvai		Lourens et al., 2005
2.128	2.148	C2r.1n Reunion		Lourens et al., 2005
			C2r.2r-1	Lourens et al., 2005
2.581	3.032	C2An.1n Gauss		Lourens et al., 2005
3.116	3.207	C2An.2n		Lourens et al., 2005
3.330	3.596	C2An.3n		Lourens et al., 2005
4.187	4.300	C3n.1n Cochiti		Lourens et al., 2005
4.493	4.631	C3n.2n Nunivak		Lourens et al., 2005
4.799	4.896	C3n.3n Sidufjall		Lourens et al., 2005
4.997	5.235	C3n.4n Thvera		Lourens et al., 2005
6.033	6.252	C3An.1n		Lourens et al., 2005
6.436	6.733	C3An.2n		Lourens et al., 2005
7.140	7.212	C3Bn		Lourens et al., 2005
7.251	7.285	C3Br.1n		Lourens et al., 2005
7.454	7.489	C3Br.2n		Lourens et al., 2005
7.528	7.642	C4n.1n		Lourens et al., 2005
7.695	8.108	C4n.2n		Lourens et al., 2005
8.254	8.300	C4r.1n		Lourens et al., 2005
			C4r.2r-1	Lourens et al., 2005
8.769	9.098	C4An		Lourens et al., 2005
9.312	9.409	C4Ar.1n		Lourens et al., 2005
9.656	9.717	C4Ar.2n		Lourens et al., 2005
9.779	9.934	C5n.1n		Lourens et al., 2005
9.987	11.040	C5n.2n		Lourens et al., 2005
11.118	11.154	C5r.1n		Lourens et al., 2005
11.554	11.614	C5r.2n		Lourens et al., 2005
12.014	12.116	C5An.1n		Lourens et al., 2005
12.207	12.415	C5An.2n		Lourens et al., 2005
12.730	12.765	C5Ar.1n		Lourens et al., 2005
12.820	12.878	C5Ar.2n		Lourens et al., 2005
13.015	13.183	C5AAn		Lourens et al., 2005
13.369	13.605	C5ABn		Lourens et al., 2005
13.734	14.095	C5ACn		Lourens et al., 2005
14.194	14.581	C5ADn		Lourens et al., 2005
14.784	14.877	C5Bn.1n		Lourens et al., 2005
15.032	15.160	C5Bn.2n		Lourens et al., 2005
15.974	16.268	C5Cn.1n		Lourens et al., 2005
16.303	16.472	C5Cn.2n		Lourens et al., 2005
16.543	16.721	C5Cn.3n		Lourens et al., 2005
17.235	17.533	C5Dn		Lourens et al., 2005
			C5Dr-1	Lourens et al., 2005
18.056	18.524	C5En		Lourens et al., 2005
18.748	19.722	C6n		Lourens et al., 2005
20.040	20.213	C6An.1n		Lourens et al., 2005
20.439	20.709	C6An.2n		Lourens et al., 2005
21.083	21.159	C6AAn		Lourens et al., 2005
21.403	21.483	C6AAn.2n		Lourens et al., 2005
21.659	21.688	C6AAr.1n		Lourens et al., 2005
21.767	21.936	C6AAr.2n		Lourens et al., 2005
21.992	22.268	C6Bn.2n		Lourens et al., 2005
22.564	22.754	C6Cn.1n		Lourens et al., 2005
22.902	23.030	C6Cn.2n		Lourens et al., 2005
			C6r-1	Pälike et al., 2006a
23.278	23.340	C6Cn.3n		Pälike et al., 2006a
24.022	24.062	C7n.1n		Pälike et al., 2006a
24.147	24.459	C7n.2n		Pälike et al., 2006a
			C7r-1	Pälike et al., 2006a
24.756	24.984	C7An		Pälike et al., 2006a
25.110	25.248	C8n.1n		Pälike et al., 2006a
25.306	26.032	C8n.2n		Pälike et al., 2006a
26.508	27.412	C9n		Pälike et al., 2006a
			C8n.2n-1	Pälike et al., 2006a
			C9n-1,2	Pälike et al., 2006a

Table T7 (continued).

Normal polarity interval age (Ma)		Polarity chron	Cryptochron	Reference
Top	Bottom			
27.886	28.126	C10n.1n	C9r-1	Pälike et al., 2006a
28.164	28.318	C10n.2n		Pälike et al., 2006a
29.166	29.467	C11n.1n	C10r-1,2	Pälike et al., 2006a
29.536	29.957	C11n.2n		Pälike et al., 2006a
30.617	31.021	C12n	C11r.1	Pälike et al., 2006a
33.232	33.705	C13n	C12r-1,2,3,4,5,6,7,8	Pälike et al., 2006a
35.126	35.254	C15n	C13n-1	Pälike et al., 2006a
35.328	35.554	C16n.1n	C13r-1,2,3,4	Pälike et al., 2006a
35.643	36.355	C16n.2n		Pälike et al., 2006a
36.668	37.520	C17n.1n		Pälike et al., 2006a
37.656	37.907	C17n.2n		Pälike et al., 2006a
37.956	38.159	C17n.3n		Pälike et al., 2006a
38.449	39.554	C18n.1n		Pälike et al., 2006a
39.602	40.084	C18n.2n		Pälike et al., 2006a
41.358	41.510	C19n		Pälike et al., 2006a
42.536	43.789	C20n		Cande and Kent, 1995
46.264	47.906	C21n		Cande and Kent, 1995
49.037	49.714	C22n		Cande and Kent, 1995
50.778	50.946	C23n.1n		Cande and Kent, 1995
51.047	51.743	C23n.2n		Cande and Kent, 1995
52.364	52.663	C24n.1n		Cande and Kent, 1995
52.757	52.801	C24n.2n		Cande and Kent, 1995
52.903	53.347	C24n.3n		Cande and Kent, 1995
55.904	56.391	C25n	C24r-1,2,3,4,5,6,7,8,9,10,11	Cande and Kent, 1995
57.554	57.911	C26n	C25r-1,2,3,4,5	Cande and Kent, 1995
60.920	61.276	C27n	C26r-1,2,3,4,5,6,7	Cande and Kent, 1995
62.499	63.634	C28n		Cande and Kent, 1995
63.976	64.745	C29n	C28r-1	Cande and Kent, 1995
65.578	67.610	C30n		Cande and Kent, 1995
67.735	68.737	C31n		Cande and Kent, 1995
71.071	71.338	C32n.1n		Cande and Kent, 1995
71.587	73.004	C32n.2n		Cande and Kent, 1995
73.291	73.374	C32r.1n		Cande and Kent, 1995
73.619	79.075	C33n		Cande and Kent, 1995
83.000	118.000	C34n		Cande and Kent, 1995


Table T8. Cultivation experiments using sediment and/or basalt samples, Expedition 329. (Continued on next page.)

Medium name	Solid/Liquid	Sample type	Target physiology	Electron donor	Electron acceptor	Carbon source	Nitrogen source	Incubation temperature (°C)	pH	Remarks
SPG-1	Liquid	Sediment	Aerobic hydrogenotrophic autotrophs	H ₂	O ₂	CO ₂	NH ₄ ⁺	10	7.0	
SPG-2	Liquid	Sediment	Aerobic hydrogenotrophic autotrophs	H ₂ , yeast extract	O ₂	CO ₂ , yeast extract	NH ₄ ⁺	10	7.0	
SPG-3	Liquid	Sediment	Hydrogenotrophic iron-reducing autotrophs	H ₂	Amorphous FeOOH	CO ₂	NH ₄ ⁺	10	7.0	
SPG-4	Liquid	Sediment	Heterotrophs	Glucose, peptone, yeast extract	O ₂	Glucose, peptone, yeast extract	NH ₄ ⁺	10	7.0	
SPG-5	Liquid	Sediment	Nitrate-reducing, iron-oxidizing autotrophs	FeCl ₂	NO ₃ ⁻	CO ₂	NH ₄ ⁺ or NO ₃ ⁻	10	7.0	
SPG-6	Liquid	Sediment	Hydrogenotrophic nitrate-reducing autotrophs	H ₂	NO ₃ ⁻	CO ₂	NH ₄ ⁺ or NO ₃ ⁻	10	7.0	
SPG-7	Liquid	Sediment	Hydrogenotrophic nitrate-reducing autotrophs	H ₂ , yeast extract	NO ₃ ⁻	CO ₂	NH ₄ ⁺ or NO ₃ ⁻	10	7.0	
SPG-8	Liquid	Sediment	Sulfur- and/or H ₂ -oxidizing chemolithoautotrophs	H ₂ , S ₂ O ₃ ²⁻	O ₂	CO ₂	NH ₄ ⁺	10	7.0	
SPG-9	Liquid	Sediment	Aerobic organotrophs	Tryptone, yeast extract	O ₂	Tryptone, yeast extract	NH ₄ ⁺	10	7.0	
SPG-10	Liquid	Sediment	Hydrogenotrophic and/or acetate-methanogens	H ₂ , acetate	CO ₂	CO ₂ or acetate	NH ₄ ⁺	10	7.2	Cysteine (0.05%)
SPG-11	Liquid	Sediment	Methanogens	Methanol	CO ₂	CO ₂ or methanol	NH ₄ ⁺	10	7.2	Cysteine (0.05%), FeCl ₂ (1 mM)
SPG-12	Liquid	Sediment	Heterotrophic sulfate reducers	Lactate, yeast extract	SO ₄ ²⁻	Lactate, yeast extract	NH ₄ ⁺	10	7.2	
SPG-13	Liquid	Sediment	Sulfur reducers	H ₂ , yeast extract	S ₂ O ₃ ²⁻	H ₂ , yeast extract	NH ₄ ⁺	10	7.2	
SPG-14	Liquid	Sediment	Hydrogen and/or acetate-oxidizing sulfur reducers	H ₂ , acetate	S ₂ O ₃ ²⁻	CO ₂ , acetate	NH ₄ ⁺	10	7.2	
SPG-15	Liquid	Sediment	Fermenters	Casamino acids, yeast extract	Casamino acids, yeast extract	Casamino acids, yeast extract	NH ₄ ⁺	10	7.2	
SPG-16	Liquid	Sediment	Sulfate reducers	H ₂ , acetate	SO ₄ ²⁻	CO ₂	NH ₄ ⁺	10	7.2	
SPG-17	Liquid	Sediment	Nitrate reducers	H ₂ , yeast extract	NO ₃ ⁻	CO ₂	NH ₄ ⁺	10	7.2	
SPG329-1	Liquid	Sediment	Aerobic heterotrophs	Various dissolved organic matter	O ₂	Various dissolved organic matter	Various dissolved organic matter	10	7.0	
SPG329-2	Liquid	Sediment	Fermenters	Various dissolved organic matter	Various dissolved organic matter	Various dissolved organic matter	Various dissolved organic matter	10	7.0	
SPG329-3	Liquid	Sediment	Autotrophic hydrogenotrophic nitrate reducers	H ₂	NO ₃ ⁻	CO ₂	NO ₃ ⁻	10	7.0	
SPG329-4	Liquid	Sediment	Heterotrophic nitrate reducers	Various dissolved organic matter	NO ₃ ⁻	Various dissolved organic matter	Various dissolved organic matter	10	7.0	
SPG329-5	Liquid	Sediment	Aerobic ammonium-oxidizing autotrophs	NH ₄ ⁺	O ₂	CO ₂	NH ₄ ⁺	10	7.0	
SPG329-6	Liquid	Sediment	Aerobic autotrophic nitrite oxidizers	NO ₂ ⁻	O ₂	CO ₂	NO ₂ ⁻	10	7.0	
SPG329-7	Liquid	Sediment	Anaerobic hydrogenotrophs	H ₂	CO ₂	CO ₂ , acetate, methylated compounds	NH ₄ ⁺	10	7.0	



Table T8 (continued).

Medium name	Solid/Liquid	Sample type	Target physiology	Electron donor	Electron acceptor	Carbon source	Nitrogen source	Incubation temperature (°C)	pH	Remarks
SPG329-8	Liquid	Sediment	Aerobic hydrogenotrophic autotrophs	H ₂	O ₂	CO ₂	NH ₄ ⁺	10	7.0	
SPG329-9	Liquid	Sediment	Autotrophic iron-oxidizing autotrophs	Fe ²⁺	O ₂	CO ₂	NH ₄ ⁺	10	7.0	
Marine 2216 (Difco)	Solid and liquid	Sediment	Aerobic heterotrophs	Various dissolved organic matter	O ₂	Various dissolved organic matter	Various dissolved organic matter	10	~7.6	1%, 10%, and 100% of media
Marine R2A (Fluka)	Solid	Sediment	Aerobic heterotrophs	Various dissolved organic matter	O ₂	Various dissolved organic matter	Various dissolved organic matter	10	~7.2	Prepared with seawater
TSA agar (Oxoid)	Solid	Sediment	Aerobic heterotrophs	Various dissolved organic matter	O ₂	Various dissolved organic matter	Various dissolved organic matter	10	~7.3	Prepared with seawater
TSB (Oxoid)	Liquid	Sediment	Aerobic heterotrophs	Various dissolved organic matter	O ₂	Various dissolved organic matter	Various dissolved organic matter	10	~7.3	Prepared with seawater
TCBS agar (Difco)	Solid	Sediment	Vibrios	Various dissolved organic matter	O ₂	Various dissolved organic matter	Various dissolved organic matter	10	~8.6	
Actinobacteria agar	Solid	Sediment	Actinobacteria	Various dissolved organic matter	O ₂	Various dissolved organic matter	Various dissolved organic matter	10	~7.6	Prepared with seawater
Sediment extract agar	Solid	Sediment	Aerobic bacteria	Various dissolved organic matter	O ₂	Various dissolved organic matter	Various dissolved organic matter	10	~7.6	
Monomer mix medium-1 (Mmm1)	Liquid	Sediment	Aerobic heterotrophs	Various dissolved organic matter	O ₂	Various dissolved organic matter	Various dissolved organic matter	4	~7.8	Setup for all sites + various depths + dilution series
Monomer mix medium-2 (Mmm2)	Liquid	Sediment	Anaerobic heterotrophs	Various dissolved organic matter	Various (no O ₂)	Various dissolved organic matter	Various dissolved organic matter	4	~7.8	(no oxic incubations at SPG-12)
SPG-ASW	Liquid	Sediment	Hydrogenotrophic autotrophs	H ₂	Various	CO ₂	NH ₄ ⁺	4	~7.8	
SPG-JL	Liquid	Sediment and basalt	Anaerobic methane-oxidizing consortium	Various dissolved organic matter, H ₂	NO ₃ ⁻ , SO ₄ ²⁻	Various dissolved organic matter	Various dissolved organic matter	10	~7.8	0.01% marine broth 2216 is supplemented. Primarily targeting Site U1371

Table T9. Radioactive and stable isotopic substrates used for incubation experiments of sediment slurry, Expedition 329.

Experiment type	Metabolism	Compound	Radioactive isotope				Stable isotope			
			Activity (kBq/ μ L)	Added volume (μ L)	Activity in vial (kBq/vial)	Specific activity (kBq/ μ M)	Concentration label (μ M/ μ L) (M)	Label (%)	Added volume (μ L)	Final concentration in vial (μ M)
A	Autotrophy	14 C bicarbonate	3.70	80	296	1.42				
B	Autotrophy	14 C bicarbonate	3.70	80	296	1.42				
	Nitrification	15 N ammonium 33 P phosphate	37	8	296	3700	1	99	8	200
C	Autotrophy N fixation	14 C bicarbonate	3.70	80	296	1.42				
		15 N dinitrogen gas						99		1 mL gas
		33 P phosphate	37	8	296	3700				
D	Autotrophy	14 C bicarbonate	3.70	80	296	1.42				
	Organic P uptake	33 P ATP	37	8	296	1.11E+08				
E	Heterotrophy	14 C acetate	0.84	80	67	2146				
F	Heterotrophy Nitrification	14 C acetate	0.84	80	67	2146				
		15 N ammonium		8			1	99	8	200
		33 P phosphate	37	8	296	3700				
G	Heterotrophy N fixation	14 C acetate	0.84	80	67	2146				
		15 N dinitrogen gas						99		1 mL gas
		33 P phosphate	37	8	296	3700				
H	Nitrate reduction	15 N nitrate		8			1	99	8	200
	Autotrophy	13 C bicarbonate		80			1	99	80	2000

Table T10. Radioactive tracers used for cell-viability assays, Expedition 329.

Isotope	Compound	Concentration (μ M)	Activity (kBq)
14 C	ATP	0.5	25.9
14 C	Leucine	0.5	288.6
14 C	Thymidine	1.8	17.1

Table T11. Stable isotope–tracer incubation experiments for single cell–level metabolic assay, Expedition 329.

Metabolism	Carbon source			Nitrogen source			Headspace of vial
	13 C substrate	Concentration		15 N substrate	Concentration		
		(mM/vial)	(mM)*		(mM/vial)	(mM)*	
Autotrophy	Bicarbonate	15	1.2	Ammonia	1.5	0.12	3.3% O ₂ in N ₂
Heterotrophy	Glucose	15	1.2	Ammonia	1.5	0.12	3.3% O ₂ in N ₂
Heterotrophy	Pyruvate	15	1.2	Ammonia	1.5	0.12	3.3% O ₂ in N ₂
Heterotrophy	Acetate	15	1.2	Ammonia	1.5	0.12	3.3% O ₂ in N ₂
Heterotrophy (oligotrophy)	Amino acids [†]	15	1.2	Amino acids [†]	15	1.2	3.3% O ₂ in N ₂
Methanotrophy	Methane		~0.7 [‡]	Ammonia	1.5	0.12	1.7% O ₂ , 43% N ₂ , 43% 13 CH ₄ (+15 psi)
(Control without 13 C)	No addition	0	0	Ammonia	1.5	0.12	3.3% O ₂ in N ₂
(Negative control 1)	No addition	0	0	No addition	0	0	3.3% O ₂ in N ₂
(Negative control 2: autoclaved sediment)	Bicarbonate glucose	15	1.2	Ammonia	1.5	0.12	3.3% O ₂ in N ₂

* = tentative value based on 80% average porosity (accurate concentration of each sample was determined by actual porosity data measured onboard). [†] = mixture of 20 different kinds of 13 C- and 15 N-labeled amino acid (>99%). [‡] = as dissolved CH₄ concentration. NanoSIMS and molecular ecological techniques were used.

Table T12. Wireline tool string downhole measurements, Expedition 329.

Tool string	Tool	Measurement	Sampling interval (cm)	Approximate vertical resolution (cm)
Triple combination	HNGS	Spectral gamma ray	15	51
	GPIT	Tool orientation	0.25 and 15	NA
	HLDS	Bulk density	2.5 and 15	38/46
	DIT	Resistivity	15	200/150/76
Formation MicroScanner	HNGS	Spectral gamma ray	15	51
	GPIT	Tool orientation	0.25 and 15	NA
	FMS	Microresistivity imaging	0.25	0.5

All tool and tool string names are trademarks of Schlumberger. Sampling interval based on optimal logging speed. NA = not applicable. For definitions of tool acronyms, see Table T13.

Table T13. Acronyms and units used for downhole wireline tools and measurements, Expedition 329.

Tool	Output	Explanation	Unit
DIT		Dual Induction Tool	
	IDPH	Deep induction resistivity	Ωm
	IMPH	Medium induction resistivity	Ωm
	SFLU	Spherically focused resistivity	Ωm
FMS		Formation MicroScanner	
	C1, C2	Orthogonal hole diameters	Inch
	P1AZ	Pad 1 azimuth Spatially oriented resistivity images of borehole wall	Degrees
GPIT		General Purpose Inclinometry Tool	
	DEVI	Hole deviation	Degrees
	HAZI	Hole azimuth	Degrees
	Fx, Fy, Fz Ax, Ay, Az	Earth's magnetic field (three orthogonal components) Acceleration (three orthogonal components)	Degrees m/s^2
HLDS		Hostile Environment Litho-Density Sonde	
	RHOM	Bulk density	g/cm^3
	PEFL	Photoelectric effect	barn/e^-
	LCAL DRH	Caliper (measure of borehole diameter) Bulk density correction	Inch g/cm^3
HNGS		Hostile Environment Gamma Ray Sonde	
	HSGR	Standard (total) gamma ray	gAPI
	HCGR	Computed gamma ray (HSGR minus uranium contribution)	gAPI
	HFK	Potassium	wt%
	HTHO HURA	Thorium Uranium	ppm ppm

For the complete list of acronyms used in IODP and for additional information about tool physics, consult IODP-USIO Science Services, LDEO, at iodp.ideo.columbia.edu/TOOLS_LABS/tools.html.